NETWORKING OF C_{60} BALLS BY MEANS OF VARIOUS CHEMICAL STRATEGIES

Thesis submitted to
the University of Calicut in partial fulfilment of
the requirements for the degree of

DOCTOR OF PHILOSOPHY IN CHEMISTRY
in the Faculty of Science

By

USHA M.

Under the guidance of
Dr. Resmi M.R.

Research and Post Graduate Department of Chemistry
Sree Neelakanta Government Sanskrit College, Pattambi
(Affiliated to the University of Calicut, Kerala, India)
December 2022

Sree Neelakanta Govt.Sanskrit College
Pattambi, Palakkad Dt, Kerala - 679 306
(Accredited by NAAC with A+ Grade)
Ph: 0466-2212223
e-mail: sngscollege@gmail.com
website: www.sngscollege.org

Date: 30. 12. 2022

CERTIFICATE

Certified that the thesis entitled "**Networking of C_{60} balls by means of various chemical strategies**", submitted by **Ms. Usha M.** is an authentic record of research work carried out by her under my supervision at the Research and Post Graduate Department of Chemistry, SNGS College, Pattambi in partial fulfillment of the requirements for the award of degree of Doctor of Philosophy in Chemistry of the University of Calicut, and has not been included in any other thesis submitted previously for the award of any other degree.

Pattambi

Dr. Resmi M.R
(Supervising Guide)
Professor
Research and Post Graduate
Department of Chemistry

SreeNeelakanta Govt. Sanskrit College
Pattambi, Palakkad Dt, Kerala - 679 306
(Accredited by NAAC with A Grade)
Ph: 0466-2212223
e-mail: sngscollege@gmail.com
Website: www.sngscollege.org

CERTIFICATE

This is to certify that the thesis entitled "**NETWORKING OF C_{60} BALLS BY MEANS OF VARIOUS CHEMICAL STRATEGIES**", bound herewith is a bonafide research work done by Ms. Usha M. under my supervision at the Research and Post Graduate Department of Chemistry, SNGS College, Pattambi in partial fulfillment of the requirements for the award of the degree of Doctor of Philosophy in Chemistry of the University of Calicut. I also certify that the corrections/suggestions from the adjudicators have been incorporated in the revised thesis.

Pattambi
22.08.2023

Dr. Resmi M.R.
(Supervising Guide)
Professor
Research and Post Graduate
Department of Chemistry
SNGS College, Pattambi

DECLARATION

I hereby declare that the present work entitled "**Networking of C_{60} balls by means of various chemical stratrgies**" is an authentic record of the original work done by me under the guidance of Dr. Resmi M.R., Professor, Research and Post Graduate Department of Chemistry, SNGS College, Pattambi in partial fulfillment of the requirement for the award of degree of Doctor of Philosophy in Chemistry of the University of Calicut, and has not been included in any other thesis submitted previously for the award of any other degree.

Place: Pattambi **Usha M.**
Date: 30.12.2022

Dedicated To

My Family, My Colleagues
&
All My Respected Teachers

ACKNOWLEDGEMENTS

Firstly, I would like to express my sincere gratitude to my research guide, Dr. Resmi M.R for her valuable suggestions and careful guidance during the entire course of my research work. I am thankful for the freedom that she had given me and also for the fruitful discussions through the entire period of my research. I specially aknowledge her patience and commitment, particularly during the thesis correction period.

I also thank Dr. P Raveendran, Professor, Department of Chemistry, University of Calicut for his valuable suggestions and support during the entire course of my research. I am grateful for the the fruitful dicscussions during the preparation of my thesis.

I express my gratitude to Dr. Binith N.N, Professor, Department of Chemistry, University of Calicut for her support. Her passion and dedication to research always surprised me and I was very much encouraged by her during the period of my research.

I would like to thank Dr. Priyakumari C. P., Assistant professor, Department of Chemistry, IIT Palakkad for her collaboration and support.

I am thankful to Dr Sunil John, Principal, SNGS College, Pattambi for for his support and encouragement. My sincere thanks are due to Dr Anil kumar V, (V C Nominee of our RAC), Professor, Department of Mathematics, University of Calicut and Dr. H. K. Santhosh, Associate Professor, Department of Malayalam, Senior Research Guide, SNGS College, Pattambi.

I am thankful to Prof. T. Pradeep, IIT Madras for helpful discussions. Dr. M. Eswaramoorthy, JNCASR, Bangalore is acknowledged for support.

My special thanks to my labmates Sreeja and Shaniba for their encouragement and support. I would like to thank all my dear colleagues and all research students of SNGS College, Pattambi. I acknowledge all teaching and non teaching staff, of SNGS College, Pattambi. I am thankful to all my lab staff, especially Surendrettan, for his valuable support.

I acknowledge my senior Dr. Rajeena U., presently at the Regional Centre of Advanced Technologies and Materials, Palacky University, Šlechtitelu 27, Olomouc, Czech Republic for her valuable help.

Kerala State Council for Science, Technology and Environment (KSCSTE) is acknowledged for funding for the research facilities. JNCASR (Bangalore), C-SIF (University of Calicut), SAIF (CUSAT, Kochi), PSG College (Coimbatore) and the DST-FIST facilities in the department are acknowledged.

Finally, I would like to thank my parents and my in-laws. They stood with me and supported me in every step of my life. Especially, I owe a deep sense of gratitude to my father, who was the first person who taught me the importance of education, in spite of being an illiterate person himself. I am also thankful to my husband, Mr. Sajeev N. for his motivation and support that he gave me throughout my life. Thanks to my children for their love and co-operation during my entire research period.

Thank you all.

Usha M.

PREFACE

The Ph.D. research work presented here focus on the networking of fullerene balls and the preparation of novel functional materials thereby which contain highly crosslinked fullerene cages possessing various unique properties, fulfilling the requirements of future applications. The development of fullerene-based nanomaterials like, polymeric fullerene oxide (PFO) network, fullerols, Partially Hydrogenated Fullerol network (PHF), two different ternary nanocomposite of Graphene, nanotube and fullerenes (GNF1 & GNF2) are included in this dissertation. The different stratergies adapted for their preparations are discussed in detail. The formation of carbon nano tubes and their accidental incorporation in the prepared nanocomposites, in a simple laboratory set up glorifies the importance of this work. The photocatalytic and electrochemical performances of the prepared nanomaterials are presented in detail.

Entire work of this Ph.D. thesis are included in six chapters and a short description of each one of them is given below:

Chapter 1: chapter 1 encompasses an introduction and literature review of different fullerene based materials, their networking strategies and their applications in electrochemical sensing, photocatalytic dye degradation and photocatalytic H_2O_2 generation and hydrogen storage. The structure and bonding in fullerenes, various methods adopted for their synthesis, properties and applications are discussed here. Also, a brief introduction of other nano allotropic forms of carbon like graphene

and carbon nanotubes are provided. The importance of carbon nanostructures as hydrogen storage materials are also presented in this chapter. The main objectives of this research work are also included in the chapter.

Chapter 2: In chapter 2, the various experimental procedures adopted in the present work are described in detail and the chemicals used for their preparation are listed. Among these, preparation of mesoporous polymeric fullerene oxide framework, its nanocomposite with titania are described. The computational details of Density Functional Theory calculations used for investigating the [3+2] cycloadditions involved in the PFO networking is given. Also, the experimental procedures adapted for the preparation of Reduced Hydroxy Graphene (RHG), fullerols, Partially Hydrogenated Fullerol network (PHF), ternary composite of Graphene, nanotube and fullerenes (GNF1 & GNF2) were discussed in detail. Prepared nanomaterials are studied by various surface, spectroscopic, and microscopic characterisation techniques like Fourier transform infrared spectroscopy (FTIR), X-ray Diffraction (XRD), Raman spectroscopy, X-ray Photoelectron spectroscopy (XPS), Field emission scanning electron microscopy (FE-SEM), Transmission electron microscopy (TEM), Atomic force microscopy (AFM), BET surface area analysis, UV-Visible diffused reflectance spectroscopy (UV-DRS), Photoluminescence spectroscopy (PL) are discussed. Electrochemical measurements, instrumentation and procedures used for the electrochemical sensing studies of developed PFO, GNF1, and GNF2 systems are included in the chapter. Additionally photocatalytic

dye degradation studies and photocatalytic H_2O_2 production by PFO and PFO/TiO_2 nanocomposite are presented.

Chapter 3: In chapter 3, the preparation, characterisation and applications of highly cross-linked fullerene oxide cages originated from fully brominated fullerene, $C_{60}Br_{24}$ through its thermal treatment is presented in detail. In addition, DFT calculations performed to understand the mechanism and energetics of networking of fullerene balls via [3+2] cycloadditions are also presented. The prepared poly (fullerene oxide) framework is characterised by various microscopic and spectroscopic techniques like SEM, TEM, Surface area measurements (BET), XRD, FTIR, RAMAN, XPS, AFM, UV-DRS studies and Photoluminescence studies (PL). As visible light active semicondoctor, the photo catalytic performance of PFO and its nanocomposite with TiO_2 (PFO/TiO_2) is evaluated with two reactions. Photocatalytic mineralisation of a model dye, methylene blue as well as photocatalytic generation of hydrogen peroxide from water are studied and the results are presented in this chapter, A schematic energy level diagram is constructed showing the band gap of PFO and mechanism of photocatalytic process is also included here. In addition, another application of PFO, as an enzyme-free, mediator-fee and binder-free fourth generation electrochemical biosensing platform for trace level detection of glucose is investigated and parameters like sensitivity, selectivity, limit of detection and linear range are compared with glucose biosensors present in literature.

Chapter 4: In chapter 4, the preparation of hydroxylated derivatives of fullerene (fullerols) by the sonochemical reaction of C_{60} with H_2O_2 and

their networking achieved by ether linkages, as a consequence of hydrazine reduction are disussed in detail. The hydrazine reduction also results in partial hydrogenation of the network. The Partially Hydrogenated Fullerol (PHF) network formed is characterised by various spectroscopic and microscopic techniques such as, FTIR, Raman spectroscopy, AFM, SEM, and XPS analysis. The mechanism of hydrogenation of fullerol clusters during hydrazine reduction is suggested to be through the formation of diimides from hydrazine, fullerols being functioned as the required oxidising agents. The subsequent addition of diimides to 6-6 bonds of C_{60} balls generated results in the hydrogenation of the network. The formation of some aromatic fragments as a consequence of breakage of few fullerene balls by virtue of gentle fragmentation due to heavy hydrogenation is also evident from FTIR and Raman spectroscopic investigations of PHF.

Enzyme-free and binder-free electrochemical biosensing performance of PHF is evaluated with the biomarker, H_2O_2, using the developed sensor electrode, Cu^{2+}-phen-dione@PHF/GCE and its various sensor parameters such as sensitivity, selectivity, limit of detection and linear range are compared with other enzyme free hydrogen peroxide electrochemical sensors reported in literature and the results are summarised in this chapter.

Chapter 5: In chapter 5, two ternary nanocomposites, hydrogenated and hydroxy functionalized Graphene-Nanotube-Fullerene (GNF1 and GNF2) are presented. GNF1 is prepared by by the hydrazine reduction of the aqueous dispersion of an oxidized mixture of PFO and RHG. GNF2 is prepared by the hydrazine reduction of a mixture of fullerol

clusters and hydroxy graphene dispersion in water. GNF1 and GNF2 thus prepared are characterised by various spectroscopic and microscopic techniques and are presented in this chapter. Accidental incorporation of nanotubes is observed in SEM, TEM and AFM analyses of both the nanocomposites prepared. Evidence for heavy hydrogenation is also presented by FTIR and Raman spectroscopic investigations. Enzyme-free electrochemical sensing studies are performed for the important biomarker H_2O_2, using the modified glassy carbon electrodes, Cu^{2+}-phen-dione@GNF1/GCE and Cu^{2+}-phen- dione@GNF2/GCE are presented in this chapter and the evaluation of sensing parameters, sensitivity, selectivity, LOD and linear range are included in this chapter along with a comparison with other similar sensors from literature.

Chapter 6: In chapter 6, a summary of the entire work is presented.

Chapter 7: In chapter 7, the future scope of the developed nanomaterials are included.

CONTENTS

ABBREVIATIONS

PFO	-	Poly Fullerene Oxide
PHF	-	Partially Hydrogenated Fullerol network
GNF1 & GNF2	-	Graphene-Nanotube-Fullerene ternary hybrid.
RHG	-	Reduced Hydroxy Graphene
CNTs	-	Carbon Nano Tubes
SWCNTs	-	Single Walled Carbon NanoTubes
MWCNTs	-	Multi Walled Carbon NanoTubes
CNMs	-	Carbon – based nanomaterials

CHAPTER 1

INTRODUCTION AND LITERATURE SURVEY

1.1.Carbon-based nanomaterials

Carbon is unique among the elements because of its incredible ability to form a strong bond with other elements and also due to its capacity to show the phenomenon of allotropism.[1] It is known to exist in various diverse physical forms such as graphite, diamond, and amorphous carbon for centuries and has played an important role historically in human development. Carbon-based nanomaterials (CNMs) are recent additions to the carbon family which include many diverse forms of carbon such as graphene, carbon nanotubes, fullerenes, graphene quantum dots, graphene nanoribbon, nano onions, nanodiamonds, etc.[2] Because of their unique structural features and dimensionalities, they are expected to exhibit outstanding chemical and physical properties and therefore have attracted enormous attention among the global research community. Many of them have already been materialized such as excellent mechanical strength, high electrical and thermal conductivities, outstanding optical properties and so on.[3–5] Laser irradiation of graphite, from polycyclic aromatic hydrocarbons, electrical arc heating and resistive arc heating of graphite, chemical vapor deposition, etc. are some of the synthetic strategies adopted for the production of CNMs. Advanced applications of carbon-based nanomaterials in various fields such as biomedical engineering as multifunctional materials, in drug delivery as versatile nanocarriers, energy storage, biosensors, power generation, wastewater treatment, microelectronics, etc. are hot topics in the current research scenario.[6–10] Thus, hybridizing nanocarbon forms into composite materials has emerged as a popular strategy to develop advance functional materials suitable for diverse applications in many fields.

1.2.Fullerenes

Fullerenes, "the wonderful molecules", are made up of carbon atoms. In the 1970's the possibility for the existence of polyhedral carbon clusters was predicted by a group of scientists [11] and this was materialized in 1985 when Kroto et al. studied the mass spectra of carbon vapours produced by the laser irradiation of graphite. They observed that the most abundant peaks in the mass spectrum corresponding to the masses of 720 and 840. They could attribute these peaks to the formation of C_{60} and C_{70} in the vapour.[12–15] The fullerene family consists of C_{60}, C_{70}, C_{72}, C_{76}, and C_{80} molecules, etc. amongst which C_{60} is the most stable one.[16] The discovery of fullerenes was the first stepping stone of nanocarbon research and it expanded the number of known allotropes of carbon from diamond, graphite, and amorphous carbon to an additional large number of different types of nanocarbon forms. C_{60} was named “Buckminsterfullerene” ("bucky balls" in short) because of its resemblance to the structures of geodesic domes designed by famous American architect Buckminster Fuller.[17] Fullerenes are also detected in outer space. Interestingly, large amounts of C_{60} and C_{70} have been found in a blast of gas from a dying star, and the presence of C_{60}^{+} in the clouds of molecules and dust is confirmed by spectroscopic investigations.[18,19]

1.3.Structure and bonding in C_{60}

In the C_{60} molecule (Figure 1.1), the carbon atoms are found to be present at the vertices of a regular truncated icosahedron with 32 faces (12 pentagons and 20 hexagons). Each carbon atom is bonded to three other carbon atoms and is sp^2 hybridized. 90 covalent bonds are

present of which 60 are slightly longer (the bonds between two adjacent hexagons or [6,6] bonds) and are termed single bonds. The remaining 30 bonds are slightly shorter (the bonds between an adjacent hexagon and a pentagon ring or [6,5] bonds) and are considered double bonds. It is considered as the most symmetric molecule with 120 possible symmetry operations.[20–22]

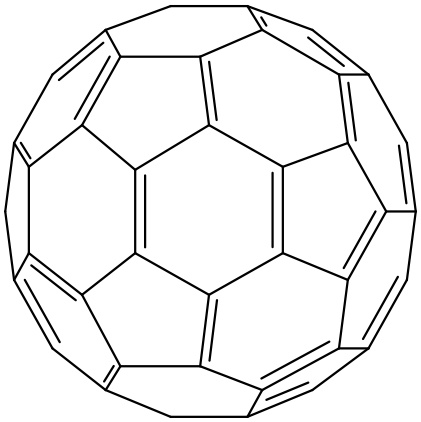

Figure 1.1: Buckminsterfullerene

1.4. Synthesis of fullerenes

There are many methods reported for the synthesis of fullerenes. As mentioned earlier, C_{60} was first synthesized by the laser vapourization of the carbon in an inert atmosphere, in the year 1985. However, fullerene research was in a stagnant state except theoretical reports because of the absence of bulk synthetic strategies until the year 1990. This was the time Kratschmer and coworkers [23] came up with the arc discharge method by which bulk production of fullerenes was materialized. Fullerenes are also produced by the pyrolysis of naphthalene in an argon atmosphere at 1000 °C. There are reports for

the synthesis of C_{60} from carbon soot as well. [24,25] Zhang et al. reported a method to synthesize C_{60} from $CHCl_3$ by using an UT-FVP apparatus under mild conditions.[26] The major drawback of all these methods is the fact that only small amount of fullerenes can be produced at a time. The reaction conditions generally adopted for some of the fullerene synthetic strategies are given below.

1.4.1. Laser irradiation of graphite

In this method, a pulsed laser beam is used for evaporating a graphite disc in an inert He atmosphere. Alternatively, this can be done with a CW-Nd: YAG laser in Ar gas flow, or with stationary CO_2 laser radiation. [27, 28]

1.4.2. Laser irradiation of PAHs.

In this method, C_{60} is produced when Polycyclic Aromatic Hydrocarbons (PAHs) consisting of 60 or more carbon atoms are exposed to a pulsed laser beam. The resulting soot formed by the condensation of vapours contains C_{60}, formed by the photofragmentation of large PAHs (>60 carbon atoms).[29] Large PAH molecules are synthesized by bottom-up approaches from smaller PAHs so that they can be used to produce C_{60}.[30, 31]

1.4.3. Electrical arc heating of graphite.

In the method reported by Kratschmer et al.[32] for the large scale synthesis of fullerenes, an electrical arc is produced between two graphite electrodes in an inert atmosphere of helium resulting in the formation of condensed carbon soot. From this soot, fullerenes are extracted by toluene solvent and subsequently toluene is removed by

heating in a rotary evaporator. High purity C_{60} is separated by liquid chromatography.[33,34]

1.4.4. Resistive arc heating of graphite

In this method, one of the graphite electrodes is resistively heated to high temperatures and subjected to arc discharge using second graphite electrode. Vaporized carbon condenses to form soot, from which C_{60} is extracted by solvent extraction method.[35]

Various methods of fullerene preparation are summarized schematically in Figure 1.2.

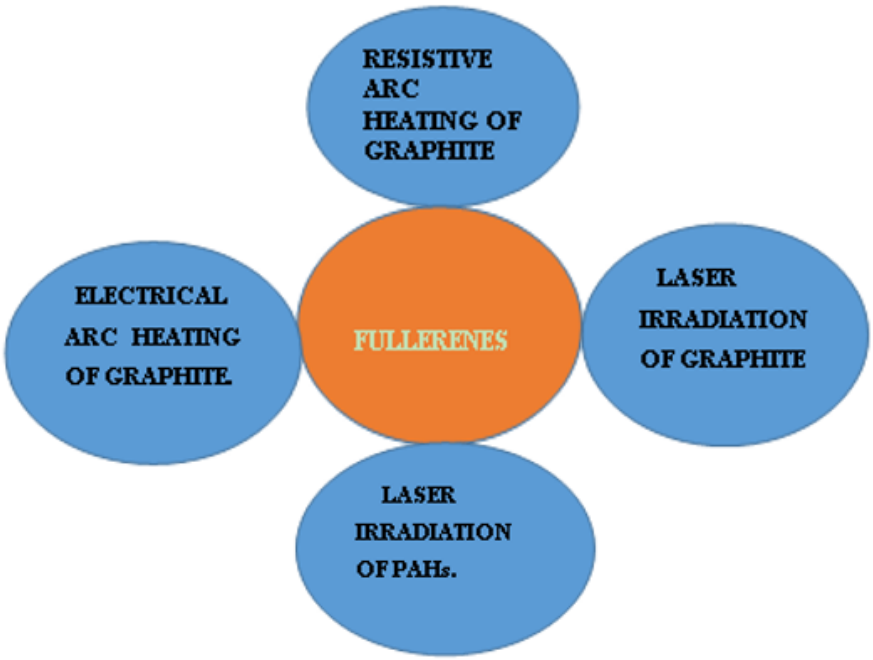

Figure 1.2.: Schematic representation of various preparation methods of fullerenes.

1.5. Properties of fullerenes

C_{60} is a black powdery material which is soft and slippery. Because of weak intermolecular forces acting between the molecules and hence less energy is needed to overcome these forces, it has a low melting point than graphite and diamond. Fullerenes are insoluble in most of the polar solvents and C_{60} forms a deep purple colour solution in toluene and many other solvents. Fullerenes are soluble in most aromatic solvents and their solubility depends upon the factors like polarizability, polarity, molecular size, and cohesive energy density.[36] Fullerenes are known to change their structure under high pressure. In general, they are stable molecules, but can accept electrons when they are engaged in chemical reactions. Most of the reactions of C_{60} are occurring at [6,6] junctions and thus form thermodynamically stable products. Because of the unique optical properties of C_{60}, it is employed as the fluorescent probe to detect solvent polarity effects, molecular associations, and complex formation with both polar and nonpolar molecules.[37]

C_{60} cannot conduct electricity, they normally act as electrical insulators. When doped with alkali metals the resulting compound becomes conducting or even acts as a superconductor. Ivetic et al. reported that endohedral $Cu@C_{60}$ and CuO/C_{60} mixture exhibits good electrical conductivity [38]. Fullerene network self-assembled on metal-covered semiconductor surfaces, are known to exhibit good electrical conductivity.[39]

Among the different fullerenes discovered, C_{60} and C_{70} are the most stable.[40] Kroto et al. presented chemical and geodesic rules, according

to which fullerenes, C_n for which n= 24, 28, 32, 36, 50, 60, 70 should have enhanced stability compared to their neighbours.[41,42] There are reports that fullerenes were stable up to 500 °C, but they decomposed immediately at 800 °C into amorphous carbon.[43] Endohedral fullerenes show quite excellent magnetic properties, which makes them suitable for potential applications in atomic clocks, molecular magnets, spin probes, and Magnetic Resonance Imaging, and spintronics.[44]

1.6. Reactivity of fullerenes

Because of the absence of super-aromaticity and considerable bond localization, fullerenes can be functionalized easily with addition reactions. Both endohedral and exohedral functionalization are possible for fullerenes. Fullerenes comprising of atoms or molecules inside their cages are termed endohedral derivatives. Covalent bond formations to carbon atoms lead to exohedral derivatives where functionalization happen outside the cage.

The chemical reactivity of fullerene (C_{60}) is similar to that of any other electron-deficient polyene. C_{60} readily undergo the reactions with electron rich species. Substitution reactions are rarely seen in C_{60}, but they can be easily subjected to various types of addition reactions such as reduction, halogenation, oxidation, and metallation reactions.

C_{60} readily undergo addition reactions at [6,6] junctions (1,2 additions) forming thermodynamically stable products.[45] Thachikawa et al. proposed that alkyl radical binds to the carbon atom of C_{60} at the top site forming alkylated C_{60} product through strong C-C bonds with a

binding energy of 31.8-35.1 kcal/mol.[46] There are reports for the formation of a dative bond complex when C_{60} reacts with piperidine molecule that exhibits versatile electronic properties.[47] C_{60} molecule forms 1, 3-dipolar adducts with ozone and diazomethane, that lead to the curvature of carbon surfaces at the reaction sites. Some important categories covalent functionalization reactions of C_{60} are summarized below.

1.6.1. Oxidation reactions

Chemical oxidation of C_{60} yields a highly oxidized analogue, $C_{60}O_n$ in which oxygen containing functional polar groups present on the carbon surfaces that is capable of enhancing its solubility in most of the polar solvents.[48] There are reports for the oxidation of C_{60} molecule with various oxidants like 3-chloroperoxy benzoic acid, 4-methyl morpholine N-oxide, Chromium (VI) oxide, and oxone monopersulphate under ultrasonication at room temperature forming $C_{60}O_n$..[49] Oxidation of C_{60} by ozone (ozonolysis) is reported earlier in the solid state as well as in solutions.[50,51] C_{60} solution in toluene when exposed to visible light results in the formation of fullerene epoxides, and they will aggregate in solutions as large clusters which may found to have important application in photovoltaics.[52]

1.6.2. Reduction reactions

Fullerenes readily undergo reduction reactions with various reducing agents. Its reduction reaction with Na and liq. NH_3 produced the hydrogenated products $C_{60}H_{18}$, $C_{60}H_{36}$.[45,53] There are reports for the hydrogenation of C_{60} in benzene using H_2 under atmospheric pressure with Pt/C and Pd/C as catalysts. Reduction reaction of C_{60} with di-imide, hydroboration reaction, hydrozirconation, etc. were also reported.[54,55] C_{60} can be reduced by anhydrous hydrazine in CH_3OH to yield a mixture of fullerene hydrides like $C_{60}H_2$, $C_{60}H_4$, $C_{60}H_8$ and other more highly reduced fullerenes like $C_{60}H_{38}$, $C_{60}H_{40}$, $C_{60}H_{42}$, $C_{60}H_{48}$ etc. were obtained by the Birch reduction of the products obtained by hydrazine reduction.[56] There are reports for the isolation of reduced fullerene isomer, 1,2-$C_{60}H_2$ by $NaBH_4$ reduction or Zn(Cu) couple reduction.[57]

1.6.3. Halogenation reactions

C_{60} molecule reacts with halogens forming corresponding halo fullerenes. Troshin et al. reported the reaction of C_{60} with liquid Br_2. Various brominated products like $C_{60}Br_6$, $C_{60}Br_8$, $C_{60}Br_{12}$, $C_{60}Br_{24}$ etc. could be separated in their study. Adamson et al. reported that UV irradiation of a solution of C_{60} in CCl_4 produced chlorinated C_{60}.

1.6.4. Nucleophilic addition reactions

Because of the electron deficient nature of C_{60}, it is susceptible to nucleophilic addition reactions. The mechanism of addition reaction is similar to that of electron deficient polyene. Initially, the nucleophile attacks one of the double bonds (6,6 bond) of the C_{60} molecule and

subsequently leading to the formation of an intermediate, which then reacts with the eletrophile present, forming the corresponding addition products. The alkylation of C_{60} with organolithium, the attack of the Grignard reagent, reaction with primary and secondary amines, alkyl cyanides, piperidines, potassium hydroxide etc. are some of the examples in this category.[58] Biglova et al. proposed that nucleophilic cyclopropanation of C_{60} proceeds via a concerted addition-elimination pathway. The formation of methano-fullerenes are believed to follow this mechanism.[59]

1.6.5. Hydroxylation reactions

Fullerene molecules can undergo hydroxylation reaction to form hydroxylated fullerenes or fullerols. There are reports for the direct hydroxylation of fullerene with 30% H_2O_2 in aqueous media under ultrasonication.[60] Isakova et al. proposed a method for the synthesis of polyhydroxylated fullerenes directly from soot containing iron nanoparticles stabilized by carbon shell.[61] Hydroxyl group rich fullerenes can function as excellent hydrogen bond catalyst with high activity, stability and better selectivity. Hydroxylated fullerenes are found to have important application in fullerene chemistry since hydroxylation increases the solubility of fullerene molecules, especially in water and they are widely used in medicinal field because of their ability to prevent the aggregation of protein molecules associated with many human diseases. Fully hydroxylated fullerenes show excellent antioxidant activity and also can be used in the field of electrochemical biosensing.[62]

Polyhydroxylated fullerenes are excellent free radical scavengers [62] and show higher conductivity and solubility in water.[63, 64] The insolubility of fullerenes can be solved by the functionalization of the molecule which will bring about a drastic change in its solubility.[65, 66] Kokubo et al. reported that highly hydroxylated fullerenes can be obtained ($C_{60}(OH)_{44}.8H_2O$) by the direct hydroxylation of C_{60} in the presence of phase transfer catalysts.[67]

1.7. Networking of fullerene balls

The unique electrical properties make fullerenes a preferred building block in the field of polymer chemistry, which may lead to the discovery of many novel fullerene-based architectures with networking of fullerene balls having extraordinary properties and practical applications.[68, 69] Generally, polymerization of fullerenes or their derivatives can be achieved under certain conditions of temperatures. Alternatively, polymerizations can be materialized under the influence of light (photopolymerization).[70] Fullerene polymers and fullerene polymer composites are interesting functional materials which exhibit superior photophysical, electrical and magnetic properties suitable for a variety of potential applications which were originally absent in the parent fullerene precursors.[71, 72] There are polymerized fullerenes in which C_{60} balls are directly linked together through covalent bonds.[73] In some other cases, fullerene balls are introduced in between the other polymer chains which can improve their solubility and processability.[73] In one of the reports, Chen et al. have described a chemically modified fullerene polymer capable of showing excellent photoconductive

performance and paramagnetic behaviour.[74] Fullerene precursors can be subjected to a variety of polymerization methods such as anionic polymerization [75], stable free radical polymerization [76], atom transfer free radical polymerization, [77] etc. are found to have important applications. [78] Teng et al. reported that alkyl functionalized fullerenes can be used to react with azido functionalized polystyrene by [3+2] cycloaddition 'click' chemistry to obtain two types of fullerene polymers. In one type, C_{60} is binding to the end of a PS chain whereas in the other C_{60} is binding at the joining point of the two PS chains. [79]

1.8. Applications of fullerenes

The unique carbon cage structure of fullerenes, their unusual electronic properties and their immense derivatization possibilities make them a suitable candidate for many important applications, especially in the field of organic photovoltaic cells, portable power sources, antioxidants, and bio-pharmaceuticals and so on. The applications of Fullerene-based materials as therapeutic agents are well known [80]. For example, they are widely employed as antioxidants, antiviral, anti-HIV, and also radical scavengers. Fullerene molecules easily fit into the hydrophobic cavity of HIV protease, thus inhibiting substrates to the catalytic active site of enzymes. Enzyme inhibition, DNA cleavage, and photodynamic therapy are some of the areas in which fullerene based materials can be employed successfully. [81–85]

Additionally, fullerenes can function as a reinforcement-materials. Fullerene-based metal nanocomposites are examples. Fullerene-based nanocomposites are advanced functional materials and

lot of research interest can be found in this emerging area. [86] Water soluble fullerenes are found to have important applications in the bio-medical field.[66, 87, 88] Self-assembled fullerene nanostructures are used for many applications like adsorption, catalysis, energy storage, solar cells, drug delivery, polymer solar cells, photovoltaics, electrocatalysis, and environmental remediation.[89, 90] Various applications of fullerene are summarized schematically in Figure 1.3.

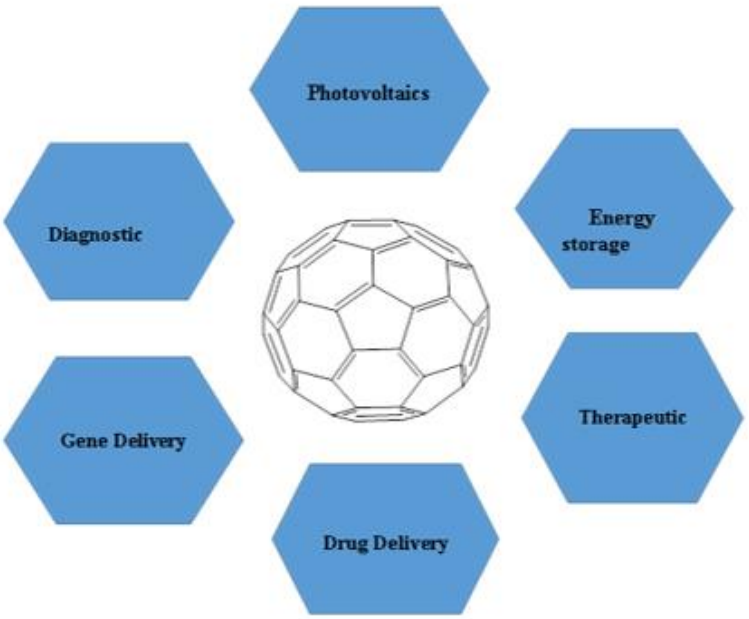

Figure 1.3: Schematic representation of various applications of fullerenes.

Fullerenes are used in ceramics for thermal management, as they reduce the thermal conductivity of bulk ceramics. [91] Hydrophilic oxidized fullerenes and their derivatives are used as cytotoxic agents and

also act as a support for nano-biocatalytic systems. Zygouri et al. reported the synthesis of a primary aliphatic amine (octadecylamine) attached fullerene derivatives, which are found to have important applications in medicine and biochemistry. [92] Photo-induced electron transfer may occur in systems containing many functionalized fullerenes. [93] Both fullerenes and hydroxylated fullerenes are capable of preventing the aggregation of proteins, thus, capable of preventing many human diseases associated with protein aggregation. [93, 94] Silicone-supported C_{60} is found to have an important application in photodynamic solar water disinfection. [95]

1.9. Electrochemical sensing studies with fullerene-based materials

Electrochemical sensors can be placed as an integral part of chemical sensors. They are preferred for commercial applications because of their cost effectiveness and their capacity to act as an important tool for providing a sensitive, selective, and fast determination of a wide range of analytes. Carbon-based materials like CNTs, Glassy Carbon Electrodes, Graphene, Carbon black, etc. are preferred functional materials generally employed to develop superior electrochemical sensing platforms. [96–98] In electrochemical biosensing, the recognition system utilizes a biochemical mechanism for detecting and quantitatively measuring the different biomarkers present in body fluids. Non-invasive monitoring of biochemical markers is another area in which wearable electrochemical sensors can be utilized. Recently, there is an ever-growing demand for such personalized sensing devices. [99] Because of the unique physicochemical and electrochemical

properties along with biocompatibility characteristics of many fullerene based materials, they find many applications in the field of electrochemical biosensing and bio-nanotechnology. There are reports in which fullerenes are effectively utilized in DNA biosensing.[100] Here, C_{60} provides an immobilization platform for DNA. Fullerene-based biosensors attract lot of research attention because of high sensitivity, selectivity, and good reproducibility exhibited by them in electrochemical biosensing.[101, 102] An electrochemical sensor fabricated with fullerene-MWCNT as the sensing platform have been studied by Taouri et al. for the detection of vanillin, a food additive. [103] An electrochemical sensor based on fullerene nanorods employed for the detection of paraben an endocrine disruptor is also reported. Hybrid nanostructures with CNT and fullerenes provide a fast, efficient, reliable, low-cost biosensor suitable for applications in pharmaceutical and clinical analysis. [104–106]

Mazloum-Ardakani et al. reported glassy carbon electrode modified with fullerene-functionalized MWCNTs and ionic liquid which can exhibit excellent electrocatalytic activity towards catecholamines. [107] Similarly, the electrochemical determination of caffeine can be performed with a C_{60}/MWCNT/Nafion/GC Electrode. [108]

1.10. Photocatalysis with fullerene-based materials

Photocatalysis refers to the acceleration of a photoreaction rate in the presence of a catalyst. Such catalysts are known as photocatalysts. They are substances that are capable of accelerating the chemical reaction by absorbing light or photons and providing the charge carriers (electrons or holes) generated for oxidation or reduction reactions to chemical species. [109–111] When a photocatalyst is irradiated with a photon, there is a possibility for two simultaneous processes, oxidation using photogenerated holes and reduction using photogenerated electrons. The basic requirement for a heterogenous semiconductor photocatalyst is that it should possess an adequate bandgap sufficient to overcome the redox potential necessary for generating oxygenated or reduced species. Carbon-based nanomaterials (CNMs) are capable of improving the photacatalytic performance of a semiconductor in multiple ways. The most widely used CNMs for this purpose are graphene, carbon nanotubes, fullerene, g-C_3N_4, Carbon Quantum Dots, etc. The major barriers associated with many pure semiconductor photocatalysts include their low light absorptivity, high charge recombination rates, low quantum yield, and so on. CNMs are capable of assisting the semiconductors to overcome these barriers with their superior properties such as large surface area, high thermal and chemical stability, favorable electronic conductivity, etc. In addition, there are CNMs capable of functioning as organic semiconductors themselves and perform as excellent photocatalysts. However, the problems of charge recombination and narrow visible light absorption can exist in

the case of pristine CNMs as well. Making the nanocomposites of CNMs with other semiconductor photocatalysts is one way of addressing these issues. C_{60}, a zero-dimensional allotropic form of carbon when combined with other semiconductor materials show excellent photocatalytic properties. Fullerene/semiconductor nanocomposites can be prepared by various synthetic strategies such as sol-gel method, hydrothermal method, solvothermal method, and impregnation methods. Fullerenes, in particular, have attracted the attention of many researchers due to their capability to improve the photocatalytic performance of their nanocomposites mainly because of their narrow bandgap suitable for visible light harvesting and ability to trigger the generation of reactive oxygen species like singlet oxygen radicals, superoxide radicals, and hydroxyl radicals in photochemical conditions.[37, 112–114]

1.10.1. Photocatalytic dye degradation

Photocatalysis under sunlight irradiation can be effectively utilized for environmental cleaning purposes. Dye effluents from many industries are important source of water pollution and their oxidation and mineralization using photocatalysis has been area of intense research which comes under the category of advanced oxidation processes. [115] Among the various model dyes used for such investigations, methylene blue is a commonly preferred one. Methylene blue dye is a thiazine cationic dye widely employed in the textile industry for coloring cotton, wool, etc. It is poisonous and causes breathing problems, vomiting, and mental disorders. These dyes if

directly discharged into water bodies, can cause adverse health effects. The degradation of methylene blue dye using a photocatalyst depends upon several factors like irradiation time, catalyst loading, pH of the solution, initial concentration of the dye, etc. The mechanism of the photocatalytic dye degradation and mineralization can be summarized as follows (Figure 1.4.):

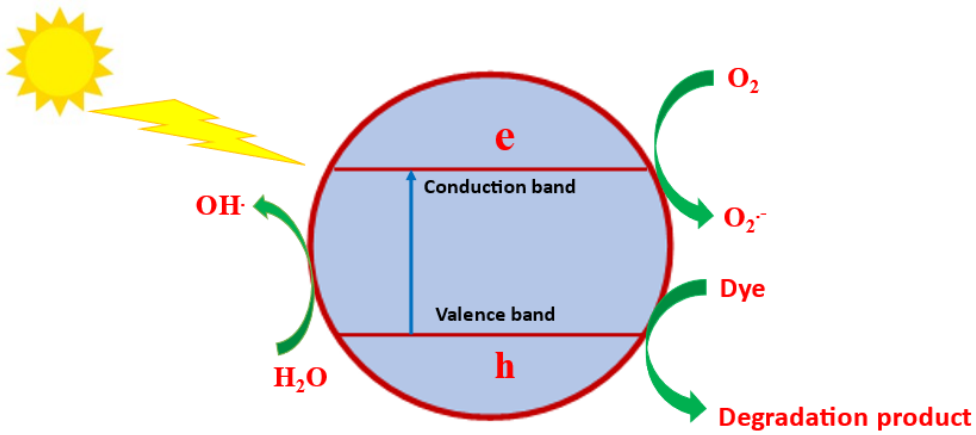

Figure 1.4: Mechanism of photocatalytic dye degradation

Under irradiation, photogenerated electrons are promoted to a higher conduction band by leaving holes in the valence band. Both the photogenerated charge carriers migrate to the surface of the catalyst. The holes react with water to produce $^{\cdot}OH$ radical on the semiconductor surface, which are powerful oxidizing agents to degrade the dye molecules. While the photogenerated electrons react with O_2 to form a

superoxide radical anion, $O_2^{\cdot -}$, that may take part in further oxidation processes.

1.10.2. Photocatalytic hydrogen peroxide generation

H_2O_2 is considered as a promising liquid fuel for the future and an environmentally benign oxidant. Its photocatalytic production is an emerging technology of great importance in a green chemistry point of view because it utilizes only water and oxygen in the presence of sunlight. [116] There are reports for the photocatalytic H_2O_2 production from O_2 reduction, with organic semiconductor photocatalysts like alkali metal doped graphitic C_3N_4 shows enhanced photocatalytic performance with an H_2O_2 production rate of 10.2 mmol/h/g, which is 89.5 times that of pristine C_3N_4. Photocatalytic H_2O_2 production is also achieved from oxygen under visible light irradiation over phosphate ion–coated Pd deposited reductive surfaces of $BiVO_4$ nanoparticles. [117–119]. Water soluble fullerene functionalized materials can be used extensively in photocatalytic H_2O_2 producton. [107, 108]

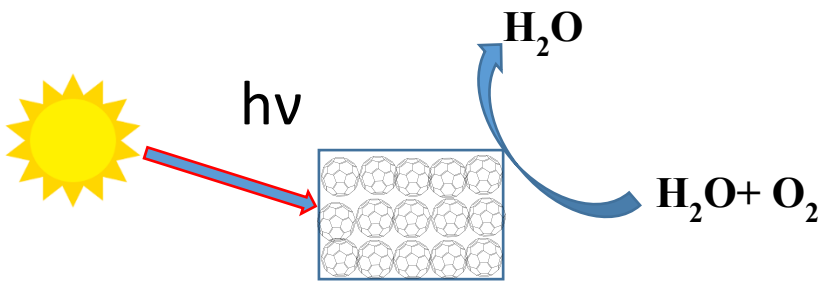

Figure 1.5: Schematic of fullerene-based material in photocatalytic H_2O_2 production.

The photocatalytic production of H_2O_2 from H_2O and O_2 is a sustainable reaction with standard Gibbs free energy change ($\Delta G°$) of 117 kJ/mol.

$$2H_2O + O_2 \longrightarrow 2H_2O_2,\ \Delta G° = 117\ kJ/mol.$$

The basic principle behind H_2O_2 production is governed by two photocatalytic mechanisms:

In the first mechanism, H_2O_2 is generated by a sequential two-step single electron indirect reduction,

$$O_2 \longrightarrow O_2^{\cdot-} \longrightarrow H_2O_2$$

According to this mechanism, the holes in the valence band would oxidize H_2O to oxygen and H^+ ions and the electrons in the conduction band would react with adsorbed oxygen and convert it into H_2O_2.

Second mechanism involves a two-electron one-step process.

In this mechanism, O_2 would directly react with two H^+ ions forming H_2O_2. [116]

$$O_2 + 2H^+ \longrightarrow H_2O_2$$

Shiraishi et al. reported a highly selective method for H_2O_2 production on graphitic carbon nitride photocatalysts. [122] Photocatalytic H_2O_2 production in pure water using graphitic carbon nitride decorated by oxidative red phosphorus provides a new strategy for H_2O_2 production due to their structural and photoelectrical properties.[123]

Quantum dots have been explored as a highly efficient photocatalytic system for H_2O_2 production under visible light with a high concentration of 126 mmol/L. [124] Zinc oxide in the aerated aqueous phase, octahedral $Cd_3(C_3N_3S_3)_2$ co-ordination polymer, photocatalytic Resorcinol-Formaldehyde resins, etc. are other photocatalytic systems employed for H_2O_2 production. [125–130]

1.11. Graphene

Graphene is one of the allotropic forms of carbon, in which carbon atoms are arranged in a honeycomb-like two-dimensional lattice. In 2010, Andre Geim and Konstantin Novoselov got Nobel prize in physics for their discovery of graphene in 2004. Graphene can be considered as a zero-band gap semiconductor with excellent electronic properties. It has got many unique properties such as outstanding mechanical stability, optical transparency, and extraordinary electrical conductivity and so on. These unique physical and chemical properties of graphene have attracted a lot of research attention in recent past. [131–134] It can be visualized as the mother material for other nanoforms of carbon. For example, it can be wrapped to form zero-dimensional fullerene, rolled to form one-dimensional carbon nanotube, and stacked on top of one another to form three-dimensional graphite. Chemical exfoliation, mechanical exfoliation and chemical vapor deposition (CVD) are some of the common methods employed for the synthesis of graphene. [135–138] Graphene based materials find important applications in various fields such as fuel cell technology, photothermal therapy, gene delivery, drug delivery, batteries, solar cells, mechanical

transduction, etc. [139–141] Another important class of applications of graphene and graphene-based nanomaterials are in the field of biosensing. In electrochemical biosensing, graphene-modified electrode surfaces exhibit better selectivity and sensitivity towards analyte molecules. The excellent electrical conductivity, fast electron transfer rate, and high surface-to-volume ratio make graphene a suitable platform for electrochemical sensing. Graphene-based biosensors are preferred in the sensing of important biomolecules like proteins, neurotransmitters, DNA, enzymes etc. [142–144]

1.12. Carbon nanotubes

Carbon Nanotubes (CNTs) are discovered in 1991 by Iijima. [145]. There are two types of CNTS, single-walled CNT and multi-walled CNTs. SWCNTs were first reported in 1993. MWCNTs are the concentric tubes with rolled up graphene sheets around a hollow area [146]. CNTs have outstanding mechanical, thermal, electrical, and optical properties which makes them a promising material in nanotechnology. [147] They are widely used in energy storage devices like Li batteries, and supercapacitors, and the electrochemical sensors. Hydrogen storage capacities of CNTs were reported to be 110 mb/g. [148] CNT-based biosensors are an important class of biosensors and in electrochemical sensing, they are employed for the electrochemical detection of important biomarkers like H_2O_2, glucose, ascorbic acid, uric acid, dopamine, etc. They are characterized by excellent sensitivity, reproducibility, better sensitivity, and fast electron transfer properties.

1.13. Graphene- Nanotube- Fullerene ternary hybrids

Even though there are many reports on the synthesis of hybrid nanostructures of graphene and fullerenes, only few reports are present on the ternary hybrids graphene, nanotubes and fullerenes. [149] Gupta et al. reported the formation of fullerenes and carbon nanotubes by the bubbling of graphene film that is formed on the anode surface by the unzipped graphite under extreme temperature and pressure conditions. [150]

1.14. Carbon nanostructures for Hydrogen Storage

Fuel cells based on hydrogen fuel is considered as a promising technology for future energy production. A major hurdle in the commercialization of this technology is the difficulty in the storage and transportation of hydrogen. Carbon nanostructures like CNT has shown promising results in the field of hydrogen storage.[151, 152] Design and development of advanced functional materials are going on in this research area. A three-dimensional pillared graphene framework with hybrid fullerene and nanotube pillars have shown excellent H_2 storage capacity.[153]

1.15. Hydrogenation of double bonds via diimide formation

Hydrazine reagent in combination with an oxidizing species is known to hydrogenate compounds with multiple bonds. This reaction is known to proceed via initial formation of an active reducing agent diimide (NH=NH) which initially form an adduct and then it is dissociated in to nitrogen gas and the hydrogenated product.[154]

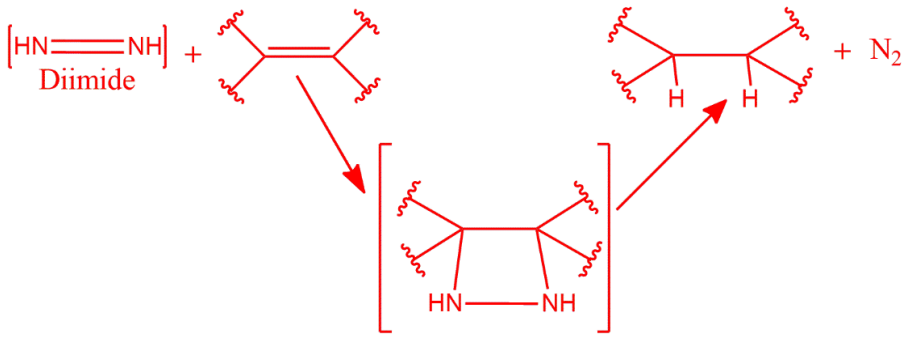

Figure 1.6: Hydrogenation of double bond via diimide formation

1.16. Objectives of the Thesis

The main objectives of the present research are:

(1) Preparation of a new class of highly efficient, nanostructured, polymeric fullerene oxide framework (PFO) by thermal [3+2] cycloadditions of fullerene oxides formed by the thermal decomposition of $C_{60}Br_{24}$ and its characterization with various spectroscopic and microscopic methods and application as a biosensing platform for trace amounts of glucose.

(2) To understand the mechanism of interlinking of C_{60} balls in polymeric Fullerene Oxide Frameworks by Density Functional Theory calculations.

(3) To prepare PFO/TiO_2 (5%) nanocomposite by mechanical mixing followed by calcination at 200 °C and the characterization of photocatalytic system produced by means of various spectroscopic and microscopic methods.

(4) To investigate the photocatalytic performance of PFO and PFO/TiO_2 nanocomposite by the degradation and mineralization

of methylene blue dye as well as by photocatalytic H_2O_2 production.

(5) To prepare polyhydroxylated fullerene derivative (fullerol) by the direct hydroxylation of C_{60} with 30% H_2O_2.

(6) To prepare Partially Hydrogenated Fullerol (PHF) network, its characterization by various microscopic and spectroscopic techniques and to investigate its application as a sensing platform for the H_2O_2 electrochemical sensing

(7) To prepare hydrogen and hydroxy functionalized Graphene-Nanotube-Fullerene Ternary hybrid (GNF1) by mechanical mixing of PFO and reduced hydroxy graphene (RHG) followed by calcination at 250 °C and subsequent hydrazine reduction of the aqueous dispersion of this mixture and its characterization by employing various microscopic and spectroscopic techniques.

(8) To Prepare hydrogen and hydroxy functionalized Graphene-Nanotube-Fullerene Ternary hybrid (GNF2) by the hydrazine reduction of a co-dispersion of fullerols and hydroxygraphene and the characterization of prepared GNF2 by various microscopic and spectroscopic techniques and to investigate its application as a sensing platform for H_2O_2 electrochemical sensing.

References

(1) Hirsch, A. Principles of Fullerene Reactivity. *Fuller. Relat. Struct.* **1999**, 1–65. https://doi.org/10.1007/3-540-68117-5_1.

(2) Patel, K. D.; Singh, R. K.; Kim, H.-W. Carbon-Based Nanomaterials as an Emerging Platform for Theranostics. *Mater. Horiz.* **2019**, *6* (3), 434–469. https://doi.org/10.1039/C8MH00966J.

(3) Crevillen, A. G.; Escarpa, A.; García, C. D. Chapter 1 Carbon-Based Nanomaterials in Analytical Chemistry. **2018**, 1–36. https://doi.org/10.1039/9781788012751-00001.

(4) Maiti, D.; Tong, X.; Mou, X.; Yang, K. Carbon-Based Nanomaterials for Biomedical Applications: A Recent Study. *Front. Pharmacol.* **2019**, *9*.

(5) Zaytseva, O.; Neumann, G. Carbon Nanomaterials: Production, Impact on Plant Development, Agricultural and Environmental Applications. *Chem. Biol. Technol. Agric.* **2016**, *3* (1), 17. https://doi.org/10.1186/s40538-016-0070-8.

(6) Rao, N.; Singh, R.; Bashambu, L. Carbon-Based Nanomaterials: Synthesis and Prospective Applications. *Mater. Today Proc.* **2021**, *44*, 608–614. https://doi.org/10.1016/j.matpr.2020.10.593.

(7) Onyancha, R. B.; Ukhurebor, K. E.; Aigbe, U. O.; Osibote, O. A.; Kusuma, H. S.; Darmokoesoemo, H. A Methodical Review on Carbon-Based Nanomaterials in Energy-Related Applications. *Adsorpt. Sci. Technol.* **2022**, *2022*, e4438286. https://doi.org/10.1155/2022/4438286.

(8) Debnath, S. K.; Srivastava, R. Drug Delivery With Carbon-Based Nanomaterials as Versatile Nanocarriers: Progress and Prospects. *Front. Nanotechnol.* **2021**, *3*.

(9) Sheoran, K.; Kaur, H.; Siwal, S. S.; Saini, A. K.; Vo, D.-V. N.; Thakur, V. K. Recent Advances of Carbon-Based Nanomaterials (CBNMs) for Wastewater Treatment: Synthesis and Application. *Chemosphere* **2022**, *299*, 134364. https://doi.org/10.1016/j.chemosphere.2022.134364.

(10) Cha, C.; Shin, S. R.; Annabi, N.; Dokmeci, M. R.; Khademhosseini, A. Carbon-Based Nanomaterials: Multifunctional Materials for

Biomedical Engineering. *ACS Nano* **2013**, *7* (4), 2891–2897. https://doi.org/10.1021/nn401196a.

(11) Xu, X.; Xing, Y.; Yang, X.; Wang, G.; Cai, Z.; Shang, Z.; Pan, Y.; Zhao, X. Theoretical Study of Structure and Stability of Fullerene Derivative: $C_{50}O$. **2005**. https://doi.org/10.1002/QUA.20265.

(12) Hebard, A. F. Buckminsterfullerene. *Annu. Rev. Mater. Sci.* **1993**, *23* (1), 159–191. https://doi.org/10.1146/annurev.ms.23.080193.001111.

(13) Kroto, H. W.; Heath, J. R.; O'Brien, S. C.; Curl, R. F.; Smalley, R. E. C_{60}: Buckminsterfullerene. *Nature* **1985**, *318* (6042), 162–163. https://doi.org/10.1038/318162a0.

(14) Aldersey-Williams, H. *The Most Beautiful Molecule: The Discovery of the Buckyball*; John Wiley & Sons.

(15) Thakral, S.; Mehta, R. M. Fullerenes: An Introduction and Overview of Their Biological Properties. *Indian J. Pharm. Sci.* **2006**, *68* (1), 13. https://doi.org/10.4103/0250-474X.22957.

(16) Cataldo, F.; Iglesias-Groth, S. Fullerene. *Encycl. Astrobiol.* **2015**, 896–900. https://doi.org/10.1007/978-3-662-44185-5_604.

(17) Samal, S.; Sahoo, S. K. An Overview of Fullerene Chemistry. *Bull. Mater. Sci.* **1997**, *20* (2), 141–230. https://doi.org/10.1007/BF02744892.

(18) Maier, J. P.; Campbell, E. K. Fullerenes in Space. *Angew. Chem. Int. Ed.* **2017**, *56* (18), 4920–4929. https://doi.org/10.1002/anie.201612117.

(19) Woods, P. The Discovery of Cosmic Fullerenes. *Nat. Astron.* **2020**, *4* (4), 299–305. https://doi.org/10.1038/s41550-020-1076-5.

(20) Auvert, G.; Auvert, M. Single Covalent Bonding Structure in Fullerenes, Carbon Nanotubes and Closed Nanotubes. *Open J. Phys. Chem.* **2020**, *10* (03), 183. https://doi.org/10.4236/ojpc.2020.103011.

(21) Rathna, A.; Chandrasekhar, J. Simple Structural And Bonding Representations Of Fullerenes. *Indian J. Chem. - Sect. Inorg. Phys. Theor. Anal. Chem.* **1992**, *31* (5), F51–F55.

(22) Liu, S.; Lu, Y.-J.; Kappes, M. M.; Ibers, J. A. The Structure of the C_{60} Molecule: X-Ray Crystal Structure Determination of a Twin at 110 K.

Science **1991**, *254* (5030), 408–410. https://doi.org/10.1126/science.254.5030.408.

(23) Krätschmer, W. Formation of Fullerenes. *Nat. Fuller. Relat. Struct. Elem. Carbon* **2006**, 7–29. https://doi.org/10.1007/1-4020-4135-7_2.

(24) Amsharov, K. *Rational Synthesis of Fullerenes*; IntechOpen, 2018. https://doi.org/10.5772/intechopen.73251.

(25) Mojica, M.; Alonso, J. A.; Méndez, F. Synthesis of Fullerenes. *J. Phys. Org. Chem.* **2013**, *26* (7), 526–539. https://doi.org/10.1002/poc.3121.

(26) Zhang, H.-G.; Zhuo, Y.-Q.; Zhang, X.-M.; Zhang, L.; Xu, P.-Y.; Tian, H.-R.; Lin, S.-C.; Zhang, Q.; Xie, S.-Y.; Zheng, L.-S. Synthesis of Fullerenes from a Nonaromatic Chloroform through a Newly Developed Ultrahigh-Temperature Flash Vacuum Pyrolysis Apparatus. *Nanomaterials* **2021**, *11* (11), 3033. https://doi.org/10.3390/nano11113033.

(27) Afanas'ev, D. V.; Baranov, G. A.; Belyaev, A. A.; Dyuzhev, G. A.; Zinchenko, A. K. Fullerenes Obtained during Graphite Evaporation with Stationary CO_2 Laser Radiation. *Tech. Phys. Lett.* **2001**, *27* (5), 408–410. https://doi.org/10.1134/1.1376767.

(28) Oyama, T.; Ishii, T.; Takeuchi, K. Synthesis of Fullerenes by Ablation Using Pulsed and Cw-Nd:YAG Lasers. *Fuller. Sci. Technol.* **1997**, *5* (5), 919–933. https://doi.org/10.1080/15363839708013307.

(29) Apicella, B.; Russo, C.; Carpentieri, A.; Tregrossi, A.; Ciajolo, A. PAHs and Fullerenes as Structural and Compositional Motifs Tracing and Distinguishing Organic Carbon from Soot. *Fuel* **2022**, *309*, 122356. https://doi.org/10.1016/j.fuel.2021.122356.

(30) Gover, R. K. E.; Chamberlain, T. W.; Sarre, P. J.; Khlobystov, A. N. Piecing Together Large Polycyclic Aromatic Hydrocarbons and Fullerenes: A Combined ChemTEM Imaging and MALDI-ToF Mass Spectrometry Approach. *Front. Chem.* **2021**, *9*.

(31) Zhen, J.; Castellanos, P.; Paardekooper, D. M.; Linnartz, H.; Tielens, A. G. G. M. Laboratory formation of fullerenes from PAHs: TOP-down InterstEllar Chemistry. *Astrophys. J.* **2014**, *797* (2), L30. https://doi.org/10.1088/2041-8205/797/2/L30.

(32) Krätschmer, W. Formation of Fullerenes. *Nat. Fuller. Relat. Struct. Elem. Carbon* **2006**, 7–29. https://doi.org/10.1007/1-4020-4135-7_2.

(33) Saidane, K.; Razafinimanana, M.; Lange, H.; Huczko, A.; Baltas, M.; Gleizes, A.; Meunier, J.-L. Fullerene Synthesis in the Graphite Electrode Arc Process: Local Plasma Characteristics and Correlation with Yield. *J. Phys. Appl. Phys.* **2004**, *37* (2), 232–239.

(34) Notarianni, M.; Liu, J.; Vernon, K.; Motta, N. Synthesis and Applications of Carbon Nanomaterials for Energy Generation and Storage. *Beilstein J. Nanotechnol.* **2016**, *7*, 149–196. https://doi.org/10.3762/bjnano.7.17.

(35) Kyesmen, P. I.; Onoja, A.; Amah, A. N. Fullerenes Synthesis by Combined Resistive Heating and Arc Discharge Techniques. *SpringerPlus* **2016**, *5* (1), 1323. https://doi.org/10.1186/s40064-016-2994-7.

(36) Ruoff, R. S.; Tse, D. S.; Malhotra, R.; Lorents, D. C. Solubility of Fullerene (C_{60}) in a Variety of Solvents. *J. Phys. Chem.* **1993**, *97* (13), 3379–3383. https://doi.org/10.1021/j100115a049.

(37) Saraswati, T. E.; Setiawan, U. H.; Ihsan, M. R.; Isnaeni, I.; Herbani, Y. The Study of the Optical Properties of C_{60} Fullerene in Different Organic Solvents. *Open Chem.* **2019**, *17* (1), 1198–1212. https://doi.org/10.1515/chem-2019-0117.

(38) Ivetić, M.; Mojović, Z.; Matija, L. Electrical Conductivity of Fullerene Derivatives. *Mater. Sci. Forum* **2003**, *413*, 49–52. https://doi.org/10.4028/www.scientific.net/MSF.413.49.

(39) Mihalyuk, A. N.; Utas, T. V.; Eremeev, S. V.; Hsing, C. R.; Wei, C. M.; Zotov, A. V.; Saranin, A. A. Structural and Electronic Properties of C_{60} Fullerene Network Self-Assembled on Metal-Covered Semiconductor Surfaces. *J. Chem. Phys.* **2021**, *154* (10), 104703. https://doi.org/10.1063/5.0040483.

(40) Khamatgalimov, A. R.; Kovalenko, V. I. Substructural Approach for Assessing the Stability of Higher Fullerenes. *Int. J. Mol. Sci.* **2021**, *22* (7), 3760. https://doi.org/10.3390/ijms22073760.

(41) Kroto, H. W. The Stability of the Fullerenes C_n, with n = 24, 28, 32, 36, 50, 60 and 70. *Nature* **1987**, *329* (6139), 529–531. https://doi.org/10.1038/329529a0.

(42) Fowler, P. W. Fullerene Stability and Structure. *Contemp. Phys.* **1996**, *37* (3), 235–247. https://doi.org/10.1080/00107519608217530.

(43) Suchanek, W. L.; Yoshimura, M.; Gogotsi, Y. G. Stability of Fullerenes under Hydrothermal Conditions. *J. Mater. Res.* **1999**, *14* (2), 323–326. https://doi.org/10.1557/JMR.1999.0046.

(44) Dallas, P.; Harding, R.; Cornes, S.; Sinha, S.; Zhou, S.; Rašović, I.; Laird, E.; Porfyrakis, K. Magnetic Properties of Endohedral Fullerenes: Applications and Perspectives. In *21st Century Nanoscience – A Handbook*; CRC Press, 2020.

(45) Taylor, R. Addition Reactions of Fullerenes. *Comptes Rendus Chim.* **2006**, *9* (7), 982–1000. https://doi.org/10.1016/j.crci.2006.01.004.

(46) Tachikawa, H.; Kawabata, H. Addition Reaction of Alkyl Radical to C_{60} Fullerene: Density Functional Theory Study. *Jpn. J. Appl. Phys.* **2015**, *55* (2S), 02BB01. https://doi.org/10.7567/JJAP.55.02BB01.

(47) Lo, R.; Manna, D.; Lamanec, M.; Wang, W.; Bakandritsos, A.; Dračínský, M.; Zbořil, R.; Nachtigallová, D.; Hobza, P. Addition Reaction between Piperidine and C_{60} to Form 1,4-Disubstituted C_{60} Proceeds through van Der Waals and Dative Bond Complexes: Theoretical and Experimental Study. *J. Am. Chem. Soc.* **2021**, *143* (29), 10930–10939. https://doi.org/10.1021/jacs.1c01542.

(48) Zygouri, P.; Spyrou, K.; Mitsari, E.; Barrio, M.; Macovez, R.; Patila, M.; Stamatis, H.; Verginadis, I. I.; Velalopoulou, A. P.; Evangelou, A. M.; Sideratou, Z.; Gournis, D.; Rudolf, P. A Facile Approach to Hydrophilic Oxidized Fullerenes and Their Derivatives as Cytotoxic Agents and Supports for Nanobiocatalytic Systems. *Sci. Rep.* **2020**, *10* (1), 1–13. https://doi.org/10.1038/s41598-020-65117-7.

(49) Ko, W.-B.; Baek, K.-N. The Oxidation of Fullerenes (C_{60}, C_{70}) with Various Oxidants under Ultrasonication. *Phys. Solid State* **2002**, *44* (3), 424–426. https://doi.org/10.1134/1.1462660.

(50) Bulgakov, R.; Sabirov, D.; Dzhemilev, U. Oxidation of Fullerenes with Ozone. *Russ. Chem. Bull.* **2013**, *62*, 304–324. https://doi.org/10.1007/s11172-013-0043-z.

(51) Deng, J.-P.; Mou, C.-Y.; Han, C.-C. Oxidation of Fullerenes by Ozone. *Fuller. Sci. Technol.* **1997**, *5* (7), 1325–1336. https://doi.org/10.1080/15363839708013323.

(52) Dattani, R.; Gibson, K. F.; Few, S.; Borg, A. J.; DiMaggio, P. A.; Nelson, J.; Kazarian, S. G.; Cabral, J. T. Fullerene Oxidation and Clustering in Solution Induced by Light. *J. Colloid Interface Sci.* **2015**, *446*, 24–30. https://doi.org/10.1016/j.jcis.2015.01.005.

(53) Haufler, R. E.; Conceicao, J.; Chibante, L. P. F.; Chai, Y.; Byrne, N. E.; Flanagan, S.; Haley, M. M.; O'Brien, S. C.; Pan, C.; et al., . Efficient Production of C_{60} (Buckminsterfullerene), $C_{60}H_{36}$, and the Solvated Buckide Ion. *J. Phys. Chem.* **1990**, *94* (24), 8634–8636. https://doi.org/10.1021/j100387a005.

(54) Henderson, C. C.; Cahill, P. A. $C_{60}H_2$: Synthesis of the Simplest C_{60} Hydrocarbon Derivative. *Science* **1993**, *259* (5103), 1885–1887. https://doi.org/10.1126/science.259.5103.1885.

(55) Ballenweg, S.; Gleiter, R.; Krätschmer, W. Hydrogenation of Buckminsterfullerene C_{60} via Hydrozirconation: A New Way to Organofullerenes. *Tetrahedron Lett.* **1993**, *34* (23), 3737–3740. https://doi.org/10.1016/S0040-4039(00)79214-8.

(56) Billups, W. E.; Luo, W.; Gonzalez, A.; Arguello, D.; Alemany, L. B.; Marriott, T.; Saunders, M.; Jiménez-Vázquez, H. A.; Khong, A. Reduction of C_{60} Using Anhydrous Hydrazine. *Tetrahedron Lett.* **1997**, *38* (2), 171–174. https://doi.org/10.1016/S0040-4039(97)83014-6.

(57) Cataldo, F.; Iglesias-Groth, S. *Fulleranes: The Hydrogenated Fullerenes*; Springer Science & Business Media, 2010.

(58) Wright, J. *Nucleophilic Addition to Fullerenes - Diamond Films*. Texas Powerful Smart. https://www.texaspowerfulsmart.com/diamond-films/nucleophilic-addition-to-fullerenes.html (accessed 2022-10-29).

(59) N. Biglova, Y.; G. Mustafin, A. Nucleophilic Cyclopropanation of [60] Fullerene by the Addition–Elimination Mechanism. *RSC Adv.* **2019**, *9* (39), 22428–22498. https://doi.org/10.1039/C9RA04036F.

(60) Afreen, S.; Kokubo, K.; Muthoosamy, K.; Manickam, S. Hydration or Hydroxylation: Direct Synthesis of Fullerenol from Pristine Fullerene [C_{60}] via Acoustic Cavitation in the Presence of Hydrogen Peroxide. *RSC Adv.* **2017**, *7* (51), 31930–31939. https://doi.org/10.1039/C7RA03799F.

(61) Isakova, V. G.; Goncharova, E. A.; Bayukov, O. A.; Churilov, G. N. Hydroxylation of Fullerenes Modified with Iron Nanoparticles. *Russ. J. Appl. Chem.* **2011**, *84* (7), 1165–1169. https://doi.org/10.1134/S107042721107007X.

(62) Grebowski, J.; Konopko, A.; Krokosz, A.; DiLabio, G. A.; Litwinienko, G. Antioxidant Activity of Highly Hydroxylated Fullerene C_{60} and Its Interactions with the Analogue of α-Tocopherol. *Free Radic. Biol. Med.* **2020**, *160*, 734–744. https://doi.org/10.1016/j.freeradbiomed.2020.08.017.

(63) Deng, F.; Yang, Y.; Hwang, S.; Shon, Y.-S.; Chen, S. Fullerene-Functionalized Gold Nanoparticles: Electrochemical and Spectroscopic Properties. *Anal. Chem.* **2004**, *76* (20), 6102–6107. https://doi.org/10.1021/ac0495891.

(64) Peyghan, A. A.; Soleymanabadi, H.; Moradi, M. Structural and Electronic Properties of Pyrrolidine-Functionalized [60] Fullerenes. *J. Phys. Chem. Solids* **2013**, *11* (74), 1594–1598. https://doi.org/10.1016/j.jpcs.2013.05.030.

(65) Huang, Y.-Y.; Sharma, S. K.; Yin, R.; Agrawal, T.; Chiang, L. Y.; Hamblin, M. R. Functionalized Fullerenes in Photodynamic Therapy. *J. Biomed. Nanotechnol.* **2014**, *10* (9), 1918–1936. https://doi.org/10.1166/jbn.2014.1963.

(66) Rašović, I. Water-Soluble Fullerenes for Medical Applications. *Mater. Sci. Technol.* **2017**, *33* (7), 777–794. https://doi.org/10.1080/02670836.2016.1198114.

(67) Kokubo, K.; Shirakawa, S.; Kobayashi, N.; Aoshima, H.; Oshima, T. Facile and Scalable Synthesis of a Highly Hydroxylated Water-Soluble Fullerenol as a Single Nanoparticle. *Nano Res.* **2011**, *4*, 204–215. https://doi.org/10.1007/s12274-010-0071-z.

(68) Hirsch, A. Fullerene Polymers. *Adv. Mater.* **1993**, *5* (11), 859–861. https://doi.org/10.1002/adma.19930051116.

(69) Giacalone, F.; Martín, N. Fullerene Polymers: Synthetic Strategies, Properties and Applications. In *Encyclopedia of Polymer Science and Technology*; John Wiley & Sons, Ltd, 2007. https://doi.org/10.1002/0471440264.pst553.

(70) Makarova, T.; Sundqvist, B. Electrical and Magnetic Properties of Undoped Fullerene Polymers. *Front. Multifunct. Nanosyst.* **2002**, 291–312. https://doi.org/10.1007/978-94-010-0341-4_22.

(71) Eklund, P. C.; Rao, A. M. *Fullerene Polymers and Fullerene Polymer Composites*; Springer Science & Business Media, 2013.

(72) Makarova, T. L. Magnetism in Polymerized Fullerenes. *J. Magn. Magn. Mater.* **2004**, *272–276*, E1263–E1268. https://doi.org/10.1016/j.jmmm.2003.12.305.

(73) Harris, P. J. F. Fullerene Polymers: A Brief Review. *C* **2020**, *6* (4), 71. https://doi.org/10.3390/c6040071.

(74) Chen, Y.; Huang, Z.-E.; Cai, R.; Fan, D.; Hou, X.; Yan, X.; Chen, S.; Jin, W.; Pan, D.; Wang, S. Photoconductivity and Paramagnetism of Fullerene Chemically Modified Polymers. *J. Appl. Polym. Sci.* **1996**, *61* (12), 2185–2190. https://doi.org/10.1002/(SICI)1097-4628(19960919)61:12<2185::AID-APP18>3.0.CO;2-6.

(75) Natori, I.; Natori, S.; Hirose, Y. Synthesis of Functionalized Fullerene-C_{60} by the Living Anionic Polymerization Technique. *J. Appl. Polym. Sci.* **2011**, *120*. https://doi.org/10.1002/app.33223.

(76) Mehrotra, R.; Lal, D.; Tripathi, V. S.; Mathur, G. N. Preparation and Charecterization of Bromofullerenes in New Stoichiometry. *Carbon Lett.* **2003**, *4* (4), 175–179.

(77) Cao, T.; Webber, S. E. Free-Radical Copolymerization of Fullerenes with Styrene. *Macromolecules* **1995**, *28* (10), 3741–3743. https://doi.org/10.1021/ma00114a033.

(78) Wang, C.; Guo, Z.-X.; Fu, S.; Wu, W.; Zhu, D. Polymers Containing Fullerene or Carbon Nanotube Structures. *Prog. Polym. Sci.* **2004**, *29* (11), 1079–1141. https://doi.org/10.1016/j.progpolymsci.2004.08.001.

(79) Teng, F.-A.; Guo, Y.; He, J.; Zhang, Y.; Han, Z.; Li, H. Convenient Syntheses of Fullerynes for "clicking" into Fullerene Polymers. *Des. Monomers Polym.* **2017**, *20* (1), 283–292. https://doi.org/10.1080/15685551.2016.1256462.

(80) Bhakta. *Fullerene and its applications: A review*. **2020**; 32 (2), 159-163. https://www.jiaomr.in/article.asp?issn=0972-1363;

(81) Bakry, R.; Vallant, R. M.; Najam-ul-Haq, M.; Rainer, M.; Szabo, Z.; Huck, C. W.; Bonn, G. K. Medicinal Applications of Fullerenes. *Int. J. Nanomedicine* **2007**, *2* (4), 639–649.

(82) Dellinger, A.; Zhou, Z.; Connor, J.; Madhankumar, A. B.; Pamujula, S.; Sayes, C. M.; Kepley, C. L. *Application of fullerenes in nanomedicine: an update*. https://doi.org/10.2217/nnm.13.99. https://doi.org/10.2217/nnm.13.99.

(83) Mohan Gokhale, M.; Ravindra Somani, R. Fullerenes: Chemistry and Its Applications. *Mini-Rev. Org. Chem.* **2015**, *12* (4), 355–366.

(84) Jensen, A. W.; Wilson, S. R.; Schuster, D. I. Biological Applications of Fullerenes. *Bioorg. Med. Chem.* **1996**, *4* (6), 767–779. https://doi.org/10.1016/0968-0896(96)00081-8.

(85) Petrovic, D.; Seke, M.; Srdjenovic, B.; Djordjevic, A. Applications of Anti/Prooxidant Fullerenes in Nanomedicine along with Fullerenes Influence on the Immune System. *J. Nanomater.* **2015**, *2015*, e565638. https://doi.org/10.1155/2015/565638.

(86) Hu, Y.; Shenderova, O. A.; Hu, Z.; Padgett, C. W.; Brenner, D. W. Carbon Nanostructures for Advanced Composites. *Rep. Prog. Phys.* **2006**, *69* (6), 1847–1895. https://doi.org/10.1088/0034-4885/69/6/R05.

(87) P., A. K.; V., V. N.; Joshi, G.; Mehta, K. P. Fabrication and Applications of Fullerene-Based Metal Nanocomposites: A Review. *J. Mater. Res.* **2021**, *36* (1), 114–128. https://doi.org/10.1557/s43578-020-00094-1.

(88) Ajay Kumar, P.; Vishnu Namboodiri, V.; Joshi, G.; Mehta, K. P. Fabrication and Applications of Fullerene-Based Metal Nanocomposites: A Review. *J. Mater. Res.* **2021**, *36*, 114–128. https://doi.org/10.1557/s43578-020-00094-1.

(89) Baskar, A. V.; Benzigar, M. R.; Talapaneni, S. N.; Singh, G.; Karakoti, A. S.; Yi, J.; Al-Muhtaseb, A. H.; Ariga, K.; Ajayan, P. M.; Vinu, A. Self-Assembled Fullerene Nanostructures: Synthesis and Applications. *Adv. Funct. Mater.* **2022**, *32* (6), 2106924. https://doi.org/10.1002/adfm.202106924.

(90) Kamanina, N. V.; Kamanina, N. V. *Introductory Chapter: Why the Study of Fullerenes Is so Important?*; IntechOpen, 2018. https://doi.org/10.5772/intechopen.74812.

(91) Yowell, L. L.; Mayeaux, B. M.; Wang, H.; Barrera, E. V. Application of Carbon Nanotubes and Fullerenes for Thermal Management in Ceramics. *MRS Online Proc. Libr. OPL* **2000**, *633*, A17.4. https://doi.org/10.1557/PROC-633-A17.4.

(92) Zygouri, P.; Spyrou, K.; Mitsari, E.; Barrio, M.; Macovez, R.; Patila, M.; Stamatis, H.; Verginadis, I. I.; Velalopoulou, A. P.; Evangelou, A. M.; Sideratou, Z.; Gournis, D.; Rudolf, P. A Facile Approach to Hydrophilic Oxidized Fullerenes and Their Derivatives as Cytotoxic Agents and Supports for Nanobiocatalytic Systems. *Sci. Rep.* **2020**, *10* (1), 1–13. https://doi.org/10.1038/s41598-020-65117-7.

(93) Armaroli, N. Photoinduced Energy Transfer Processes in Functionalized Fullerenes. *Fuller. Synth. Optoelectron. Prop.* **2002**, 137–162. https://doi.org/10.1007/978-94-015-9902-3_5.

(94) Bai, C.; Lao, Z.; Chen, Y.; Tang, Y.; Wei, G. Pristine and Hydroxylated Fullerenes Prevent the Aggregation of Human Islet Amyloid Polypeptide and Display Different Inhibitory Mechanisms. *Front. Chem.* **2020**, *8*.

(95) Manjón, F.; Santana-Magaña, M.; García-Fresnadillo, D.; Orellana, G. Are Silicone-Supported [C_{60}]-Fullerenes an Alternative to Ru(Ii) Polypyridyls for Photodynamic Solar Water Disinfection? *Photochem. Photobiol. Sci.* **2014**, *13* (2), 397. https://doi.org/10.1039/c3pp50361e.

(96) Power, A. C.; Gorey, B.; Chandra, S.; Chapman, J. Carbon Nanomaterials and Their Application to Electrochemical Sensors: A Review. *Nanotechnol. Rev.* **2018**, *7* (1), 19–41. https://doi.org/10.1515/ntrev-2017-0160.

(97) Zhang, C.; Du, X. Electrochemical Sensors Based on Carbon Nanomaterial Used in Diagnosing Metabolic Disease. *Front. Chem.* **2020**, *8*.

(98) Kour, R.; Arya, S.; Young, S.-J.; Gupta, V.; Bandhoria, P.; Khosla, A. Review—Recent Advances in Carbon Nanomaterials as Electrochemical Biosensors. *J. Electrochem. Soc.* **2020**, *167* (3), 037555. https://doi.org/10.1149/1945-7111/ab6bc4.

(99) Teymourian, H.; Parrilla, M.; Sempionatto, J. R.; Montiel, N. F.; Barfidokht, A.; Van Echelpoel, R.; De Wael, K.; Wang, J. Wearable Electrochemical Sensors for the Monitoring and Screening of Drugs. *ACSSens.***2020**,*5*(9),2679–2700. https://doi.org/10.1021/acssensors.0c01318.

(100) Holzinger, M.; Le Goff, A.; Cosnier, S. Nanomaterials for Biosensing Applications: A Review. *Front. Chem.* **2014**, *2*.

(101) Pilehvar, S.; De Wael, K. Recent Advances in Electrochemical Biosensors Based on Fullerene-C_{60} Nano-Structured Platforms. *Biosensors* **2015**, *5* (4), 712–735. https://doi.org/10.3390/bios5040712.

(102) Yáñez-Sedeño, P.; Campuzano, S.; Pingarrón, J. M. Fullerenes in Electrochemical Catalytic and Affinity Biosensing: A Review. *C* **2017**, *3* (3), 21. https://doi.org/10.3390/c3030021.

(103) Taouri, L.; Bourouina, M.; Bourouina-Bacha, S.; Hauchard, D. Fullerene-MWCNT Nanostructured-Based Electrochemical Sensor for the Detection of Vanillin as Food Additive. *J. Food Compos. Anal.* **2021**, *100*, 103811. https://doi.org/10.1016/j.jfca.2021.103811.

(104) Rather, J. A.; Harthi, A. J. A.; Khudaish, E. A.; Qurashi, A.; Munam, A.; Kannan, P. An Electrochemical Sensor Based on Fullerene Nanorods for the Detection of Paraben, an Endocrine Disruptor. *Anal. Methods* **2016**, *8* (28), 5690–5700. https://doi.org/10.1039/C6AY01489E.

(105) Gergeroglu, H.; Yildirim, S.; Ebeoglugil, M. F. Nano-Carbons in Biosensor Applications: An Overview of Carbon Nanotubes (CNTs) and Fullerenes (C60). *SN Appl. Sci.* **2020**, *2* (4), 1–22. https://doi.org/10.1007/s42452-020-2404-1.

(106) Ghalkhani, M.; Ghorbani-Bidkorbeh, F. Development of Carbon Nanostructured Based Electrochemical Sensors for Pharmaceutical Analysis. *Iran. J. Pharm. Res. IJPR* **2019**, *18* (2), 658–669. https://doi.org/10.22037/ijpr.2019.1100645.

(107) Mazloum-Ardakani, M.; Khoshroo, A. High Performance Electrochemical Sensor Based on Fullerene-Functionalized Carbon Nanotubes/Ionic Liquid: Determination of Some Catecholamines. *Electrochem. Commun.***2014**, *Complete* (42), 9–12. https://doi.org/10.1016/j.elecom.2014.01.026.

(108) Tajeu, K. Y.; Dongmo, L. M.; Tonle, I. K. Fullerene/MWCNT/Nafion Modified Glassy Carbon Electrode for the Electrochemical Determination of Caffeine. *Am. J. Anal. Chem.* **2020**, *11* (2), 114–127. https://doi.org/10.4236/ajac.2020.112009.

(109) Zhu, S.; Wang, D. Photocatalysis: Basic Principles, Diverse Forms of Implementations and Emerging Scientific Opportunities. *Adv. Energy Mater.* **2017**, *7* (23), 1700841. https://doi.org/10.1002/aenm.201700841.

(110) Umar, M.; Abdul, H. Photocatalytic Degradation of Organic Pollutants in Water. In *Organic Pollutants - Monitoring, Risk and Treatment*; Rashed, M. N., Ed.; InTech, 2013. https://doi.org/10.5772/53699.

(111) Serpone, N.; Emeline, A. V. Semiconductor Photocatalysis — Past, Present, and Future Outlook. *J. Phys. Chem. Lett.* **2012**, *3* (5), 673–677. https://doi.org/10.1021/jz300071j.

(112) Pan, Y.; Liu, X.; Zhang, W.; Liu, Z.; Zeng, G.; Shao, B.; Liang, Q.; He, Q.; Yuan, X.; Huang, D.; Chen, M. Advances in Photocatalysis Based on Fullerene C_{60} and Its Derivatives: Properties, Mechanism, Synthesis, and Applications. *Appl. Catal. B Environ.* **2020**, *265*, 118579. https://doi.org/10.1016/j.apcatb.2019.118579.

(113) Huang, L.; Zhao, J. C_{60}-Bodipy Dyad Triplet Photosensitizers as Organic Photocatalysts for Photocatalytic Tandem Oxidation/[3+2] Cycloaddition Reactions to Prepare Pyrrolo[2,1-a]Isoquinoline. *Chem. Commun.* **2013**, *49* (36), 3751. https://doi.org/10.1039/c3cc41494a.

(114) Song, L.; Guo, C.; Li, T.; Zhang, S. C_{60}/Graphene/g-C_3N_4 Composite Photocatalyst and Mutually- Reinforcing Synergy to Improve Hydrogen Production in Splitting Water under Visible Light Radiation. *Ceram. Int.* **2017**,*43*(10),7901–7907. https://doi.org/10.1016/j.ceramint.2017.03.115.

(115) Deng, Y.; Zhao, R. Advanced Oxidation Processes (AOPs) in Wastewater Treatment. *Curr. Pollut. Rep.* **2015**, *1* (3), 167–176. https://doi.org/10.1007/s40726-015-0015-z.

(116) Hou, H.; Zeng, X.; Zhang, X. Production of Hydrogen Peroxide by Photocatalytic Processes. *Angew. Chem. Int. Ed.* **2020**, *59* (40), 17356–17376. https://doi.org/10.1002/anie.201911609.

(117) Wu, S.; Quan, X. Design Principles and Strategies of Photocatalytic H_2O_2 Production from O_2 Reduction. *ACS EST Eng.* **2022**, *2* (6), 1068–1079. https://doi.org/10.1021/acsestengg.1c00456.

(118) Wu, S.; Yu, H.; Chen, S.; Quan, X. Enhanced Photocatalytic H_2O_2 Production over Carbon Nitride by Doping and Defect Engineering. *ACS Catal.* **2020**, *10* (24), 14380–14389. https://doi.org/10.1021/acscatal.0c03359.

(119) Fuku, K.; Takioka, R.; Iwamura, K.; Todoroki, M.; Sayama, K.; Ikenaga, N. Photocatalytic H_2O_2 Production from O_2 under Visible Light Irradiation over Phosphate Ion-Coated Pd Nanoparticles-Supported $BiVO_4$. *Appl. Catal. B Environ.* **2020**, *272*, 119003. https://doi.org/10.1016/j.apcatb.2020.119003.

(120) Yao, S.; Yuan, X.; Jiang, L.; Xiong, T.; Zhang, J. Recent Progress on Fullerene-Based Materials: Synthesis, Properties, Modifications, and Photocatalytic Applications. *Materials* **2020**, *13* (13), 2924. https://doi.org/10.3390/ma13132924.

(121) Moor, K. J.; Kim, J.-H. Simple Synthetic Method Toward Solid Supported C_{60} Visible Light-Activated Photocatalysts. *Environ. Sci. Technol.* **2014**, *48* (5), 2785–2791. https://doi.org/10.1021/es405283w.

(122) Shiraishi, Y.; Kanazawa, S.; Sugano, Y.; Tsukamoto, D.; Sakamoto, H.; Ichikawa, S.; Hirai, T. Highly Selective Production of Hydrogen Peroxide on Graphitic Carbon Nitride ($g\text{-}C_3N_4$) Photocatalyst Activated by Visible Light. *ACS Catal.* **2014**, *4* (3), 774–780. https://doi.org/10.1021/cs401208c.

(123) Zhang, J.; Lang, J.; Wei, Y.; Zheng, Q.; Liu, L.; Hu, Y. H.; Zhou, B.; Yuan, C.; Long, M. Efficient Photocatalytic H_2O_2 Production from Oxygen and Pure Water over Graphitic Carbon Nitride Decorated by Oxidative Red Phosphorus. *Appl. Catal. B Environ.* **2021**, *298*. https://doi.org/10.1016/j.apcatb.2021.120522.

(124) Ji, W.; Xu, Z.; Zhang, S.; Li, Y.; Bao, Z.; Zhao, Z.; Xie, L.; Zhong, X.; Wei, Z.; Wang, J. High-Efficiency Visible-Light Photocatalytic H_2O_2 Production Using CdSe-Based Core/Shell Quantum Dots. *Catal. Sci. Technol.* **2022**, *12* (9), 2865–2871. https://doi.org/10.1039/D2CY00269H.

(125) Zhang, J.; Lang, J.; Wei, Y.; Zheng, Q.; Liu, L.; Hu, Y.-H.; Zhou, B.; Yuan, C.; Long, M. Efficient Photocatalytic H_2O_2 Production from Oxygen and Pure Water over Graphitic Carbon Nitride Decorated by Oxidative Red Phosphorus. *Appl. Catal. B Environ.* **2021**, *298*, 120522. https://doi.org/10.1016/j.apcatb.2021.120522.

(126) Domènech, X.; Ayllón, J. A.; Peral, J. H_2O_2 Formation from Photocatalytic Processes at the ZnO/Water Interface. *Environ. Sci. Pollut. Res. Int.* **2001**, *8* (4), 285–287. https://doi.org/10.1007/BF02987409.

(127) Ji, W.; Xu, Z.; Zhang, S.; Li, Y.; Bao, Z.; Zhao, Z.; Xie, L.; Zhong, X.; Wei, Z.; Wang, J. High-Efficiency Visible-Light Photocatalytic H_2O_2 Production Using CdSe-Based Core/Shell Quantum Dots. *Catal. Sci. Technol.* **2022**, *12* (9), 2865–2871. https://doi.org/10.1039/D2CY00269H.

(128) Bercot, M.; Piwnica, A. [Aneurysm of the ascending aorta complicating chronic aortic dissection with operated aortic insufficiency. *Coeur Med. Interne* **1972**, *11* (4), 775–778.

(129) Song, H.; Wei, L.; Chen, L.; Zhang, H.; Su, J. Photocatalytic Production of Hydrogen Peroxide over Modified Semiconductor Materials: A Minireview. *Top. Catal.* **2020**, *63* (9), 895–912. https://doi.org/10.1007/s11244-020-01317-9.

(130) Shiraishi, Y.; Hagi, T.; Matsumoto, M.; Tanaka, S.; Ichikawa, S.; Hirai, T. Solar-to-Hydrogen Peroxide Energy Conversion on Resorcinol–Formaldehyde Resin Photocatalysts Prepared by Acid-Catalysed Polycondensation. *Commun. Chem.* **2020**, *3* (1), 1–9. https://doi.org/10.1038/s42004-020-00421-x.

(131) Hasan, A. *Electrical and Chemical Properties of Graphene over Composite Materials: A Technical Review – Material Science Research India*. https://www.materialsciencejournal.org/vol16no2/electrical-and-chemical-properties-of-graphene-over-composite-materials-a-technical-review/ (accessed 2022-10-15).

(132) Liao, G.; Hu, J.; Chen, Z.; Zhang, R.; Wang, G.; Kuang, T. Preparation, Properties, and Applications of Graphene-Based Hydrogels. *Front. Chem.* **2018**, *6*.

(133) Sharma, N.; Dev Gupta, R.; Chandmal Sharma, R.; Dayal, S.; Singh Yadav, A. Graphene: An Overview of Its Characteristics and Applications. *Mater. Today Proc.* **2021**, *47*, 2752–2755. https://doi.org/10.1016/j.matpr.2021.03.086.

(134) Rudrapati, R.; Rudrapati, R. *Graphene: Fabrication Methods, Properties, and Applications in Modern Industries*; IntechOpen, 2020. https://doi.org/10.5772/intechopen.92258.

(135) Viculis, L. M.; Mack, J. J.; Kaner, R. B. A Chemical Route to Carbon Nanoscrolls. *Science* **2003**, *299* (5611), 1361–1361. https://doi.org/10.1126/science.1078842.

(136) Novoselov, K. S.; Geim, A. K.; Morozov, S. V.; Jiang, D.; Zhang, Y.; Dubonos, S. V.; Grigorieva, I. V.; Firsov, A. A. Electric Field Effect in Atomically Thin Carbon Films. *Science* **2004**, *306* (5696), 666–669. https://doi.org/10.1126/science.1102896.

(137) Park, S.; Ruoff, R. S. Chemical Methods for the Production of Graphenes. *Nat. Nanotechnol.* **2009**, *4* (4), 217–224. https://doi.org/10.1038/nnano.2009.58.

(138) Bhuyan, M. S. A.; Uddin, M. N.; Islam, M. M.; Bipasha, F. A.; Hossain, S. S. Synthesis of Graphene. *Int. Nano Lett.* **2016**, *6* (2), 65–83. https://doi.org/10.1007/s40089-015-0176-1.

(139) Nguyen, B. H.; Nguyen, V. H. Promising Applications of Graphene and Graphene-Based Nanostructures. *Adv. Nat. Sci. Nanosci. Nanotechnol.* **2016**, *7* (2), 023002. https://doi.org/10.1088/2043-6262/7/2/023002.

(140) Chung, C.; Kim, Y.-K.; Shin, D.; Ryoo, S.-R.; Hong, B. H.; Min, D.-H. Biomedical Applications of Graphene and Graphene Oxide. *Acc. Chem. Res.* **2013**, *46* (10), 2211–2224. https://doi.org/10.1021/ar300159f.

(141) Carvalho, A. F.; Kulyk, B.; Fernandes, A. J. S.; Fortunato, E.; Costa, F. M. A Review on the Applications of Graphene in Mechanical Transduction. *Adv. Mater.* **2022**, *34* (8), 2101326. https://doi.org/10.1002/adma.202101326.

(142) Bahadır, E. B.; Sezgintürk, M. K. Applications of Graphene in Electrochemical Sensing and Biosensing. *TrAC Trends Anal. Chem.* **2016**, *76*, 1–14. https://doi.org/10.1016/j.trac.2015.07.008.

(143) Gan, T.; Hu, S. Electrochemical Sensors Based on Graphene Materials. *Microchim. Acta* **2011**, *175* (1), 1–19. https://doi.org/10.1007/s00604-011-0639-7.

(144) Zhang, M.; Halder, A.; Cao, X.; Hou, C.; Chi, Q.; Zhang, M.; Halder, A.; Cao, X.; Hou, C.; Chi, Q. *Graphene-Paper Based Electrochemical Sensors*; IntechOpen, 2017. https://doi.org/10.5772/intechopen.68186.

(145) Iijima, S. Helical Microtubules of Graphitic Carbon. *Nature* **1991**, *354*, 56–58. https://doi.org/10.1038/354056a0.

(146) Ong, Y. T.; Ahmad, A. L.; Zein, S. H. S.; Tan, S. H. A Review on Carbon Nanotubes in an Environmental Protection and Green Engineering Perspective. *Braz. J. Chem. Eng.* **2010**, *27* (2), 227–242. https://doi.org/10.1590/S0104-66322010000200002.

(147) Jagadeesan, A. K.; Thangavelu, K.; Dhananjeyan, V. *Carbon Nanotubes: Synthesis, Properties and Applications*; IntechOpen, 2020. https://doi.org/10.5772/intechopen.92995.

(148) Kavan, L.; Dunsch, L.; Kataura, H. Electrochemical Tuning of Electronic Structure of Carbon Nanotubes and Fullerene Peapods. *Carbon* **2004**, *42* (5), 1011–1019. https://doi.org/10.1016/j.carbon.2003.12.024.

(149) Chen, M.; Guan, R.; Yang, S. Hybrids of Fullerenes and 2D Nanomaterials. *Adv. Sci.* **2018**, *6* (1), 1800941. https://doi.org/10.1002/advs.201800941.

(150) Gupta, V. Graphene as Intermediate Phase in Fullerene and Carbon Nanotube Growth: A Young–Laplace Surface-Tension Model. *Appl. Phys. Lett.* **2010**, *97* (18), 181910. https://doi.org/10.1063/1.3509403.

(151) Froudakis, G. E. Hydrogen Storage in Nanotubes & Nanostructures. *Mater. Today* **2011**, *14* (7), 324–328. https://doi.org/10.1016/S1369-7021(11)70162-6.

(152) Lobo, R.; Ribeiro, J.; Inok, F. Hydrogen Uptake and Release in Carbon Nanotube Electrocatalysts. *Nanomaterials* **2021**, *11* (4), 975. https://doi.org/10.3390/nano11040975.

(153) Bi, L.; Yin, J.; Huang, X.; Wang, Y.; Yang, Z. Graphene Pillared with Hybrid Fullerene and Nanotube as a Novel 3D Framework for

Hydrogen Storage: A DFT and GCMC Study. *Int. J. Hydrog. Energy* **2020**, *45* (35), 17637–17648. https://doi.org/10.1016/j.ijhydene.2020.04.227.

(154) Corey, E. J.0; Mock, W. L. Chemistry of Diimide. III. Hydrogen Transfer to Multiple Bonds by Dissociation of the Diimide-Anthracene Adduct, Anthracene-9,10-Biimine. *J. Am. Chem. Soc.* **1962**, *84* (4), 685–686. https://doi.org/10.1021/ja00863a045.

CHAPTER 2

MATERIALS AND METHODS

2.1 Experimental procedures

In the present study, we have developed a method for the preparation of an interconnected, three-dimensional, mesoporous polymeric fullerene oxide framework via thermal [3+2] cycloadditions of monomeric C_{60} and fullerene oxides. $C_{60}O_n$ are formed by the thermal decomposition of $C_{60}Br_{24}$, causing the elimination of Br_2 molecules in an oxygen atmosphere at an elevated temperature of 200 °C. A Density Functional Theory calculation is performed with Gaussian 16 using M06-2X functional and 6-31g basis set. The Poly Fullerene Oxide (PFO) is characterized with various spectroscopic and microscopic techniques and its 5% nanocomposite with P25 TiO_2 is prepared. Methylene blue is taken as a model dye to investigate photocatalytic dye degradation applications of PFO and the developed PFO/TiO_2 nanocomposite under sunlight irradiation. Photocatalytic H_2O_2 production by the sunlight-assisted reaction of water and oxygen using PFO/TiO_2 nanocomposite is also performed. Further, in the next study, fullerols (poly hydroxy derivatives of C_{60}) are prepared by the direct ultrasonication of C_{60} with 30% H_2O_2. Subsequently, the aqueous dispersion of fullerols is subjected to hydrazine reduction resulting in the formation of a partially hydrogenated fullerol network (PHF). The prepared nanomaterial is characterized by different spectroscopic and microscopic techniques. Reduced hydroxy graphene is prepared adapting a strategy reported from our lab earlier[1], which is then mechanically mixed with PFO in 1:1 weight ratio and calcined at 250 °C. This mixture is then dispersed fully in water and is subjected to

hydrazine reduction to produce hydrogenated ternary composite of graphene, carbon nanotube and fullerene (GNF1). Next, the hydrazine reduction of fullerols along with hydroxygraphene (HG) prepared from fluorographite is carried out to obtain another partially hydrogenated ternary nanocomposite of graphene, carbon nanotube and fullerene (GNF2). Electrochemical sensing investigations employing the prepared nanomaterials PFO, PHF, GNF1, and GNF2 as sensing platforms are carried out. The procedure adopted for the development of these novel nanomaterials and the experimental conditions employed for their photocatalytic and electrochemical sensing applications are summarized in this chapter.

The important chemicals used in for the investigations presented in this thesis are listed in the table given below:

All the chemical used in the work are of analytical grade and deionized water is used throughout the experiments.

Table 2.1 List of chemicals used for the preparation and applications of the nanomaterials studied

Sl No.	Chemicals used	Name of manufacturer
1	Fullerene	Sigma Aldrich Chemicals Pvt. Ltd. India
2	Liq. Br_2 capsules	Sigma Aldrich Chemicals Pvt. Ltd. India
3	Toluene	Merck, ACS Reagent
4	Isopropyl Alcohol (IPA)	Merck, ACS Reagent
5	Potassium Chloride	Sigma Aldrich, > 99%
6	Potassium ferrocyanide	Merck, ACS Reagent
7	Potassium ferricyanide	Merck, ACS Reagent

8	Phosphate buffer tablet (PBS tablet) pH 7.4	Sigma Aldrich
9	Glucose	Sigma Aldrich
10	Hydrogen peroxide	Merck, ACS Reagent
11	Uric acid	Sigma Aldrich, > 99%
12	L-Ascorbic acid	Sigma Aldrich
13	Dopamine hydrochloride	Sigma Aldrich
14	Sodium hydroxide	Merck
15	Methanol	Merck
16	Ethanol	Merck
17	Acetone	Loba chemie, India
18	Hydrazine hydrochloride	Loba chemie, India
19	1,10- phenanthroline	Sigma Aldrich
20	Methylene blue dye	Merck
21	Graphite flakes	Merck
22	Alumina powder (0.3 micron)	Sigma Aldrich
23	N,N – Diethyl-p-phenylene Diamine	Sigma Aldrich
24	Horse Radish Peroxidase enzyme	Sigma Aldrich
26	Heptane	Merck
27	Copper Sulphate	Merck
28	Sulphuric acid	Nice Chemicals, Laboratory reagent
29	Hydrochloric acid	Nice Chemicals, Laboratory reagent
30	Deionized water	Nice, Laboratory reagent
31	Potassium bromide	Sigma Aldrich
32	P25 Titania	Merck
33	Flourographite	Sigma Aldrich, > 61 wt % Fluorine
34	Sodium nitrate	Merck
35	Potassium permanganate	Merck

2.2. Preparation methods

2.2.1. Preparation of polymeric fullerene oxide (PFO)

Polymeric Fullerene oxide (PFO) is prepared by the thermal treatment of $C_{60}Br_{24}$. Initially, $C_{60}Br_{24}$ is prepared by a method described by Birket et al. [2] For this about 0.2033 g of C_{60} is ground well in an agate mortar for 15 min, 20 ml of liquid bromine is added, stirred for 8 h, and is allowed to stay at room temperature, overnight. Orange-yellow crystals of $C_{60}Br_{24}$ is observed to be separated slowly. This sample is collected and then heated in the presence of air (Tubular Furnace) at 200 °C, for 18 h. [3] This mixture of oligomeric and polymeric fullerene oxides formed is collected and washed repeatedly with toluene for separating the toluene-soluble, low-molecular-weight fullerene oxide fragments and PFO. The dark brown coloured solid, poly fullerene oxide (PFO) powder is then dried in an oven to remove residual solvent and used for characterization and further studies.

2.2.2. Preparation of 5% PFO/TiO_2 nanocomposite

To prepare 5% PFO/TiO_2 nanocomposite, about 2 g of commercial Degussa P25 TiO_2 powder is treated with 0.1 g of PFO by mechanical solid-state mixing in an agate mortar for 1 h, followed by calcination at 250 °C for 5 h and the resulting PFO/TiO_2 (20:1) nanocomposite is employed for further photocatalytic studies.

2.2.3. Preparation of Hydroxy Graphene (HG) and Reduced Hydroxy Graphene (RHG)

Hydroxy Graphene (HG) and Reduced Hydroxy Graphene (RHG) are prepared starting from flourographite following a procedure reported from this lab.[4] For this about 100 mg of the flourographite powder is mixed with 10 ml of ethanolic NaOH (10 g NaOH in 100 ml ethanol) and maintained at 100 °C for 24 h in an RB flask fitted with a water condenser. The black-coloured hydroxy graphene (HG) obtained is washed with acetone and distilled water and dried. The resulting HG is dispersed in 1:1 ethanolic–water mixture by ultrasonication (6.5 L bath sonicator, 200 W) for 2 h, and the contents are transferred into an autoclave and kept overnight at 180 °C. [1] The solvothermally reduced hydroxy graphene (RHG) obtained is washed with acetone & water and then dried. The RHG thus prepared is used for further studies.

2.2.4. Preparation of fullerols

In this method, 200 mg of C_{60} is treated with 20 ml of 30% H_2O_2 [5] and is subjected to ultrasonication (30% amplitude, 200 W) for 1 h. The temperature is maintained by using a water bath to 30 °C. Initially, the mixture was colourless and it turns to brown after 30 min ultrasonication. The unreacted C_{60} is again treated with H_2O_2 followed by ultrasonication and the resulting fullerol can be separated as a white precipitate by treating it with 85 ml of the mixture of three solvents 2-propanol, Diethyl ether, heptane in the volume ratio 7:5:5 respectively and keeping for two days.[5, 6] The resulting white-coloured fullerol

precipitate is washed several times with methanol and distilled water and is dried at 60 °C.

2.2.5. Preparation of partially Hydrogenated Fullerol network (PHF)

For this, 100 ml of fullerol dispersion is treated with 1 ml of hydrazine solution and the reaction mixture is kept at 100 °C in an RB flask fitted with a water condenser for 24 h. The white deposit formed on the walls of the container is washed with methanol and distilled water. The undissolved portion, Partially Hydrogenated Fullerol (PHF) network formed is separated, dried and characterized.

2.2.6. Preparation of hydrogen and hydroxy functionalized Graphene-Nanotube-Fullerene ternary hybrid (GNF1) from the aqueous dispersion of PFO/ RHG mixture.

In this procedure, 50% PFO/RHG mixture is prepared by the mechanical mixing of about 0.1 g of PFO with 0.1 g of RHG in an agate mortar for 30 min. Then, it is calcined at 250 °C for 3 h in a muffle furnace. The resulting mixture is then dispersed fully in water and is treated with 1 ml of hydrazine solution in an RB flask equipped with a water condenser for 24 h at 100 °C. The precipitate formed is washed with ethanol & water and dried at 60 °C resulted in the formation of hydrogenated ternary composite of graphene, carbon nanotube and fullerene (GNF1).

2.2.7. Preparation of hydrogen and hydroxy functionalized Graphene-Nanotube-Fullerene ternary hybrid (GNF2) from fullerol and hydroxy graphene dispersion.

GNF2 is prepared by the hydrazine reduction method.[7, 8] For this, 50 ml of an aqueous dispersion of fullerol and hydroxygraphene are taken in an RB flask equipped with water condenser, 1 ml of hydrazine solution is added and refluxed for 24 h at 100 °C. The precipitate of GNF2 formed is centrifuged, washed with ethanol and subsequently with water and dried at 60 °C and used for further studies.

2.2.8. Preparation of Graphene

Graphene is prepared by the hydrazine reduction of hydroxy graphene. [1] About 1 ml of hydrazine reagent is treated with 100 ml of HG dispersion. The resulting mixture is heated in an RB flask fitted with a water condenser at 100 °C for 24 h. The black colored solid obtained is the graphene formed which is then washed with methanol and distilled water and dried at 60 °C.

2.3. Electrochemical sensing studies

All electrochemical sensing studies are performed with a mini potentiostat (Digi-Ivy, DY2000 series)

2.3.1. Cyclic Voltammetry

Cyclic Voltammetry (CV) is one of the most acceptable potentiodynamic electrochemical measurements and is generally used for the detection of analyte molecules in a solution.[9,10] In a typical CV

measurement, the potential of the working electrode is initially ramped linearly versus time in a particular direction and is repeated in the opposite direction to complete one cycle.

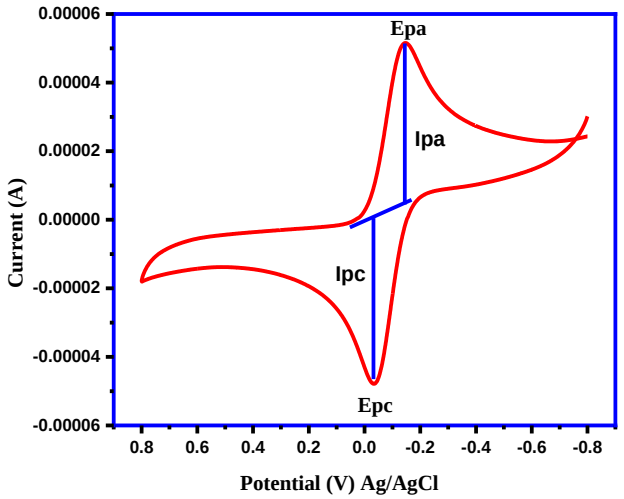

Figure 2.1: A typical Cyclic Voltammogram (CV) showing the redox peaks of 5 mM ferricyanide/Ferrocyanide system in 0.1 M KCl (supporting electrolyte) and PBS buffer at bare GCE. Scan rate is 50 mV/s.

Then current in the working electrode is measured and plotted vs. potential which will give the cyclic voltammogram. Three electrode system is preferred in cyclic voltammetric measurements. The working electrode, counter electrode, and reference electrode are employed and the potential is measured between the working electrode and reference electrode while the current is measured between the working electrode and counter electrode. A typical cyclic voltammogram is shown in Figure 2.1.

From the cyclic voltammogram, anodic potential, E_{pa}, Cathodic potential, E_{pc}, anodic current, I_{pa}, cathodic current, and I_{pc} are measured. The peak current is given by the Randles-Sevcik equation.[5]

$$Ip= (2.69x10^{-5})n^{3/2} ACD^{1/2}v^{1/2} \quad (2.1)$$

Ip is the peak current and n is the number of electrons involved in redox reactions.

A is the area of the electrode surface (cm^2)

C is the concentration of electroactive species in the solution (mol/cm^3)

D is the diffusion coefficient (m^2/s)

V is scan rate (V/s)

Cyclic voltametric measurements are used in the electrochemical analysis of organic, and inorganic compounds and polymers. [11] The kinetics of an electrochemical reaction is best understood from CV measurements. If the reaction is reversible, oxidation peak of CV will be similar in shape to the reduction peak. [10] The separation between peak potentials is given by the equation:

$$\Delta E_p = E_{pa} – E_{pc} = 59 \text{ mV/n} \quad (2.2)$$

For a reversible electrochemical reaction, the ratio of anodic peak current to cathodic peak current is independent of the scan rate. For an irreversible electrochemical reaction, peak potentials show a considerable shift with scan rate.

All electrochemical measurements are performed using a Digi-Ivy (DY2000EN) potentiostat. The modified Glassy Carbon Electrode is used as the working electrode, Ag/AgCl is used as the reference electrode, and platinum wire is used as the counter electrode. All the measurements are carried out using 0.1 M Phosphate Buffer solution (PBS, pH 7.4) and 0.1 M KCl is used as a supporting electrolyte. 1 mM ascorbic acid,1 mM uric acid, 1 mM dopamine, 1 mM glucose, and 1 mM H_2O_2 are used as analyte molecules.

2.3.2. Differential Pulse Voltammetry (DPV)

Differential Pulse Voltammetry is a type of linear sweep voltammetric technique in which amplitude pulse potentials are superimposed on a ramp potential curve. [13] Here, a series of pulses are given to the electrode surface with a sequential increase in baseline voltage of the voltammetric cell in which voltage pulses are transmitted by a counter electrode and the resulting current is measured by the working electrode. In this technique, the current is sampled before applying the amplitude pulse and also at the end of the pulse application. The difference between the two currents is plotted against the potential of the working electrode: [14]

$$\text{E peak} = \frac{E_{1/2} - E_{pulse}}{2} \qquad (2.3)$$

In DPV there is no effective non-Faradic current and hence it is used for the detection of even very low concentrations of the analyte molecules. DPV is a highly sensitive, selective voltammetric technique,

which allows its use in studying the kinetics and thermodynamics of electrochemical reactions. [15]

2.3.3. Preparation of modified glassy carbon electrodes

Bare GCE (3 mm) is polished with alumina slurry (0.05 micron) taken in a micro polishing pad. After polishing, the electrode is rinsed well with distilled water repeatedly for several times to remove any adsorbed impurities present and dried under an IR lamp. After that 10 µl of the functional electrode material dispersion is drop-casted on the well-polished Glassy Carbon electrode surface and allowed to dry. The modified electrode surface is now ready for the electrochemical measurements.

2.3.4. Electro-Chemically active Surface Area (ECSA) measurements

The Electro-Chemically active Surface Areas of the surface-modified electrodes are calculated using cyclic voltametric measurements in 5 mM potassium ferrocyanide in PBS solution (pH 7.4) with 0.1 M KCl as supporting electrolyte using the Randles-Sevcik equation.[12]

$$Ip = 2.69 \times 10^5 AD^{1/2}n^{3/2}\gamma^{1/2}C \qquad (2.4)$$

Here, **Ip** is the Peak current, **A** is the ECSA value, **D** is the diffusion coefficient, **n** is the number of transferred electrons in the redox couple, **γ** is the scan rate and **C** is the concentration of the analyte.

2.3.5. Calculations for Sensitivities and Limits of Detection (LODs)

The sensitivities and limits of detection (LODs) can be determined from the cyclic voltammetric curves or DPV curves depending on the technique used for sensing. The limit of detection is calculated from 3*S.D (bl)/m; where S.D (bl) is the standard deviation of the blank solution determined from ten consecutive CV/DPV measurements and m is the slope of the calibration curve. The sensitivity of the modified electrodes is determined as, the slope of the calibration curve/ ECSA values.

2.4. Photocatalytic Studies

2.4.1. Photocatalytic methylene blue dye degradation studies

Photodegradation studies of methylene blue dye mineralization using different photocatalytic systems developed are performed in the presence of natural sunlight. [17–19] A Thermo-Scientific EVOLUTION 160 spectrophotometer in the wavelength range 200 to 800 nm is used to measure the absorbance of the solutions. In a typical photocatalytic degradation study, 100 ml of aqueous solution (0.01 g/l) of methylene blue and 0.05 g of the photocatalyst are taken in a beaker, stirred for 30 min in darkness, and subsequently exposed to sunlight with constant stirring. After each time interval of 15 min, about 5 ml of the reaction mixture is withdrawn. It is then centrifuged at 3500 rpm and the absorbance of the centrifugate is observed by measuring the intensity of absorption for the dye, at 668 nm. All the photodegradation studies are carried out on sunny days at hours when sunlight availability is maximum and uniform. The efficiency of photo-catalytic degradation is calculated by plotting ln C/C_0 versus irradiation time where C_0

represents the concentration of methylene blue when t= 0 and C is its concentration after irradiation for t seconds.

2.4.2. Photocatalytic H_2O_2 production

About 0.05 g of photocatalyst is mixed with 50 ml water in an RB flask which is sealed after passing oxygen gas for 10min, stirred for 30 min in darkness and the reaction mixture is irradiated under sunlight with constant stirring. H_2O_2 formed by this reaction is monitored spectrophotometrically.[16] For this, after 15 min, 5 ml of the solution is withdrawn using a syringe and centrifuged at 2000 rpm for 10 min. Then, 3 ml buffer, 50 µl Horse Radish Peroxidase enzyme, and 50 µl DPD reagent (N, N-Diethyl-p-phenylene Diamine) are added. The Absorbance of the solution is measured using a PerkinElmer UV/VIS Spectrophotometer Lambda 850 in the wavelength range of 500 to 800nm. This measurement was repeated for 30, 45, 60, 90 and120 min intervals of time. All the photo- catalytic measurements are performed on sunny days when sunlight availability is maximum. A calibration graph is plotted with absorbance at λ_{max}= 551 nm vs. concentration of H_2O_2 (10-100 µM). From the calibration graph, H_2O_2 evolved in the photocataytic reaction at different irradiation times are obtained. A graph is plotted with H_2O_2 evolution in µmol/g vs. irradiation time. The rate of H_2O_2 production is calculated in µmol/g/h at every 15 min of irradiation. The experiment is repeated with pristine P25 titania photocatalyst and the results are compared.

2.5. Electrochemical measurements for Mott-Schottky plot

Electrochemical impedance measurements of PFO modified GCE are performed with an Electrochemical Analyzer (chi1210c series). From this measurement, the Mott-Schottky plot for PFO is drawn and the flat band potential (E_f) is evaluated by extrapolating the tangent.[20, 21] Combining the band gap value obtained from the Kubelka-Munk plot as well as PL studies, the valence band spectrum obtained from the XPS analysis, and the Mott-Schottky plot, a schematic energy level diagram is constructed for PFO semiconductor photocatalyst. [22–25] Using this energy level diagram, the probable mechanism and reaction routes of photocatalytic methylene blue dye degradation are proposed.

2.6. Total Organic Carbon (TOC) Analysis

Total Organic Carbon analysis measures the amount of organic carbon present in a sample of material under investigation. [26] In the present work, TOC measurements are performed to monitor the mineralization process of the methylene blue dye. For this, 100 ml of methylene blue dye solution is treated with PFO catalyst and kept in darkness for 30 min and the resulting solution is centrifuged and the centrifugate is used for TOC measurement. After irradiating the reaction mixture in sunlight for 15 min, 30 min, 45 min, 60 min respectively and the corresponding TOC values are recorded for each of the reaction mixtures obtained, after the removal of the photocatalyst by centrifugation. All the TOC measurements are performed using a Multiparameter Water Quality Analyzer Sonde (YSI-6820-USA).

2.7. Physico-Chemical Characterisation Techniques Used

In the present work, the developed functional nanomaterials are characterized by various microscopic and macroscopic techniques. Techniques like Fourier Transform Infrared (FTIR) Spectroscopy, Scanning Electron Microscopy (SEM), Field Emission Scanning Electron Microscopy (FESEM), Transmission Electron Microscopy (TEM), Atomic Force Microscopy (AFM), Raman Spectroscopy, X-ray Photoelectron Spectroscopy (XPS), X-ray Diffraction (XRD), UV-Visible and UV-Vis Diffused Reflectance Spectroscopy, are employed for this purpose. DFT calculations are performed using MO6-2X functional and 6-31g basis set using Gaussian 16 program.

2.7.1. Fourier Transform Infrared (FTIR) Spectroscopy

FTIR spectroscopy is a powerful tool for the identification of various functional groups present in a molecule which is considered as the fingerprint of a particular molecular species. [27–29] In IR spectroscopy, the IR radiations incident on the sample are absorbed when the vibrational frequencies of the sample material are matching with the frequencies of the incident radiations. A plot of transmittance vs. wave number gives the infrared spectrum. In FTIR, an interferometer is used to collect the signal which is called the time domain spectrum. It is then converted to frequency domain spectrum by a mathematical process called Fourier transformation to obtain the FTIR spectrum.

In fullerene science as well, FTIR is considered an important non-destructive characterization technique to identify unique structural features. C_{60} is the most symmetric molecule which has a total of 174 vibrational degrees of freedom. However, because of its exceptional

symmetry, only the four F_{1u} vibrational modes are infrared active and these are observed in the FTIR spectrum of C_{60} at positions around 527 cm^{-1}, 576 cm^{-1}, 1183 $cm^{-1}$and 1428 cm^{-1}. Depending upon the nature of functionalization, additional features appear in the FTIR spectra of fullerene-based materials.

In the present work, Fourier transforms infrared (FTIR) spectra of the nanomaterials are recorded using a Perkin Elmer spectrum two L 1600300 FTIR spectrometer in the range 400-4000 cm^{-1}. Using this technique, the intact networking of fullerene balls in the PFO framework is well confirmed. Moreover, the peaks corresponding to various functional groups are also analyzed by this technique. Cage vibrations of hydrogenated C_{60} are also confirmed by FTIR spectra analysis.

2.7.2. X-ray diffraction

X-ray diffraction is a non-destructive technique that gives detailed information about the crystallographic structure as well as the chemical composition of the material. It is based on Bragg's law**:**

$$n\lambda = 2d\sin\theta, \qquad (2.6)$$

where λ is the wavelength of X-rays, d is the spacing between the planes from which diffraction occurs, and θ is the diffraction angle. [30] Here X-rays are allowed to pass through the sample and the intensity of the diffracted X-rays is measured. Materials are identified based on the diffraction pattern obtained from the X-rays that leave the material.

Small Angle X-ray diffraction is a technique that allows the determination of nanoscale or mesoscale structural features of a material. It is an important characterization technique especially for materials with mesoporous structural ordering.

In the present investigation, the low-angle X-ray diffraction analysis is carried out using a Bruker D8 Advance A25 Analytical X-Ray photoelectron spectrometer with monochromated Cu-Kα (8.04 keV) radiation (λ=1.5406) with 2θ values ranging from 0.100° to 8.997°.

2.7.3. Raman spectroscopy

Raman spectroscopy is another non-destructive spectroscopic technique used for identifying the different types of vibrational modes present in a molecule. In this technique, a monochromatic beam of radiation is allowed to pass through the material, and the shift in the energy of the non-elastically scattered radiation as a result of its interaction with molecular vibrations is recorded, which will indicate the vibrational modes present in the molecule. [31, 32] Based on the nature of the bonds, the emitting radiations show high-frequency modes of vibrations (stokes lines) and low-frequency vibrational modes (anti-stokes lines).

Raman scattering is an important tool in fullerene chemistry to understand the molecular structure and properties. C_{60} is the most symmetric molecule with 46 vibrational modes distributed over 174 vibrational degrees of freedom.[33, 34] There are ten Raman active modes in C_{60}. Among these, eight are with Hg symmetry (degenerate gerade

modes) and the other two with Ag symmetry (non-degenerate gerade modes). [35] The characteristic pentagonal pinch mode of C_{60} Ag (2) is located at 1469 cm^{-1}. [36] Cage-cage vibrations of fullerene cages are well observed in fullerene dimer oxides in the region of 15-180 cm^{-1} as evident from Raman spectroscopic measurements. [37]

For many nanocarbon structures like carbon nanotubes and graphene, a D band is observed around 1351 cm^{-1} which is a characteristic peak of disordered amorphous carbon state, and also a G band which corresponds to the hexagonal unit of carbon atom, observed around 1592 cm^{-1} and a 2D band is observed around 2672 cm^{-1}. [38] For CNTs, radial breathing modes (RBMs) will be seen at low frequency regions depending upon the diameter of the nanotubes. [39]

Raman spectral measurements are carried out using a model LabRam HR spectrometer equipped with a 532 nm laser. Raman spectra are recorded, from which modes vibrations of C_{60} balls are assigned. From Raman spectra, the presence of the D band, 2D band, and G band are confirmed for samples with nanotubes and graphene.

2.7.4. X-ray Photoelectron Spectroscopy (XPS)

X-ray Photoelectron Spectroscopy (XPS) is a powerful surface-sensitive electron spectroscopic technique based on the principle of irradiating the atoms of the sample surface of solid material with X-rays causing the ejection of electrons. [40, 41] It is also known as Electron Spectroscopy for Chemical Analysis (ESCA). In XPS spectrum, the intensity plotted vs binding energy. We can identify the type of elements

present in the sample, their oxidation state, and also the other elements to which they are bonded, from the XPS spectrum,. The survey scan gives information about the elemental composition and the percentage composition of each element in the sample. The high-resolution XPS spectra provide information about the type of orbitals in which electrons of the elements are present.

In the present investigation, the X-ray photoelectron spectroscopic analysis is carried out using a Kratos Analytical X-Ray photoelectron spectrometer with monochromated Al-Kα (1486.6 eV;15 kV; 250 W) radiation (λ=1.5418). In this work, the XPS spectra are recorded and the high-resolution C1s and O1s spectra are also analyzed for the nanomaterials prepared. A valence band spectrum of PFO is obtained from the XPS analysis.

2.7.5. Field Emission Scanning Electron Microscopy (FE-SEM)

Field emission scanning electron microscopy is an advanced microscopic technique used for imaging the microstructure of the material. [42] It is one of the most versatile and non-destructive techniques that provide topographical information at higher magnifications. In this technique, a beam of electrons is used to scan the surface of a sample where they enter into interaction with sample atoms. Secondary electrons thus generated will give an image of the sample surface.

In the present investigation, Field emission scanning electron microscopic (FE-SEM) images of the PFO and GNF1are collected using a Hitachi SU 6600 SEM microscope (accelerating potential of 10 kV).

Scanning Electron Microscopic (SEM) images of PHF and GNF2 are collected using a JEOL 6390 LA/OXFORD XMXN SEM microscope (accelerating voltage 0.5 to 30 kV).

2.7.6. Transmission Electron Microscopy (TEM)

Transmission Electron Microscopy is another microscopic technique used to predict structural information about the sample (particle size, shape, and distribution). Here, a beam of electrons is allowed to pass through the sample and they will interact with the sample atoms and the transmitted beam is employed to form a two dimensional image of the sample.[43, 44] Selected Area Electron Diffraction (SAED) is a method in TEM by which lattice parameters and crystallinity of the sample can be predicted. From the SAED pattern we can find out whether the sample is crystalline (bright dotted ring), amorphous (thick diffused continuous ring), or polycrystalline (randomly dotted ring) and chemical information of the sample also can be deduced.

In the present investigation, Transmission electron microscopic (TEM) analyses are performed using a JEOL JEM-2100 microscope operating at 200 kV. TEM images of the nanomaterial samples and the corresponding SAED patterns are recorded. The porous nature of the polymeric fullerene oxide framework (PFO) is well-predicted from the TEM image and its crystallinity is confirmed by the SAED pattern. In the case of PHF, being an electron beam sensitive material, the attempt to take TEM image caused degradation of the sample. Also, in the TEM

analysis of GNF2, the PHF coatings of the carbon nanotubes formed got largely destroyed during the TEM analysis.

2.7.7. Atomic Force Microscopy

Atomic Force Microscopy (AFM) is another surface-sensitive microscopic technique from which the surface topography of the sample can be predicted. AFM comes under the group of microscopic techniques called scanning probe Microscopic (SPM) techniques. In AFM, a sharp cantilever tip scans the sample surface and its deflections, proportional to the interatomic forces between the cantilever tip and sample surface, can be recorded by a photodiode. AFM also provides information about the thickness of the sample, thus we can find out the roughness of the sample surface and the number of layers in two-dimensional materials like graphene.

In the present investigation, AFM images of the PFO sample are collected using Multimode 8 high performance AFM in high speed ScanAsyst mode. AFM images of PHF, GNF1, and GNF2 are collected using the Scanning Probe Microscope (NTEGRA, NTMDT, Russia).

2.7.8. Surface area measurements

BET (Brunauer, Emmet, Teller) is the technique generally used to measure surface area of materials. This technique also can be used for measuring the pore size distribution. BET theory is based on the assumption that multimolecular layer adsorption occurs on localized sites of the sample surface. The BET equation is:

$$\frac{1}{\left[V_a\left(P^{\circ}/p-1\right)\right]} = \frac{C-1}{V_m C}\left(P/p^{\circ}\right) + \frac{1}{V_m C} \quad (2.7)$$

V_a is the volume of gas adsorbed at a pressure P, P° is the saturated pressure of adsorbate gas molecules, V_m is the volume of gas corresponding to the monolayer formation at STP, and C is a constant. A plot volume of the gas against relative pressure at constant temperature (for example, 77 K, liquid N_2) gives the BET adsorption isotherm. Generally, there are six types of adsorption isotherms observed for materials. In the present work, the BET adsorption isotherm of the material (PFO) is recorded by an Autosorb station 1 analyzer.

2.7.9. UV-Visible spectroscopy

UV-Visible spectroscopy is a non-destructive analytical technique, that measures the quantity of UV or Visible light that is absorbed or transmitted through a sample. The absorbance of the sample plotted against wavelength gives UV-Visible spectrum. The sample is used either in liquid or solid form. UV-Visible Diffused Reflectance spectroscopy is widely used for solid sample analysis. In the present work, the UV-Visible absorbance of the PFO in the diffuse reflectance mode is measured using a Varian, Cary 5000 spectrophotometer, and the band gap is calculated by drawing a kubelka-munk plot. Photodegradation studies of methylene blue dye using polymeric fullerene oxide are performed with a Thermo scientific EVOLUTION 160 spectrophotometer in the wavelength range 200 to 800 nm is used to measure the absorbance of the solutions. Photocatalytic production of

H_2O_2 is carried out with PFO/TiO_2 nanocomposite and its spectrophotometric determination is performed with Perkin Elmer UV/VIS Spectrophotometer Lambda 850 in the wavelength range of 400 to 800.nm.

2.7.10. Photoluminescence spectroscopy

Photoluminescence spectroscopy is a light emission spectroscopic technique used to predict the electronic structure of the material. [40] When light of specific wavelength falls on a material, excitation and de-excitation of electrons can give rise to photoluminescence spectra. In a typical PL spectrum, intensity of the emitted radiation is plotted against wavelength.

In the present investigation, Photoluminescence (PL) spectrum for PFO is collected with a Perkin Elmer LS55 luminescence spectrometer employing an excitation wavelength of 320 nm. Photoluminescence spectrum of PFO are recorded and its band gap is calculated by the equation 1240/ λ, where λ is the maximum wavelength of emission which is measured from PL spectra.

2.7.11. Density Functional Theory calculations (DFT)

Density Functional Theory (DFT) is a computational quantum mechanical modeling method which can be used to study the properties of molecules, crystals, surfaces and any type of atomic systems. DFT calculations are found to have important applications for the interpretations and prediction of properties of complex systems and the energetics of various reaction pathways at an atomic level.[45, 46]

In the present investigation, the energetics of the reaction $C_{60}O + C_{60} \rightarrow C_{120}O$ is calculated with Gaussian 16 using M06-2X functional and 6-31g basis set. The transition state of [3+2] cycloaddition bridging reactions in the PFO framework is found out and the feasibility of the reaction under the present reaction conditions is predicted using the results of DFT calculations.

References

(1) Rajeena, U.; Akbar, M.; Raveendran, P.; Ramakrishnan, R. M. Fluorographite to Hydroxy Graphene to Graphene: A Simple Wet Chemical Approach for Good Quality Graphene. *New J. Chem.* **2018**, *42* (12), 9658–9665. https://doi.org/10.1039/C8NJ01392F.

(2) Birkett, P. R.; Crane, J. D.; Hitchcock, P. B.; Kroto, H. W.; Meidine, M. F.; Taylor, R.; Walton, D. R. M. The Structural Characterization of Buckminsterfullerene Compounds. *Journal of Molecular Structure* **1993**, *292*, 1–8. https://doi.org/10.1016/0022-2860(93)80085-A.

(3) Resmi, M. R.; Ma, S.; Caprioli, R.; Pradeep, T. $C_{120}O_n$ from $C_{60}Br_{24}$. *Chemical Physics Letters* **2001**, *333* (6), 515–521. https://doi.org/10.1016/S0009-2614(00)01415-9.

(4) U, R.; M, A.; P, R.; Rm, R. Graphene reduction of P25 titania: Ti^{3+}-doped titania/graphene nanohybrids for enhanced photocatalytic hydrogen production. *Int. J. Hydrog. Energy* **2020**, *45* (16), 9564–9574.

(5) Afreen, S.; Kokubo, K.; Muthoosamy, K.; Manickam, S. Hydration or Hydroxylation: Direct Synthesis of Fullerenol from Pristine Fullerene [C_{60}] via Acoustic Cavitation in the Presence of Hydrogen Peroxide. *RSC Advances* **2017**, *7* (51), 31930–31939. https://doi.org/10.1039/C7RA03799F.

(6) Kokubo, K.; Shirakawa, S.; Kobayashi, N.; Aoshima, H.; Oshima, T. Facile and Scalable Synthesis of a Highly Hydroxylated Water-Soluble Fullerenol as a Single Nanoparticle. *Nano Research* **2011**, *4*, 204–215. https://doi.org/10.1007/s12274-010-0071-z.

(7) Stankovich, S.; Dikin, D. A.; Piner, R. D.; Kohlhaas, K. A.; Kleinhammes, A.; Jia, Y.; Wu, Y.; Nguyen, S. T.; Ruoff, R. S. Synthesis of Graphene-Based Nanosheets via Chemical Reduction of Exfoliated Graphite Oxide. *Carbon* **2007**, *45* (7), 1558–1565. https://doi.org/10.1016/j.carbon.2007.02.034.

(9) Marken, F.; Neudeck, A.; Bond, A. M. Cyclic Voltammetry. *Electroanalytical Methods* **2010**, 57–106. https://doi.org/10.1007/978-3-642-02915-8_4.

(10) Espinoza, E. M.; Clark, J. A.; Soliman, J.; Derr, J. B.; Morales, M.; Vullev, V. I. Practical Aspects of Cyclic Voltammetry: How to

Estimate Reduction Potentials When Irreversibility Prevails. *J. Electrochem. Soc.* **2019**, *166* (5), H3175. https://doi.org/10.1149/2.0241905jes.

(11) Chooto, P.; Chooto, P. *Cyclic Voltammetry and Its Applications*; IntechOpen, 2019. https://doi.org/10.5772/intechopen.83451.

(12) Brownson, D. A. C.; Banks, C. E. *The Handbook of Graphene Electrochemistry*, 4th edition.; Springer: New York, 2014.

(13) Scholz, F. Voltammetric Techniques of Analysis: The Essentials. *ChemTexts* **2015**, *1* (4), 1–24. https://doi.org/10.1007/s40828-015-0016-y.

(14) *Handbook of Instrumental Techniques for Analytical Chemistry*; Settle, F. A., Ed.; Prentice Hall PTR: Upper Saddle River, NJ, 1997.

(15) Sandford, C.; A. Edwards, M.; J. Klunder, K.; P. Hickey, D.; Li, M.; Barman, K.; S. Sigman, M.; S. White, H.; D. Minteer, S. A Synthetic Chemist's Guide to Electroanalytical Tools for Studying Reaction Mechanisms. *Chemical Science* **2019**, *10* (26), 6404–6422. https://doi.org/10.1039/C9SC01545K.

(16) Bader, H.; Sturzenegger, V.; Hoigné, J. Photometric Method for the Determination of Low Concentrations of Hydrogen Peroxide by the Peroxidase Catalyzed Oxidation of N,N-Diethyl-p-Phenylenediamine (DPD). *Water Research* **1988**, *22* (9), 1109–1115. https://doi.org/10.1016/0043-1354(88)90005-X.

(17) Balu, S.; Uma, K.; Pan, G.-T.; Yang, T. C.-K.; Ramaraj, S. K. Degradation of Methylene Blue Dye in the Presence of Visible Light Using SiO_2@α-Fe_2O_3 Nanocomposites Deposited on SnS_2 Flowers. *Materials (Basel)* **2018**, *11* (6). https://doi.org/10.3390/ma11061030.

(18) Xu, C.; Rangaiah, G. P.; Zhao, X. S. Photocatalytic Degradation of Methylene Blue by Titanium Dioxide: Experimental and Modeling Study. *Ind. Eng. Chem. Res.* **2014**, *53* (38), 14641–14649. https://doi.org/10.1021/ie502367x.

(19) Zuo, R.; Du, G.; Zhang, W.; Liu, L.; Liu, Y.; Mei, L.; Li, Z. *Photocatalytic Degradation of Methylene Blue Using TiO_2 Impregnated Diatomite*. Advances in Materials Science and Engineering. https://doi.org/10.1155/2014/170148.

(20) Patel, K.; Solanki, G. K.; Patel, K. D.; Pataniya, P.; Pathak, V. M.; Tannarana, M.; Chauhan, P.; Patel, M. Flat Band Potential Determination of $NbSe_2$ Photoelectrode Using Mott-Schottky Plot. *AIP Conference Proceedings* **2019**, *2115* (1), 030402. https://doi.org/10.1063/1.5113241.

(21) Gelderman, K.; Lee, L.; Donne, S. W. Flat-Band Potential of a Semiconductor: Using the Mott–Schottky Equation. *J. Chem. Educ.* **2007**, *84* (4), 685. https://doi.org/10.1021/ed084p685.

(22) Schumacher, L.; Marschall, R. Recent Advances in Semiconductor Heterojunctions and Z-Schemes for Photocatalytic Hydrogen Generation. *Top Curr Chem (Cham)* **2022**, *380* (6), 53. https://doi.org/10.1007/s41061-022-00406-5.

(23) Humayun, M.; Raziq, F.; Khan, A.; Luo, W. Modification Strategies of TiO2 for Potential Applications in Photocatalysis: A Critical Review. *Green Chemistry Letters and Reviews* **2018**, *11* (2), 86–102. https://doi.org/10.1080/17518253.2018.1440324.

(24) Sakar, M.; Mithun Prakash, R.; Do, T.-O. Insights into the TiO_2-Based Photocatalytic Systems and Their Mechanisms. *Catalysts* **2019**, *9* (8), 680. https://doi.org/10.3390/catal9080680.

(25) Soltani, N.; Saion, E.; Hussein, M. Z.; Erfani, M.; Abedini, A.; Bahmanrokh, G.; Navasery, M.; Vaziri, P. Visible Light-Induced Degradation of Methylene Blue in the Presence of Photocatalytic ZnS and CdS Nanoparticles. *Int J Mol Sci* **2012**, *13* (10), 12242–12258. https://doi.org/10.3390/ijms131012242.

(26) Emery, R. M.; Welch, E. B.; Christman, R. F. The Total Organic Carbon Analyzer and Its Application to Water Research. *Journal (Water Pollution Control Federation)* **1971**, *43* (9), 1834–1844.

(27) Faix, O. Fourier Transform Infrared Spectroscopy. *Methods in Lignin Chemistry* **1992**, 83–109. https://doi.org/10.1007/978-3-642-74065-7_7.

(28) Gaffney, J. S.; Marley, N. A.; Jones, D. E. Fourier Transform Infrared (FTIR) Spectroscopy. In *Characterization of Materials*; John Wiley & Sons, Ltd, 2012; pp 1–33. https://doi.org/10.1002/0471266965.com107.pub2.

(29) Silverstein, R. M.; Bassler, G. C. Spectrometric Identification of Organic Compounds. *J. Chem. Educ.* **1962**, *39* (11), 546. https://doi.org/10.1021/ed039p546.

(30) Rao, C. N. R.; Gopalakrishnan, J. *New Directions in Solid State Chemistry*; Cambridge University Press, 1997.

(31) *Principle, Instrumentation, Types and Applications of XRD*. 14impressions. https://www.14impressions.in/2020/09/principle-instrumentation-types-and.html (accessed 2022-10-20).

(32) Jones, R. R.; Hooper, D. C.; Zhang, L.; Wolverson, D.; Valev, V. K. Raman Techniques: Fundamentals and Frontiers. *Nanoscale Research Letters* **2019**, *14* (1), 231. https://doi.org/10.1186/s11671-019-3039-2.

(33) Yamamoto, K.; Saunders, M.; Khong, A.; Cross, R. J. ; Grayson, M. ; Gross, M. L.; Benedetto, A. F. and Weisman, R. B. *Isolation and Spectral Properties of Kr@C_{60}, a Stable van der Waals Molecule*. ACS Publications. https://doi.org/10.1021/ja9831498.

(34) Stewart, J. T.; Brumfield, B. E.; Gibson, B. M.; McCall, B. J. Inefficient Vibrational Cooling of C_{60} in a Supersonic Expansion. *International Scholarly Research Notices* **2013**, *2013*, e675138. https://doi.org/10.1155/2013/675138.

(35) Damle, V. H.; Sinwani, M.; Aviv, H.; Tischler, Y. R. Microcavity Enhanced Raman Spectroscopy of Fullerene C_{60} Bucky Balls. *Sensors (Basel)* **2020**, *20* (5), 1470. https://doi.org/10.3390/s20051470.

(36) Kuzmany, H.; Pfeiffer, R.; Hulman, M.; Kramberger, C. Raman Spectroscopy of Fullerenes and Fullerene-Nanotube Composites. *Philosophical Transactions: Mathematical, Physical and Engineering Sciences* **2004**, *362* (1824), 2375–2406.

(37) Eisler, H.-J.; Hennrich, F. H.; Werner, E.; Hertwig, A.; Stoermer, C.; Kappes, M. M. Superdiatomics and Picosprings: Cage−Cage Vibrations in $C_{120}O$, $C_{120}O_2$, and in Three Isomers of $C_{130}O$. *J. Phys. Chem. A* **1998**, *102* (22), 3889–3897. https://doi.org/10.1021/jp980834s.

(38) Alsulam, I. K.; Alharbi, T. M. D.; Moussa, M.; Raston, C. L. High-Yield Continuous-Flow Synthesis of Spheroidal C_{60}@Graphene Composites as Supercapacitors. *ACS Omega* **2019**, *4* (21), 19279–19286. https://doi.org/10.1021/acsomega.9b02656.

(39) Cheng, H.-C.; Liu, Y.-L.; Wu, C.-H.; Chen, W.-H. On Radial Breathing Vibration of Carbon Nanotubes. *Computer Methods in Applied Mechanics and Engineering* **2010**, *199* (45), 2820–2827. https://doi.org/10.1016/j.cma.2010.05.003.

(40) Skoog, D. A. *Principles of instrumental analysis.*

(41) Shard, A. G. Practical Guides for X-Ray Photoelectron Spectroscopy: Quantitative XPS. *Journal of Vacuum Science & Technology A* **2020**, *38* (4), 041201. https://doi.org/10.1116/1.5141395.

(42) Erlandsen, S. L.; Frethem, C.; Chen, Y. Field Emission Scanning Electron Microscopy (FESEM) Entering the 21st Century: Nanometer Resolution and Molecular Topography of Cell Structure. *Journal of Histotechnology* **2000**, *23* (3), 249–259. https://doi.org/10.1179/his.2000.23.3.249.

(43) Botton, G. Analytical Electron Microscopy. *Science of Microscopy* **2007**, 273–405. https://doi.org/10.1007/978-0-387-49762-4_4.

(44) Goodhew, P. J.; Humphreys, J.; Beanland, R. *Electron Microscopy and Analysis, Third Edition*; CRC Press, 2000.

(45) Kohn, W.; Becke, A. D.; Parr, R. G. Density Functional Theory of Electronic Structure. *J. Phys. Chem.* **1996**, *100* (31), 12974–12980. https://doi.org/10.1021/jp960669l.

(46) Kang, J. Y. L. and M. H. Density-Functional Study of the Interface Structure of C_{60}/Al(111)-(2 X 2)R30o. *Journal of the Korean Physical Society* **2009**, *54* (2), 668–672. https://doi.org/10.3938/jkps.54.668.

CHAPTER 3

PREPARATION OF MESOPOROUS POLY (FULLERENE OXIDE) FRAMEWORK BY THERMAL [3+2] CYCLOADDITIONS AND ITS PHOTOCATALYTIC AND ELECTROCHEMICAL SENSING APPLICATIONS.

3.1 Introduction

For chemists in the recent decades, carbon nanostructures such as fullerenes, carbon nanotubes, graphene, and their numerous derivatives have triggered enormous research interest. They have emerged as a class of most fascinating molecular systems from a structural chemist's point of view. From organic structural constructions to the unique material properties they exhibit, possibilities for immense potential applications of these systems emerge, pervasive to all areas of chemistry. [1–4] The unique material properties offered by these systems are essentially linked to the sp^2 hybridization, extent of π-electron delocalization, and the energy levels created in these systems. Fullerenes, in particular, have attracted attention by virtue of the narrow bandgap suitable for visible light absorption and the ability to trigger the generation of reactive oxygen species like singlet oxygen radicals, superoxide radicals, and hydroxyl radicals in photochemical conditions, with potential for photocatalytic applications. [5–8] Fullerene-based photocatalysts have been successfully employed for many specific organic transformations. The synthesis of phenols through oxidative hydroxylation of aryl boronic acids [9], photooxidation of alkenes [10], oxidative conversion of secondary benzylamines to imines [11], and synthesis of pyrrolo[2,1-a]isoquinolines through a tandem oxidation/[3+2] cycloaddition of tetrahydro-isoquinoline with N-phenyl maleimide employing C_{60}-Bodipy dyad triplet photosensitizers are some examples in this category. [6]

There has also been a keen interest in the exploitation of the carbon-based, metal-free, catalysts from a green chemistry perspective.[12–14] The concept of using semiconducting organic polymers

as photocatalyst materials, replacing inorganic semiconductors had been introduced by Yanagida et al. as early as in 1985. [15] They used poly(*p*-phenylene) (PPP) for the photocatalytic hydrogen generation under UV irradiation in the presence of an electron donor. Recent years have witnessed enormous activity in this area. In fact, the use of such polymeric carbocatalysts in photocatalysis is perceived to be of much significance with the new possibility of tailoring the specific band gaps for each reaction, particularly in the non-ultraviolet region of the electromagnetic spectrum, which can enable the strategy for the development of heterogeneous photocatalytic processes using these carbocatalysts using sunlight. For example, the use of graphitic carbon nitride (g-C_3N_4) materials for harvesting visible light have received much attention in recent years. [16–19] There have also been a few reports on the use of oxidized carbon nanomaterials for photocatalytic purposes. [20, 21] Recently, Shiraishi et al. [21] have reported the use of resorcinol–formaldehyde resins as metal-free semiconductor photocatalysts for the sunlight-assisted production of hydrogen peroxide from water. Reduced complexity in the synthetic protocols is an important attraction of these materials. From this imperative, photocatalytic studies with the fullerene-based mesoporous photocatalytic systems become important. [22–26] In fact, previous studies had reported the formation of mesoporous fullerene assembles. Template-based strategies have been widely reported for the preparation of nanoporous carbon architectures and their chemical/electrochemical applications have been demonstrated in the past. [27–31] Shrestha *et al.* have reported the formation of C_{60} crystals with bimodal pore architectures using an anti-solvent precipitation method using isopropyl alcohol as the anti-solvent from a saturated solution of C_{60} dissolved in benzene-CCl_4 mixture. [32] Also, mesoporous C_{70} cubes

with high photoluminescence were reported by Bairi *et al.* [33] However, such networks may not be suitable for photocatalytic applications since their higher photoluminescence indicates faster electron-hole recombinations preventing the transportation of charge carriers to the reactive surface sites reducing the possibility for photocatalytic transformations [33].

In this work, we suggest a simple strategy for a new class of poly (fullerene oxide) (PFO) networks that can function as semiconductor photocatalysts using sunlight. The scheme for the formation of the PFO catalyst is presented in Figure 3.1.

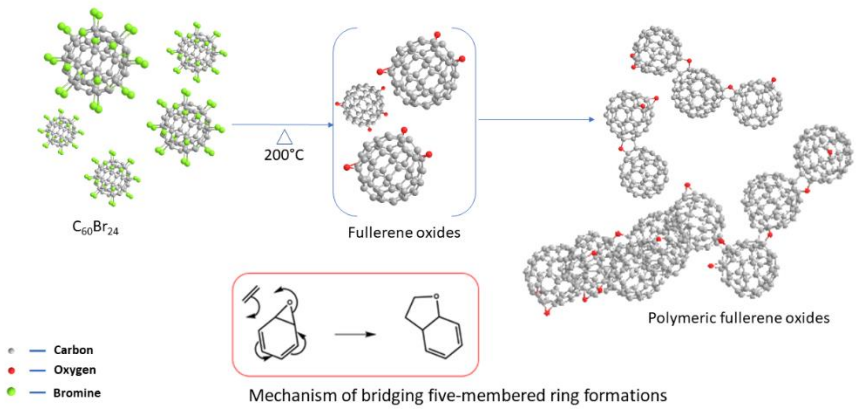

Figure 3.1: Scheme for the synthesis of nanoporous network of poly (fullerene oxide) frameworks from C_{60} via $C_{60}Br_{24}$

By virtue of its high affinity towards electron-deficient species, C_{60} reacts with excess liquid Br_2 ultimately forming its highly brominated derivative, $C_{60}Br_{24}$ [34]. Direct bromination of solid C_{60} with liquid bromine is capable of producing partially brominated fullerenes

like $C_{60}Br_8$, $C_{60}Br_{12}$, $C_{60}Br_{14}$ as intermediate products in the initial stage of the reaction. But upon increasing the reaction time up to around 8 h, these bromofullerenes again dissolve in unreacted Br_2 present in the reaction mixture and forms $C_{60}Br_{24}$. [35] This is the highest degree of bromination possible for C_{60}, for steric reasons. Bromine atoms being bulky, the 24 Br atoms fully cover the carbon core of fullerene, hindering the remaining 18 double bonds from undergoing further addition reactions. [32–35]

Bromofullerenes have been utilized as precursor materials for the synthesis of fullerene derivatives with desired properties. [40] In the present study, we describe the preparation of highly cross-linked fullerene oxide cages from fully brominated fullerene $C_{60}Br_{24}$ through its thermal treatment. At 200 °C, they readily react with oxygen forming a mixture of oxides by the eliminations of bromine atoms, without affecting fullerene cages as reported earlier by Resmi et al. [41] The oxidation and their subsequent crosslinking by [3+2] thermal cycloadditions have been established therein through electrospray mass spectroscopic studies. Fullerene epoxides constitute an interesting class of fullerene derivatives which consist of epoxide groups directly attached to the fullerene cages. Monomeric, dimeric and other smaller oligomeric oxides thus formed can be easily removed by washing with toluene, since they are soluble forms. The insoluble polymeric form of the fullerene oxide framework is expected to have a lot of epoxide rings on its surface. [42] Networked fullerene polymeric oxides are found to be semiconducting materials capable of acting as photocatalysts. They may

also be suitable for applications in devices like organic solar cells and photocurrent generation devices. Therefore, a detailed study on their material properties, as well as straightforward simple preparation methods are relevant in the current scenario where novel functional materials are the key factors causing the current technological advancements.

H_2O_2 being an environmentally benign oxidant, can be considered as a suitable liquid fuel for future and its photocatalytic production is of great importance. Photocatalytic H_2O_2 production is an the emerging research field being a green process which utilizes only water and oxygen in the presence of sunlight for the production of an important fuel like H_2O_2. [43] Barder et al. have reported a simple method for the spectrophotometric detection of H_2O_2 in which N,N-Diethyl-P-Phenylene Diamine is oxidized in a peroxidase catalyzed reaction, ideal to monitor the H_2O_2 production in photocatalytic conditions. [44] Photocatalytic H_2O_2 production is known to follow a mechanism which proceeds via the formation of reactive oxygen species (ROS) [43]. In the present work, this reaction is utilized to confirm ROS production in photocatalytic conditions when the prepared photocatalysts are employed.

Electrochemical sensors can act as an important cost-effective tool for providing a sensitive, selective and fast determination of a wide range of analytes. They can be generally categorized as potentiometric, conductometric, and amperometric sensors. Particularly, there has been lot of attention in the research field towards the development of

wearable electrochemical sensors for monitoring therapeutic drugs. [45] Carbon-based materials like CNTs and graphene, carbon black, etc. can be used as sensing platforms for biomarkers such as glucose. [46] There are different electrochemical techniques that can be employed for sensing which include cyclic voltammetry, Differential pulse voltammetry and Amperometry. [45, 47–50] Biochemical sensors are devices in which the recognition system utilizes a biochemical mechanism. [51]

Glucose is an important carbohydrate found in our blood. It carries energy to every part of our body. The normal glucose level in our blood is considered as to be in the limit 80-120 mg/dl. [52] High glucose concentration may increase the glucose level in our body and can cause serious health problems such as diabetes which may lead to cardiovascular diseases. [53–60] High glucose level in blood and related issues are found to be one of the root causes of death rate in the world. So, the monitoring of blood glucose has become a very important aspect of maintaining of good health. Electrochemical glucose biosensors play an important role in detecting blood glucose levels in a cost-effective way. In the modified electrode surfaces glucose undergoes electrochemical oxidation to form gluconic acid. Biosensors, in general, can be considered as compact analytical devices containing a biologically sensitive element associated with a physico-chemical transducer. [61] Glucose sensors include both enzymatic and enzyme-free sensors. In enzymatic sensors, enzymes are employed as the biological recognition element that recognizes the target material even in the presence of other materials. [62–64] Enzyme-based sensors provide a highly

reliable, selective and sensitive glucose monitoring. However, in fact there are some disadvantages also when enzyme based glucose sensors are concerned, such as their chemical instability, high cost, critical operating conditions and so on. And also in their development, an additional step, ie., the enzyme immobilization is needed.[65, 66] To solve these problems, enzyme free sensors like inert metals, metal alloys, metal dispersed CNTs, etc. are introduced. However, enzyme free sensors are still in a developing stage and require lot of improvement to match with enzymatic sensors in their performance. The major challenges associated with them are low sensitivity, quick loss of activity, and low selectivity. So the development of highly selective, sensitive, inexpensive, reliable, fast, and non-enzymatic glucose sensors are need of the hour. [67–74] Non-enzymatic glucose sensors are capable of regulate the interferences occurring from various electro-inactive, and electro-active species. [75] Metal oxide nanoparticles are widely used in non-enzymatic glucose sensors.[76] In the present work, PolyFullerene Oxide (PFO) prepared by the thermal decomposition of $C_{60}Br_{24}$ at higher temperatures is used as a sensor material for the electrochemical detection of glucose. Glucose sensing is performed with PFO modified Glassy Carbon Electrode. PFO based glucose sensors are found to capable of trace level detection of glucose which especially is relevant in noninvasive, more accurate as well as rapid monitoring of glucose levels in neonatal babies.

3.2 Results and discussion

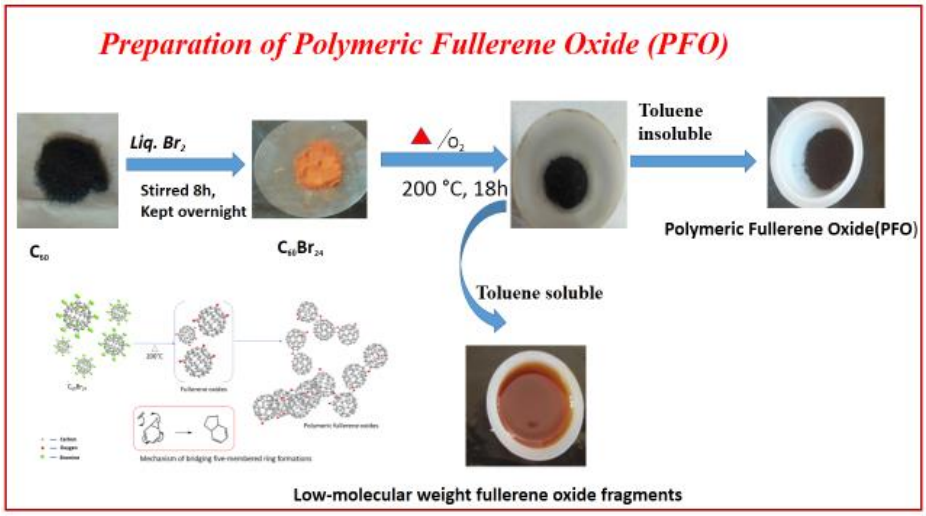

Figure 3.2: Preparation of PFO

3.2.1 SEM Analysis

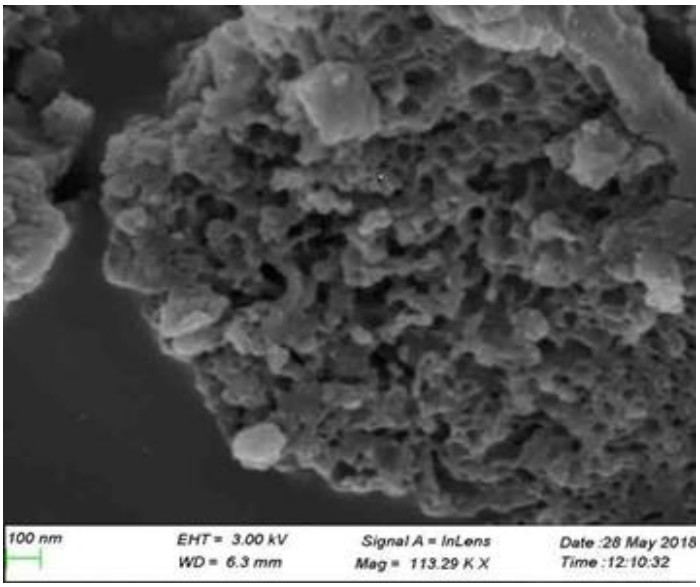

Figure 3.3 : SEM image of PFO

The SEM image is presented in Figure 3.3. The SEM image clearly show a highly porous architecture with non-uniform pore dimensions ranging from meso/micropores to larger macropores with high surface area that are interconnected, suggesting potential as a suitable catalyst.

3.2.2 TEM Analysis

TEM image of the PFO sample and the corresponding SAED pattern are presented in Figure 3.4.

The porous nature of the polymeric fullerene oxide framework is further confirmed by high resolution (HR) TEM measurements and the corresponding SAED pattern is presented in the Figure 3.4b. Some amount of the meso-structured ordering is visible in the TEM image as well.

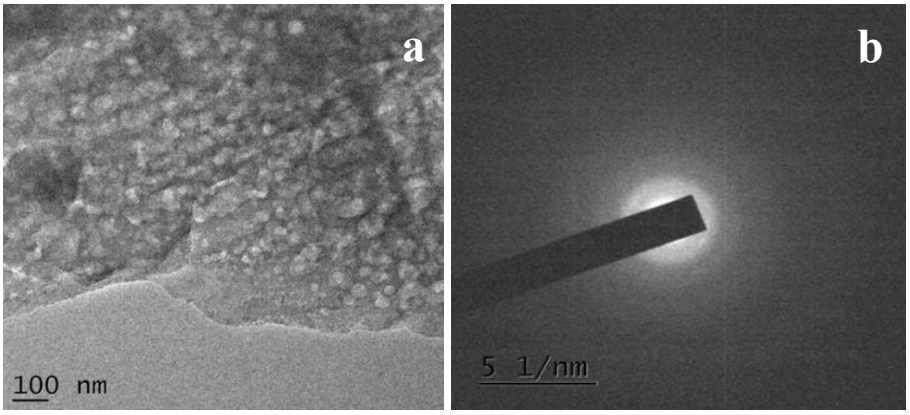

Figure 3.4: (a) TEM image (b) SAED Pattern of PFO

3.2.3 Surface area measurements (BET)

The porous structure of the fullerene framework is studied by nitrogen adsorption. The hysteresis loop observed in BET isotherm (Figure 3.5) indicates the mesoporous nature of the material and the systematic patterns observed in adsorption and desorption curves indicate the presence of some periodic inter-connections between the parallel pores in the system. Because of this peculiarity, the observed surface area (117.517 m^2/g) may not indicate the actual surface area of the material.

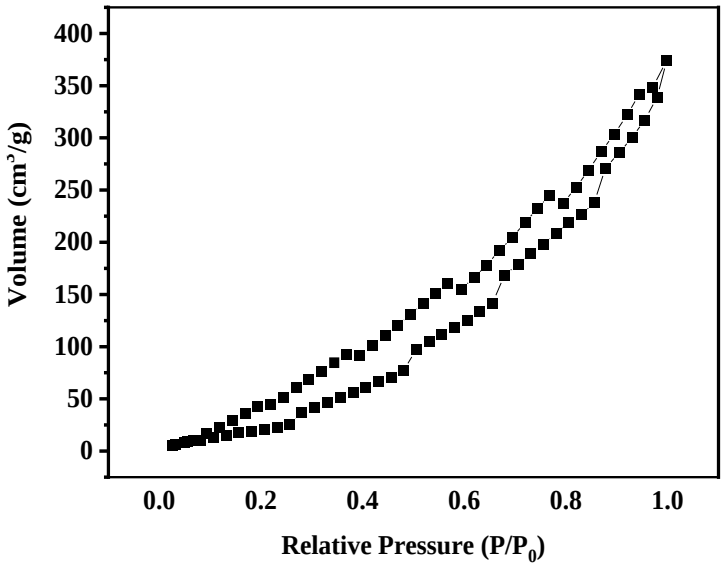

Figure 3.5: BET adsorption isotherm for PFO

3.2.4 XRD Analysis

The meso-structural order of PFO is investigated by low-angle XRD studies (Figure 3.6). The diffraction pattern obtained shows two

peaks at 0.3442 and 0.4947 indicative of the presence of lots of cross-linking of fullerenes and formation of structured mesopores and macropores.

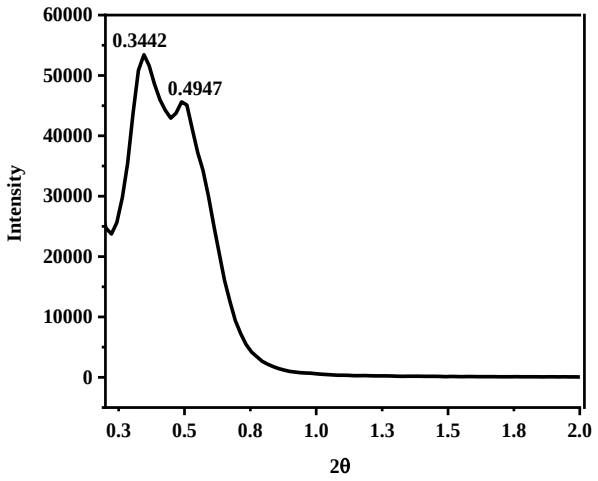

Figure 3.6 : Small Angle X-ray diffraction pattern

3.2.5 FTIR Analysis

PFO is characterized by Fourier Transform Infrared spectroscopy and vibrational spectral features are compared with that of the precursors, C_{60} and $C_{60}Br_{24}$. The FTIR spectra obtained are presented in Figure 3.7. In the FTIR of PFO, peaks observed at 527 cm^{-1}, 575 cm^{-1}, 1182 cm^{-1}, and 1423 cm^{-1} correspond to fullerene balls, confirming the presence of intact fullerene cages in the network. The characteristic peak observed at 1026 cm^{-1} corresponds to C-O stretching vibrations, indicating the formation of epoxide rings at the surface of fullerene cages. The peaks at 1613 $cm^{-1}$and 1721 cm^{-1} indicate the presence of C=C stretching vibrations and asymmetric stretching of

COO^- ions respectively. Also, the peak at 1387 cm^{-1} is characteristic of the symmetric stretching of the COO^- ions, indicative of oxidative opening of a few C_{60} balls at the periphery of the framework.

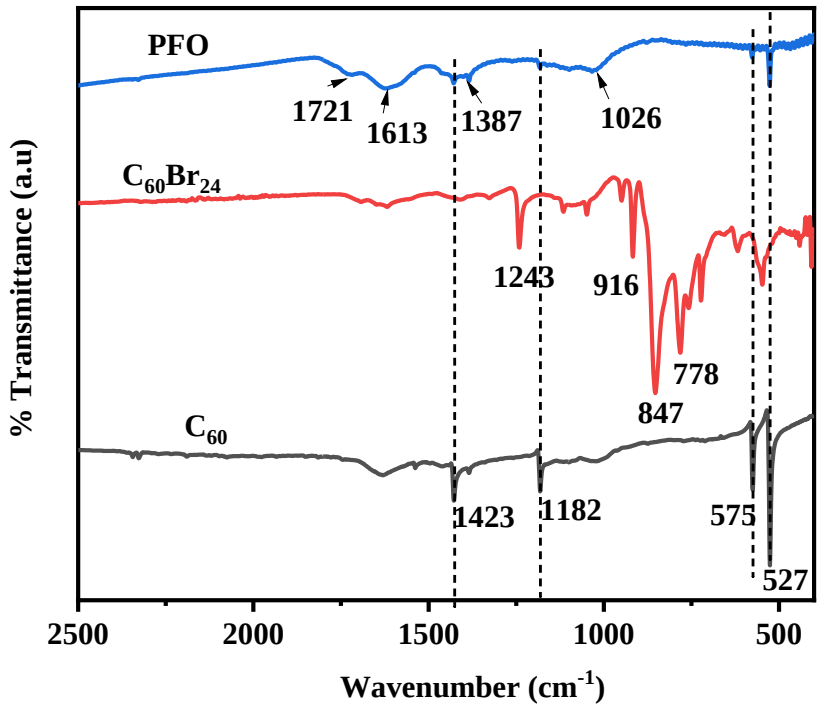

Figure 3.7 : FTIR spectra of PFO, C_{60} and $C_{60}Br_{24}$ sample

3.2.6 Raman Analysis

Raman spectra for PFO (Figure 3.8) show two distinct peaks at 1586 cm^{-1} and 1416 cm^{-1}, which tentatively can be assigned as the H_g (7) and H_g (8) modes of C_{60}, shifted due to the cross-linking of C_{60} balls and oxidation.

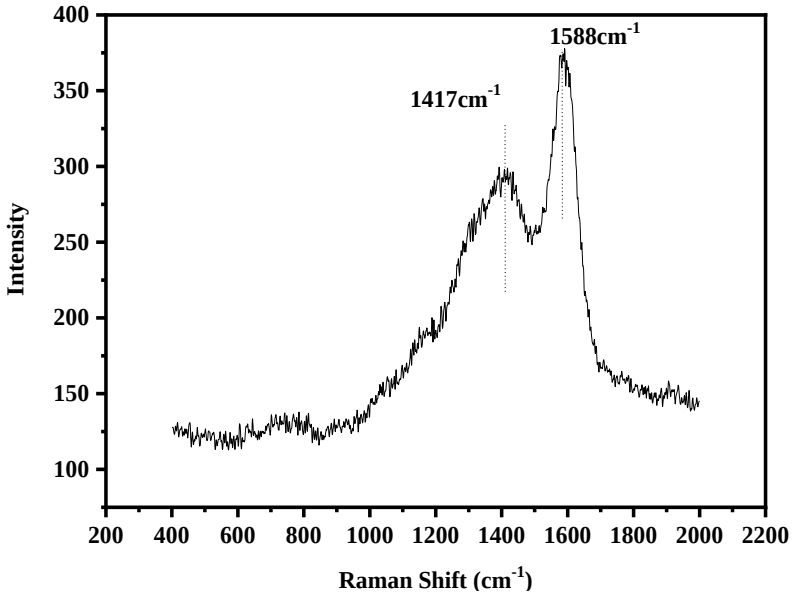

Figure 3.8 : Raman spectra of PFO

3.2.7 XPS Analysis

The X-ray Photoelectron spectra of the PFO sample are shown in Figure 3.9. The survey spectrum (Figure 3.9a) shows 82.6 % of carbon and 17.39 % of oxygen. In the High Resolution C1s XPS spectrum (Figure 3.9 b), the peak at 284.7 eV (41.76 %) can be attributed to sp^2 hybridized carbon atoms that are part of the C_{60} network and the peak at 285.6 eV (43.03 %) to the carbon atoms involved in C-O-C bonding. The small peak at 288.5 eV (15.20 %) can be attributed to C=O groups, probably by the oxidative opening of a few cages on the surface of the PFO framework. The High Resolution O1s XPS spectrum (Figure 3.9 c) indicates the presence of two types of oxygen atoms, peaks at 532.26 eV for C-O-C oxygen and 534.02 eV for C=O oxygen, consistent with the C1s spectrum.

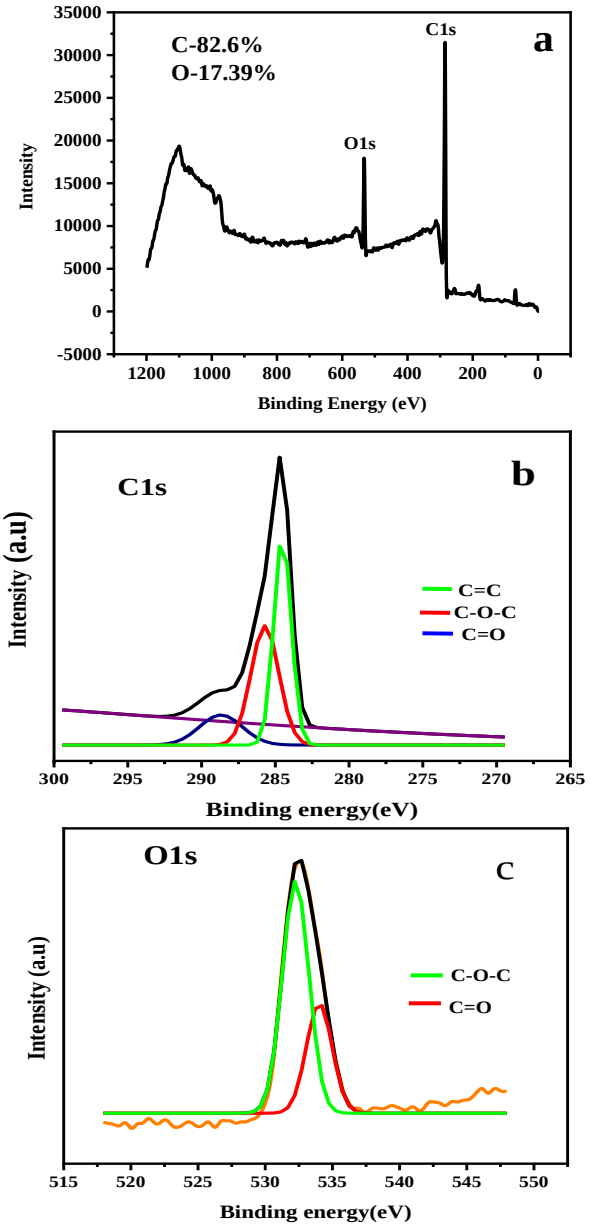

Figure 3.9: X-ray photoelectron spectra of PFO: (a) survey scan (b) High Resolution C1s spectrum (c) High Resolution O1s spectrum.

3.2.8 AFM Analysis

AFM studies of PFO powder confirm the three-dimensional nature of the network with a rough surface. The 2D and 3D AFM images are presented in Figure 3.10.

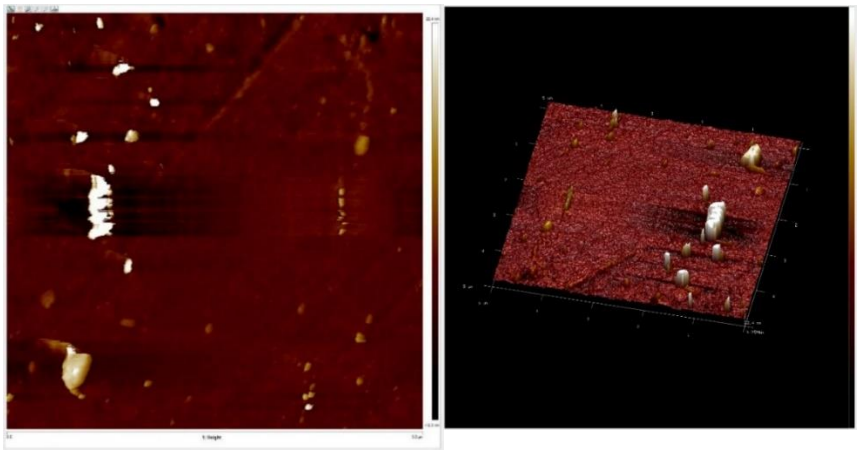

Figure 3.10: (a) 2D and (b) 3D AFM images of PFO powder.

3.2.9 UV-Vis Spectral Studies

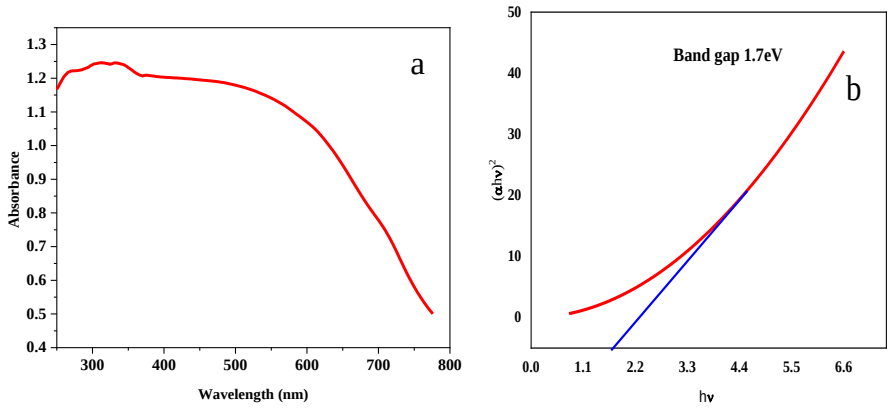

Figure 3.11: (a) UV-VIS Diffuse Reflectance Spectrum of PFO; (b) Kubelka-Munk plot of PFO

UV-VIS Diffuse Reflectance Spectrum of polymeric fullerene oxide is presented in Figure 3.11a which shows a clear absorption edge typical of semiconductors. From the Kubelka-Munk plot (Figure 3.11b), a bandgap of 1.7 eV is obtained for polymeric fullerene oxide, clearly indicating that the semiconductor is suitable for visible light harvesting.

3.2.10 Photoluminescence Studies

The photoluminescence spectrum obtained for PFO is presented in Figure 3.12.

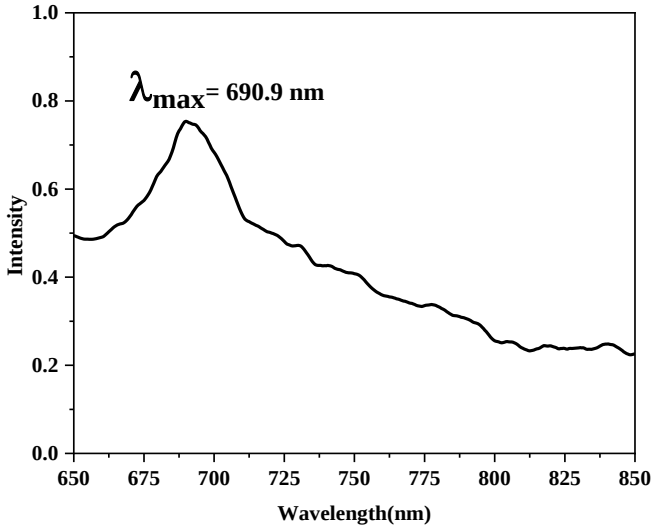

Figure 3.12: Photoluminescence spectrum obtained for PFO

The maximum wavelength of emission is found to be at 690.9 nm and the bandgap of polymeric fullerene oxide can be calculated as 1.7 eV, consistent with the value obtained from the Kubelka-Munk plot of UV-Visible DRS studies. The fact that PL intensity is rather a low

compared to many other fullerene-based materials like mesoporous C_{70} cubes reported by Bairi et al, indicates that PFO is more suited for photocatalytic applications than mesoporous C_{70} since the competing process, ie., the recombination of charge carriers, is less prominent leading to the possibility for more photocatalytic processes and ROS production.

3.2.11 Photocatalytic Methylene Blue Degradation Studies

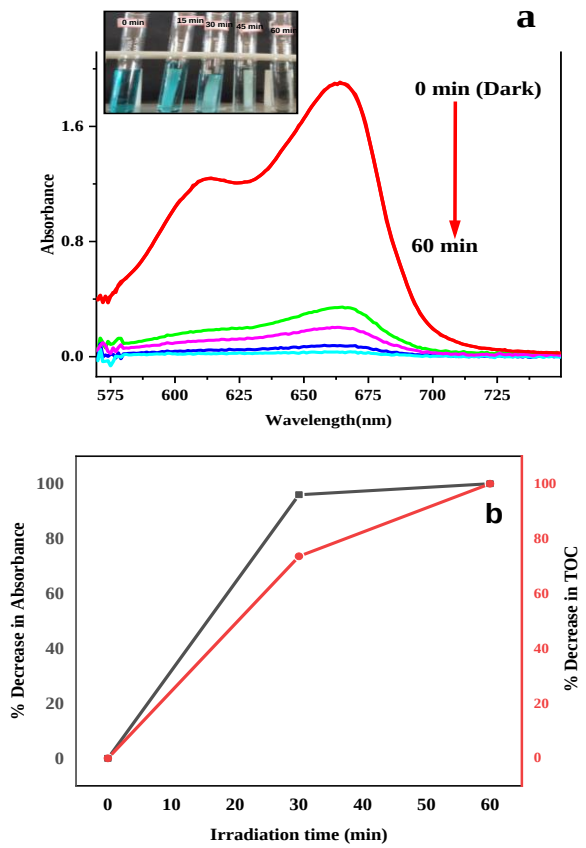

Figure 3.13: (a) UV-Vis Spectra of the reaction mixture at 0, 15, 30, 45, 60 intervals of time**;** (b) The TOC removal and decolorization efficiencies of PFO versus irradiation time.

From the Figure 3.13a, it is clear that the de-coloration of methylene blue dye solution is happening mostly in the first 15 min itself and it is slower in the later minutes of irradiation. However, from the TOC data (Figure 3.13b), it is clear that the decoloration rate is different from that of the complete demineralization rate. The TOC value after the first 30 min irradiation time indicates the formation of colorless intermediates in the reaction mixture. After the first 15 min, competition for surface cites from the intermediates will be larger, bringing down the reaction rate. Within 60 min of irradiation, the de-coloration, as well as mineralization process is almost complete.

Photocatalytic degradation of methylene blue over PFO is compared with the performance of bare C_{60}, commercial Degussa P25 TiO_2 catalyst, and PFO/TIO_2 5% nanocomposite (Figure 3.14). The nanocomposite of PFO and TiO_2 exhibited far better visible light harvesting and photocatalysis compared to pristine TiO_2, indicating a bandgap reduction for the TiO_2 catalyst. Even though the photocatalytic performance of the nanohybrid is lesser compared to bare PFO, the nanocomposite catalyst also has its importance especially considering the cost-effectiveness of the catalytic systems. By the loading of just 5% of PFO in TiO_2, the rate constant changes from a value of 0.0088 s^{-1} to 0.02452 s^{-1}. Here, PFO might be functioning as a photosensitizer, making the catalytic system suitable for visible light harvesting. Pristine polymeric fullerene oxide is found to be the most efficient catalyst among the catalytic systems studied here with a rate constant of 0.09015 s^{-1}. The photocatalytic performance of pristine C_{60} is observed

to be the least with a rate constant of 0.00374 cm^{-1}, probably due to the photochemical aggregation of fullerene balls leading to mutual quenching of the excited fullerenes.

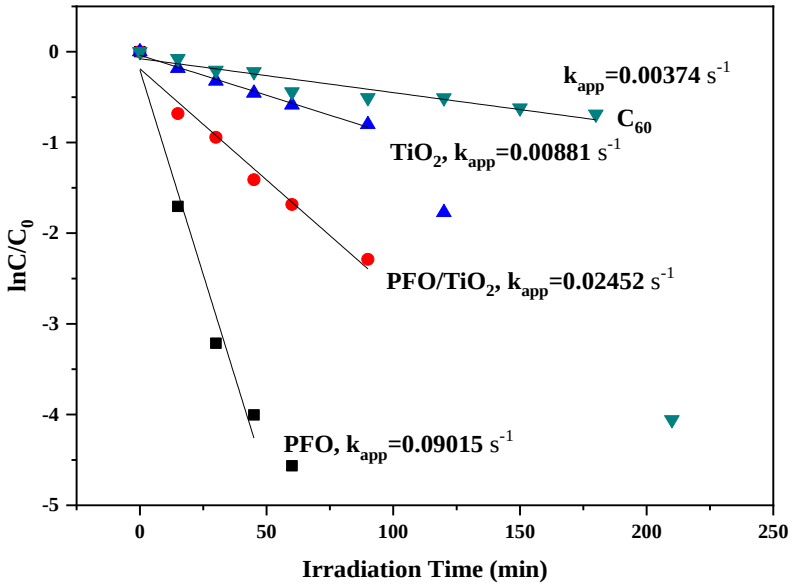

Figure 3.14: Plot of ln C/C_0 against irradiation time for the photocatalytic degradation of Methylene Blue using different photocatalytic systems.

Mechanism of the Photocatalytic Process

To investigate the probable mechanism and reaction routes, a schematic energy level diagram is constructed. With the help of electrochemical studies, the Mott-Schottky plot for PFO is drawn (Figure 3.15a) and the flat band potential (E_f) is evaluated by extrapolating the tangent which is found to be -1.14 with respect to Ag/AgCl. PFO is observed to exhibit n-type semiconductor characteristics with a positive slope for the tangent [77]. Combining the

band gap value obtained from Kubelka-Munk plot as well as PL studies, valence band spectrum obtained from the XPS analysis (Figure 3.15b), and Mott-Schottky plot, a schematic energy level diagram can be proposed which is presented in Figure 3.16 a. For PFO, the narrow bandgap can be held responsible for the visible light response. The proposed band diagram leads to the plausible mechanism of ROS production and the mechanism of the photocatalytic process involved. It is evident that the superoxide anion formation is the main primary reaction process in the dye degradation whereas the oxidation of the hydroxide ion to hydroxide radical by the holes migrated to the surface is not supported by the evaluated potential values. The holes migrated to the surface of the catalyst will not possess enough potential to carry out such a reaction. A schematic drawing of the primary processes of photocatalysis is presented in Figure 3.16b. However, it is quite possible that hydroxide radical formation is happening in the reaction mixture as a result of secondary reactions of superoxide radical anion formed in the primary process.

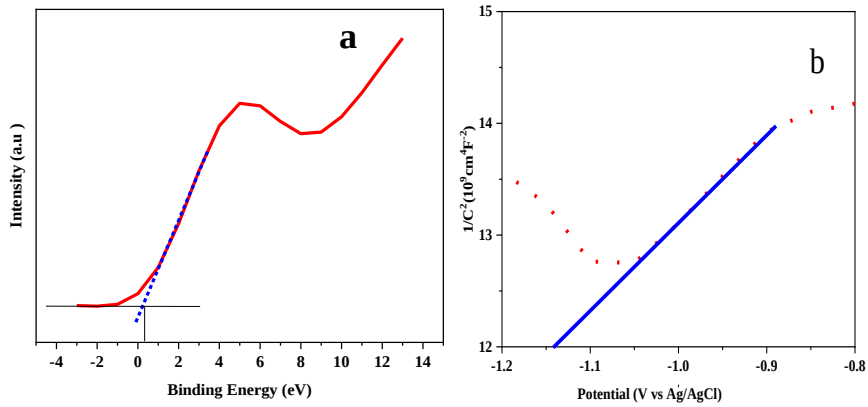

Figure 3.15: (a) Mott-Schottky plot of PFO (b) Valence band spectrum obtained from the XPS analysis

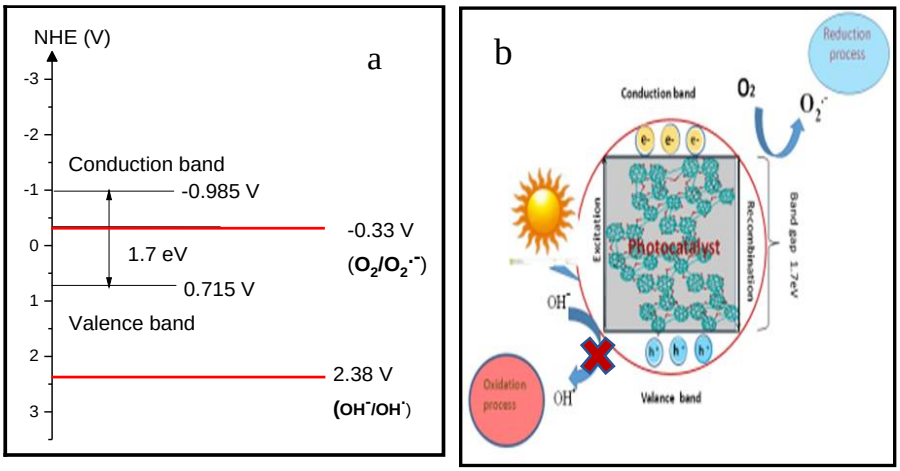

Figure 3.16: (a) Schematic energy level diagram showing the band gap of PFO; (b) Schematic diagram showing the mechanism of photocatalytic process.

Recyclability of PFO as photocatalyst is studied by repeating the photocatalytic reaction in three consecutive cycles. The results obtained are summarized in Figure 3.17.

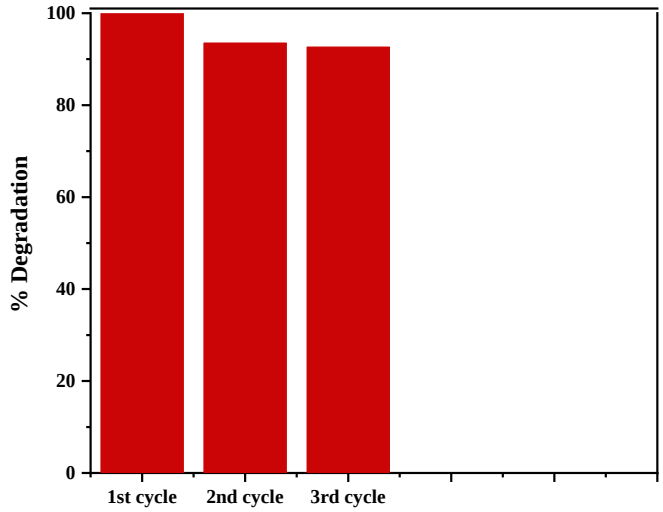

Figure 3.17: Bar diagram showing the Recyclability of PFO

3.2.12 Photocatalytic H_2O_2 production

For confirming the ROS production in the photocatalytic conditions, photocatalytic production of H_2O_2 is performed with both PFO/TiO_2 nanocomposite and bare TiO_2 and the results are given below (Figure 3.18)

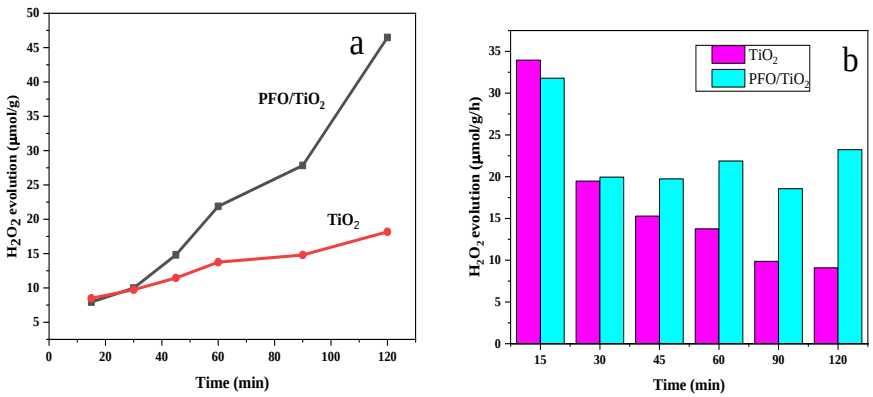

Figure 3.18: (a) Evolution of H_2O_2 with irradiation time (b**)** Rate of evolution of H_2O_2 with irradiation time

For the first 30 min, both the catalyst exhibited the same performance, however, after 30 min the performance of PFO/TiO_2 photocatalyst is observed to be far superior compared to that of P25 titania. The better performance of the nanocomposite catalyst can be attributed to higher ROS production resulting from lower recombination of charge carriers as a consequence of direct Z-scheme mechanism between PFO and TiO_2 photocatalysts.

3.2.13 DFT Calculations for the energetics of the $C_{60}O + C_{60} \rightarrow C_{120}O$ reaction.

For a better understanding of the networking of fullerene balls via [3+2] cyclo-additions, DFT calculations are performed for the reaction $C_{60}O + C_{60} \rightarrow C_{120}O$.

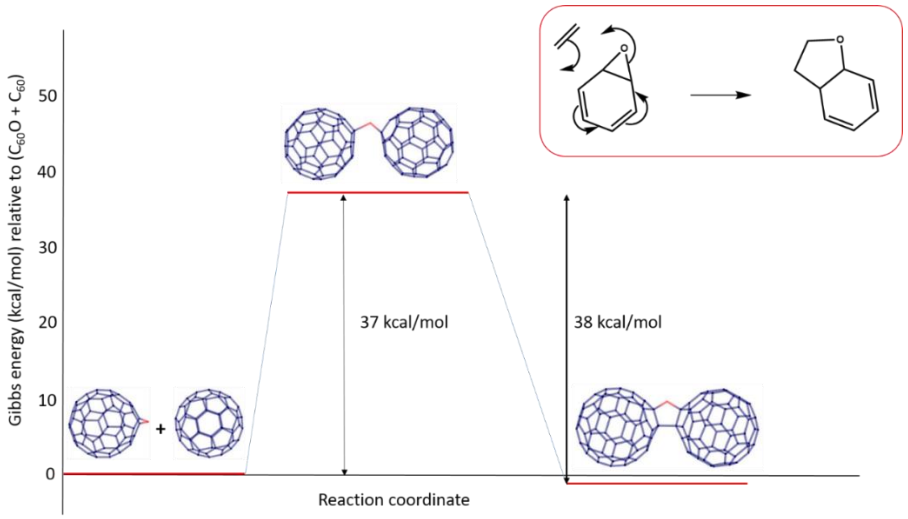

Figure 3.19: Energetics of the reaction $C_{60}O + C_{60} \rightarrow C_{120}O$, calculated using M06-2X functional and 6-31g basis set. The mechanism is shown schematically in the inset, with benzene epoxide and ethylene as model systems.

It has been proposed earlier that the reaction of C_{60} with $C_{60}O$ proceeds via the ring opening of fullerene epoxide to form a diradical, which then reacts with C_{60} to form $C_{120}O$. [78] However, it is very unlikely for this diradical to attack another fullerene, instead of recombining to form fullerene epoxide, considering that the former has an entropy cost. We have found a concerted pathway, which is similar to the mechanism reported for the dissociation of $C_{120}O$.[79] The Gibbs energy of activation

for this is 37 kcal/mol, which can be easily surmounted by the reaction temperature of 200 ˚C. Interestingly, this is 3+2 cycloaddition, assisted by the epoxide ring-opening (see inset, Fig. 3.18).

3.3 Electrochemical measurements

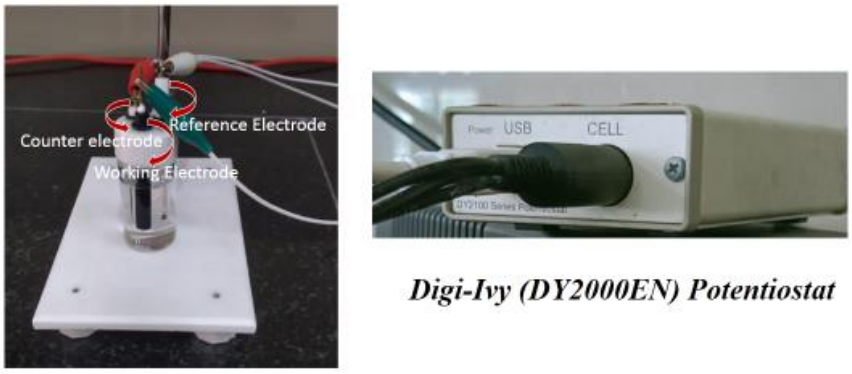

Figure 3.20: Electrochemical sensing studies: Experimental setup

Investigations on the electrochemical performance of prepared PFO modified glassy carbon electrode are carried out using potassium ferrocyanide/ferricyanide redox probe with an aim to find out the electrochemically active surface area. Cyclic voltametric measurements are performed with 5 mM potassium ferrocyanide solution, PBS buffer (pH 7.4) and 0.1 M KCl as supporting electrolyte and the resultant cyclic voltammograms for bare GCE as well as PFO modified GCE are presented in figure 3.21.

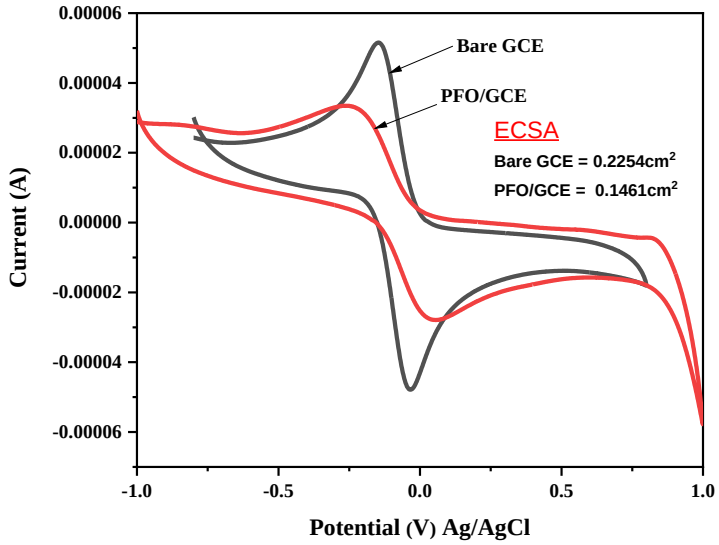

Figure 3.21: Cyclic Voltammetric (CV) curves of 5 mM $K_3[Fe(CN)_6]$ (pH 7.4 PBS) with KCl as supporting electrolyte on PFO/GCE at a scan rate of 50 mV/s.

The Electro-Chemically active Surface Area (ECSA) can be calculated using the Randles-Sevcik equation:

$$Ip = 2.69\times10^5 AD^{1/2}n^{3/2}\gamma^{1/2}C$$

Ip is the Peak current, A is the ECSA, D is the diffusion coefficient, n is the number of transferred electrons in the redox couple, γ is the scan rate and C is the concentration of the analyte. The ECSA values of bare GCE, PFO/GCE are observed to be 0.2254 cm^2, 0.1461 cm^2 respectively. The lower value of electrochemically-active surface area of PFO compared to bare GCE can be attributed to the semiconducting nature of PFO resulting in low value of peak current. The low ECSA value does not indicate lower sensing performance.

The effect of scan rate for glucose in phosphate buffer Solution (PBS pH 7.4) is studied, again by cyclic voltammetry and the results are summarized in figure 3.22. From the results, it was found that peak current increases with the increase in scan rate as shown in figure 3.22a. A calibration plot of peak current against the square root of scan rate (figure 3.22b) gives a straight line with good linearity (R^2 0.9988). From this, it can be derived that electron transfer in PFO- modified GCE is a diffusion-controlled process.

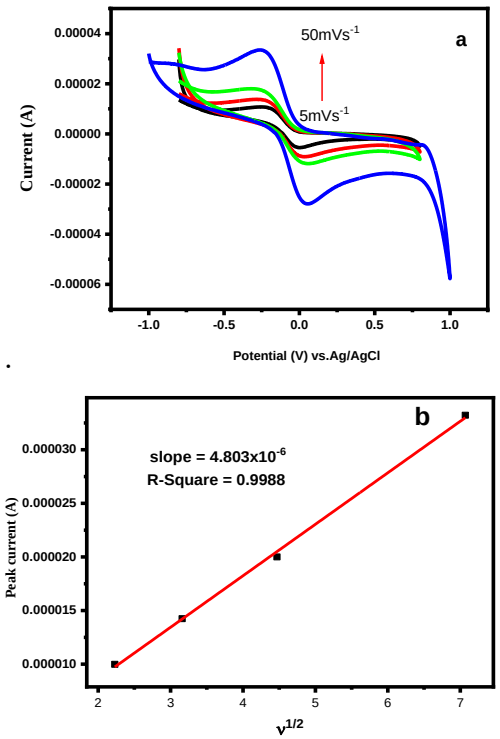

Figure 3.22 : (a) Cyclic Voltammetric (CV) curves of 5 mM $K_3[Fe(CN)_6]$ (pH 7.4 PBS) of PFO/GCE at different scan rates (b) Calibration plot of peak current Vs. the square root of the scan rate.

3.3.1 Differential Pulse Voltammetric (DPV) measurements

Differential Pulse Voltammetry is considered to be a superior method than the cyclic voltammetry for the low-level detection of analytes.[80] In the present investigation, we have selected the DPV method for glucose sensing. The PFO/GC electrode is used as the electrode in 10 ml of PBS Buffer solution (pH 7.4) with 0.1 M KCl as supporting electrolyte and. In all these cases, two oxidation peaks are found to increase in intensity, and it is observed that the peak current increases with the successive addition of glucose as shown in figure 3.23a. The variation of peak current of the oxidation peak at 0.04972 V is monitored with the different concentrations of analyte (glucose) molecules and a calibration plot of peak current against the molar concentration of glucose is made which gives a straight line with an R^2 value of 0.9917 as shown in figure 3.23b.

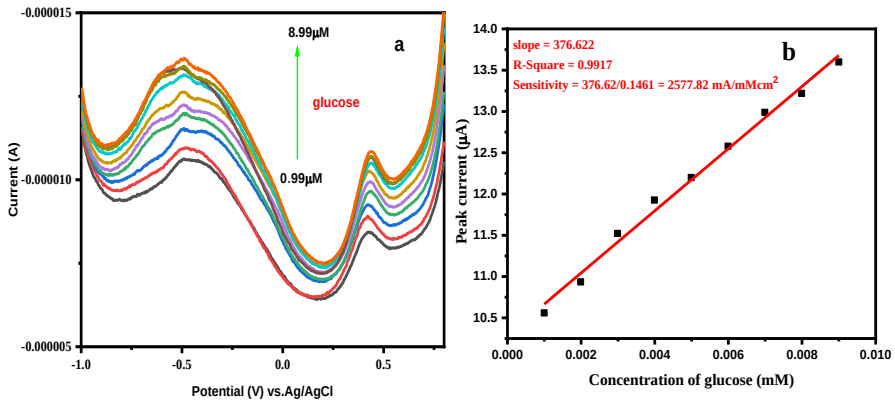

Figure 3.23: (a) Differential pulse voltammetric curves at different concentrations of glucose on PFO/GCE in PBS buffer at pH = 7.4 with 0.1 M KCl as supporting electrolyte.(b) Calibration plot for PFO/GCE, showing the linear variation in peak-current.

To investigate the possible interferences of different types of biomarkers towards the the detection of glucose, an equimolar mixture

of (1.5 mM) Uric acid, Ascorbic acid, and H_2O_2 is prepared. 10 µM of UA, AA, and H_2O_2 is added to the 0.1 M PBS solution (pH 7.4) containing 10 µM glucose. It is observed that no interferences in the determination of glucose.

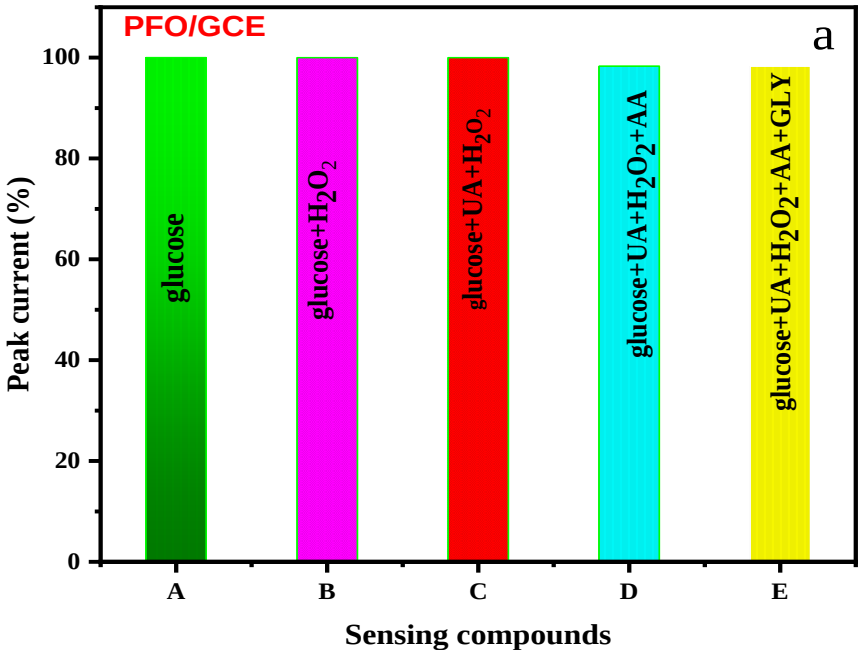

Figure 3.24: Effect of interfering compounds such as H_2O_2, Ascorbic acid (AA), Uric acid (UA), and Glycine (GLY) on the peak current of glucose with PFO/GCE sensing platform.

The Limit of Detection (LOD) of PFO/GCE is found to be 3.086 µM, calculated from the relation $3xS.D_{bl.}$ /m, where $S.D_{bl}$. is the standard deviation of the blank solution obtained from ten consecutive differential pulse voltammetric measurements and m is the slope of the calibration curve. and the sensitivity is calculated to be 2577.82 $\mu AmM^{-1}cm^{-2}$ obtained from the relation, slope of the calibration curve/ECSA of

the electrode. The linear range for PFO/GCE electrodes is observed to be 0.99 μM-9 μM. Thus, PFO can be considered as an efficient sensing platform for glucose.

3.3.4. Comparison of electrochemical glucose sensors in literature with the present work

Electrochemical performance of our electrode material, PFO is compared with that of other non-enzymatic glucose sensing electrode materials and it is summarized below in Table 3.1. It is found that PFO shows high sensitivity, better selectivity as well as a very low detection limit, thus, offering much promise as a glucose sensing platform.

Table 3.1. Electrochemical performances of non-enzymatic glucose sensing electrode materials.

Sl No.	Electrode material	Technique used	Linear range (mM)	Sensitivity ($\mu A/mMcm^2$)	Limit of Detection(μM)	Ref
1	Nanoporous PtPb	CV	1.0-16 mM	10.8	---	[75]
2	Mesoporous Pt	CV	0-10 mM	9.6	---	[69]
3	Porous Au	CV	2.0-10 mM	11.8	5	[81]
4	Pt-Pb/CNTs	CV	Upto 11 mM	17.8	1	[82]
5	MnO_2/MWCNTs	CV	10 μM-28 Mm	33.19	10	[83]
6	Cu/MWCNTs	CV	0.7-3.5 mM	251.4	0.21	[84]
7	$Ni(OH)_2$/CILE	CV	0.05-23 mM	202	6	[85]
8	Cu-in-ZIF-B	CV	---	0.412	2.76	[86]
9	ZIF-67	CV	---	0.152	1.62	[87]
10	Ag@TiO_2@ZIF-67	AMP	48 μM-1 mM	0.788	0.99	[88]
11	PFO/GCE	CV	0.99 μM-9 μM	2577.2	3.086	This work

3.3. Conclusions

In this work, we have successfully prepared a new class of highly efficient metal-free, nanostructured polymeric fullerene oxide frameworks possessing pore architectures made up of macropores and mesopores, plausibly through the interlinking via thermal [3+2] cycloadditions of fullerene oxides formed by the thermal decomposition of $C_{60}Br_{24}$. The DFT calculations to understand the interlinking of fullerene balls showed that Gibbs energy of activation is found to be 37 kcal/mol. The interlinking process is understood as [3+2] cycloaddition, assisted by the simultaneous epoxide ring-opening. Polymeric fullerene oxide network is found to be a semiconductor with narrow bandgap and is shown to function as an excellent visible light active photocatalyst. With the proposed band diagram for PFO, the plausible mechanism of ROS production and the photocatalytic process has been proposed. According to this, the superoxide anion formation is the primary reaction in the dye degradation whereas the oxidation of the hydroxide ion to hydroxide radical by the holes migrated to the surface as a primary process have been ruled out. The ROS production in photocatalytic conditions is further confirmed by carrying out photocatalytic H_2O_2 production with PFO/TiO_2 and pristine TiO_2 catalysts under sunlight irradiation, a known reaction in which ROS production is involved in the mechanism. PFO/TiO_2 catalyst is found to perform better in longer irradiation times. Polymeric fullerene oxide network is found to be a better electrochemical non- enzymatic, mediator free, sensor for the detection of biomarker, glucose. The high sensitivity, large linear range,

and the high selectivity with negligible electrochemical interferences from other substances like uric acid, H_2O_2, and ascorbic acid, exhibited by PFO makes it an excellent choice as a sensing platform for the low level detection of glucose.

References

(1) Slepičková Kasálková, N.; Slepička, P.; Švorčík, V. Carbon Nanostructures, Nanolayers, and Their Composites. *Nanomaterials* **2021**, *11* (9), 2368. https://doi.org/10.3390/nano11092368.

(2) Hu, Y.; Shenderova, O. A.; Hu, Z.; Padgett, C. W.; Brenner, D. W. Carbon Nanostructures for Advanced Composites. *Rep. Prog. Phys.* **2006**, *69* (6), 1847–1895. https://doi.org/10.1088/0034-4885/69/6/R05.

(3) Power, A. C.; Gorey, B.; Chandra, S.; Chapman, J. Carbon Nanomaterials and Their Application to Electrochemical Sensors: A Review. *Nanotechnology Reviews* **2018**, *7* (1), 19–41. https://doi.org/10.1515/ntrev-2017-0160.

(4) Thiruvengadathan, R.; Roy, S. C.; Sundriyal, P.; Bhattacharya, S. *Carbon Nanostructures*; AIP Publishing Books; AIP Publishing LLC, 2021. https://doi.org/10.1063/9780735423114.

(5) Pan, Y.; Liu, X.; Zhang, W.; Liu, Z.; Zeng, G.; Shao, B.; Liang, Q.; He, Q.; Yuan, X.; Huang, D.; Chen, M. Advances in Photocatalysis Based on Fullerene C_{60} and Its Derivatives: Properties, Mechanism, Synthesis, and Applications. *Applied Catalysis B: Environmental* **2020**, *265*, 118579. https://doi.org/10.1016/j.apcatb.2019.118579.

(6) Huang, L.; Zhao, J. C_{60}-Bodipy Dyad Triplet Photosensitizers as Organic Photocatalysts for Photocatalytic Tandem Oxidation/[3+2] Cycloaddition Reactions to Prepare Pyrrolo[2,1-a]Isoquinoline. *Chem. Commun.* **2013**, *49* (36), 3751. https://doi.org/10.1039/c3cc41494a.

(7) Song, L.; Guo, C.; Li, T.; Zhang, S. C_{60}/Graphene/g-C_3N_4 Composite Photocatalyst and Mutually- Reinforcing Synergy to Improve Hydrogen Production in Splitting Water under Visible Light

(8) Saraswati, T. E.; Setiawan, U. H.; Ihsan, M Radiation. *Ceramics International* **2017**, *43* (10), 7901–7907. https://doi.org/10.1016/j.ceramint.2017.03.115.. R.; Isnaeni, I.; Herbani, Y. The Study of the Optical Properties of C_{60} Fullerene in Different Organic Solvents. *Open Chemistry* **2019**, *17* (1), 1198–1212. https://doi.org/10.1515/chem-2019-0117.

(9) Kumar, I.; Sharma, R.; Kumar, R.; Kumar, R.; Sharma, U. C_{70} Fullerene-Catalyzed Metal-Free Photocatalytic Ipso-Hydroxylation of

Aryl Boronic Acids: Synthesis of Phenols. *Advanced Synthesis & Catalysis* **2018**, *360* (10), 2013–2019. https://doi.org/10.1002/adsc.201701573.

(10) Panagiotou, G. D.; Tzirakis, M. D.; Vakros, J.; Loukatzikou, L.; Orfanopoulos, M.; Kordulis, C.; Lycourghiotis, A. Development of [60] Fullerene Supported on Silica Catalysts for the Photo-Oxidation of Alkenes. *Applied Catalysis A: General* **2010**, *372* (1), 16–25. https://doi.org/10.1016/j.apcata.2009.09.046.

(11) Kumar, R.; Gleissner, E. H.; Tiu, E. G. V.; Yamakoshi, Y. C_{70} as a Photocatalyst for Oxidation of Secondary Benzylamines to Imines. *Org Lett* **2016**, *18* (2), 184–187. https://doi.org/10.1021/acs.orglett.5b03194.

(12) Doi, Y.; Takai, A.; Makino, S.; Radhakrishnan, L.; Suzuki, N.; Sugimoto, W.; Yamauchi, Y.; Kuroda, K. Synthesis of Mesoporous Carbon Using a Fullerenol-Based Precursor Solution via Nanocasting with SBA-15. *Chem. Lett.* **2010**, *39* (7), 777–779. https://doi.org/10.1246/cl.2010.777.

(13) Mondal, S. K. Synthesis of Novel Mesoporous Fullerene and Its Application to Electro-Oxidation of Methanol. *arXiv:1004.4046 [cond-mat]* **2011**.

(14) Liang, C.; Li, Z.; Dai, S. Mesoporous Carbon Materials: Synthesis and Modification. *Angewandte Chemie (International ed. in English)* **2008**, *47*, 3696–3717. https://doi.org/10.1002/anie.200702046.

(15) Yanagida, S.; Kabumoto, A.; Mizumoto, K.; Pac, C.; Yoshino, K. Poly(p-Phenylene)-Catalysed Photoreduction of Water to Hydrogen. *J. Chem. Soc., Chem. Commun.* **1985**, No. 8, 474–475. https://doi.org/10.1039/C39850000474.

(16) Li, C.; Xu, Y.; Tu, W.; Chen, G.; Xu, R. Metal-Free Photocatalysts for Various Applications in Energy Conversion and Environmental Purification. *Green Chemistry* **2017**, *19*, 882–899. https://doi.org/10.1039/c6gc02856j.

(17) Yao, S.; Yuan, X.; Jiang, L.; Xiong, T.; Zhang, J. Recent Progress on Fullerene-Based Materials: Synthesis, Properties, Modifications, and Photocatalytic Applications. *Materials* **2020**, *13* (13), 2924. https://doi.org/10.3390/ma13132924.

(18) Ehtisham Khan, M. State-of-the-Art Developments in Carbon-Based Metal Nanocomposites as a Catalyst: Photocatalysis. *Nanoscale Advances* **2021**, *3* (7), 1887–1900. https://doi.org/10.1039/D1NA00041A.

(19) Veerakumar, P.; Thanasekaran, P.; Subburaj, T.; Lin, K.-C. A Metal-Free Carbon-Based Catalyst: An Overview and Directions for Future Research. *C* **2018**, *4* (4), 54. https://doi.org/10.3390/c4040054.

(20) Zhang, Y.; Schilling, W.; Riemer, D.; Das, S. Metal-Free Photocatalysts for the Oxidation of Non-Activated Alcohols and the Oxygenation of Tertiary Amines Performed in Air or Oxygen. *Nat Protoc* **2020**, *15* (3), 822–839. https://doi.org/10.1038/s41596-019-0268-x.

(21) Shiraishi, Y.; Takii, T.; Hagi, T.; Mori, S.; Kofuji, Y.; Kitagawa, Y.; Tanaka, S.; Ichikawa, S.; Hirai, T. Resorcinol-Formaldehyde Resins as Metal-Free Semiconductor Photocatalysts for Solar-to-Hydrogen Peroxide Energy Conversion. *Nat Mater* **2019**, *18* (9), 985–993. https://doi.org/10.1038/s41563-019-0398-0.

(22) Benzigar, M. R.; Joseph, S.; Ilbeygi, H.; Park, D.-H.; Sarkar, S.; Chandra, G.; Umapathy, S.; Srinivasan, S.; Talapaneni, S. N.; Vinu, A. Highly Crystalline Mesoporous C_{60} with Ordered Pores: A Class of Nanomaterials for Energy Applications. *Angewandte Chemie International Edition* **2018**, *57* (2), 569–573. https://doi.org/10.1002/anie.201710888.

(23) Ignat, M.; Pastravanu, C.; Popovici, E. Mesoporous Carbon Pipes-Suitable Materials for Photocatalytic Supports. In *CAS 2010 Proceedings (International Semiconductor Conference)*; 2010; Vol. 02, pp 379–382. https://doi.org/10.1109/SMICND.2010.5650615.

(24) Chai, B.; Liao, X.; Song, F.; Zhou, H. Fullerene Modified C_3N_4 Composites with Enhanced Photocatalytic Activity under Visible Light Irradiation. *Dalton Trans.* **2013**, *43* (3), 982–989. https://doi.org/10.1039/C3DT52454J.

(25) Lian, Z.; Xu, P.; Wang, W.; Zhang, D.; Xiao, S.; Li, X.; Li, G. C_{60}-Decorated CdS/TiO_2 Mesoporous Architectures with Enhanced Photostability and Photocatalytic Activity for H_2 Evolution. *ACS Appl. Mater. Interfaces* **2015**, *7* (8), 4533–4540. https://doi.org/10.1021/am5088665.

(26) Baskar, A. V.; Ruban, A. M.; Davidraj, J. M.; Singh, G.; Al-Muhtaseb, A. H.; Lee, J. M.; Yi, J.; Vinu, A. Single-Step Synthesis of 2D Mesoporous C_{60} /Carbon Hybrids for Supercapacitor and Li-Ion Battery Applications. *BCSJ* **2021**, *94* (1), 133–140. https://doi.org/10.1246/bcsj.20200265.

(27) Zhong, Y.; Munir, R.; Balawi, A. H.; Sheikh, A. D.; Yu, L.; Tang, M.-C.; Hu, H.; Laquai, F.; Amassian, A. Mesostructured Fullerene Electrodes for Highly Efficient n–i–p Perovskite Solar Cells. *ACS Energy Lett.* **2016**, *1* (5), 1049–1056. https://doi.org/10.1021/acsenergylett.6b00455.

(28) Wang, S.; Dai, T.; Lu, Y.; Chen, Q.; Feng, L.; Sui, Z. Fullerene-Bearing Porous Polymer via Ball-Milling Approach and Its Palladium Composite for Catalytic Deallylation. *Microporous and Mesoporous Materials* **2020**.

(29) Bezzu, C. G.; Burt, L. A.; McMonagle, C. J.; Moggach, S. A.; Kariuki, B. M.; Allan, D. R.; Warren, M.; McKeown, N. B. Highly Stable Fullerene-Based Porous Molecular Crystals with Open Metal Sites. *Nat Mater* **2019**, *18* (7), 740–745. https://doi.org/10.1038/s41563-019-0361-0.

(30) Benzigar, M. R.; Joseph, S.; Saianand, G.; Gopalan, A.-I.; Sarkar, S.; Srinivasan, S.; Park, D.-H.; Kim, S.; Talapaneni, S. N.; Ramadass, K.; Vinu, A. Highly Ordered Iron Oxide-Mesoporous Fullerene Nanocomposites for Oxygen Reduction Reaction and Supercapacitor Applications. *Microporous and Mesoporous Materials* **2019**, *285*, 21–31. https://doi.org/10.1016/j.micromeso.2019.04.071.

(31) Xu, T.; Yu, D.; Du, Z.; Huang, W.; Lu, X. Two-Dimensional Mesoporous Carbon Materials Derived from Fullerene Microsheets for Energy Applications. *Chemistry* **2020**, *26* (47), 10811–10816. https://doi.org/10.1002/chem.202001404.

(32) Shrestha, L. K.; Yamauchi, Y.; Hill, J. P.; Miyazawa, K.; Ariga, K. Fullerene Crystals with Bimodal Pore Architectures Consisting of Macropores and Mesopores. *J Am Chem Soc* **2013**, *135* (2), 586–589. https://doi.org/10.1021/ja3108752.

(33) Bairi, P.; Tsuruoka, T.; Acharya, S.; Ji, Q.; Hill, J. P.; Ariga, K.; Yamauchi, Y.; Shrestha, L. K. Mesoporous Fullerene C_{70} Cubes with Highly Crystalline Frameworks and Unusually Enhanced

Photoluminescence Properties. *Mater. Horiz.* **2018**, *5* (2), 285–290. https://doi.org/10.1039/C7MH00954B.

(34) Tebbe, F. N.; Harlow, R. L.; Chase, D. B.; Thorn, D. L.; Campbell, G. C.; Calabrese, J. C.; Herron, N.; Young, R. J.; Wasserman, E. Synthesis and Single-Crystal X-Ray Structure of a Highly Symmetrical C_{60} Derivative, $C_{60}Br_{24}$.*Science* **1992**, *256* (5058), 822–825. https://doi.org/10.1126/science.256.5058.822

(35) Karel, K. Fullerene C_{60}, Graphene-Oxide and Graphene-Oxide Foil with Fullerene and Their Bromination. *IJMSA* **2014**, *3* (6), 293. https://doi.org/10.11648/j.ijmsa.20140306.13.

(36) Fowler, P. W.; Hansen, P.; Rogers, K. M.; Fajtlowicz, S. $C_{60}Br_{24}$ as a Chemical Illustration of Graph Theoretical Independence. *J. Chem. Soc., Perkin Trans. 2* **1998**, No. 7, 1531–1534. https://doi.org/10.1039/A803459A.

(37) Djordjević, A.; Vojínović-Miloradov, M.; Petranović, N.; Devečerski, A.; Lazar, D.; Ribar, B. Catalytic Preparation and Characterization of $C_{60}Br_{24}$. *Fullerene Science and Technology* **1998**, *6* (4), 689–694. https://doi.org/10.1080/10641229809350229.

(38) Đorđević, A. N.; Vojinović Miloradov, M. B.; Petranović, N. A.; Devečerski, A.; Lazar, D. V.; Ribar, B. J. Catalytic Preparation and Characterization of $C_{60}Br_{24}$. *Fullerene Science and Technology* **1998**, *6* (4), 689–694. https://doi.org/10.1080/10641229809350229.

(39) Mehrotra, R.; Lal, D.; Tripathi, V. S.; Mathur, G. N. Preparation and Charecterization of Bromofullerenes in New Stoichiometry. *Carbon letters* **2003**, *4* (4), 175–179.

(40) Huang, S.; Xiao, Z.; Wang, F.; Gan, L.; Zhang, X.; Hu, X.; Zhang, S.; Lu, M.; Pan, Q.; Xu, L. Selective Preparation of Oxygen-Rich [60]Fullerene Derivatives by Stepwise Addition of Tert-Butylperoxy Radical and Further Functionalization of the Fullerene Mixed Peroxides. *J. Org. Chem.* **2004**, *69* (7), 2442–2453. https://doi.org/10.1021/jo049974q.

(41) Resmi, M. R.; Ma, S.; Caprioli, R.; Pradeep, T. $C_{120}O_n$ from $C_{60}Br_{24}$. *Chemical Physics Letters* **2001**, *333* (6), 515–521. https://doi.org/10.1016/S0009-2614(00)01415-9.

(42) Jiang, S.-P.; Duan, S.; Liu, K.-Q.; Yang, X.-Y.; Cheng, C.; Li, J.; Wang, G.-W. Highly Efficient Synthesis of [60]Fullerene Oxides by Plasma Jet. *R Soc Open Sci* **2017**, *4* (9), 170658. https://doi.org/10.1098/rsos.170658.

(43) Hou, H.; Zeng, X.; Zhang, X. Production of Hydrogen Peroxide by Photocatalytic Processes. *Angew. Chem. Int. Ed.* **2020**, *59* (40), 17356–17376. https://doi.org/10.1002/anie.201911609.

(44) Bader, H.; Sturzenegger, V.; Hoigné, J. Photometric Method for the Determination of Low Concentrations of Hydrogen Peroxide by the Peroxidase Catalyzed Oxidation of N,N-Diethyl-p-Phenylenediamine (DPD). *Water Research* **1988**, *22* (9), 1109–1115. https://doi.org/10.1016/0043-1354(88)90005-X.

(45) Teymourian, H.; Parrilla, M.; Sempionatto, J. R.; Montiel, N. F.; Barfidokht, A.; Van Echelpoel, R.; De Wael, K.; Wang, J. Wearable Electrochemical Sensors for the Monitoring and Screening of Drugs. *ACS Sens.* **2020**, *5* (9), 2679–2700. https://doi.org/10.1021/acssensors.0c01318.

(46) Pandey, R. R.; Chusuei, C. C. Carbon Nanotubes, Graphene, and Carbon Dots as Electrochemical Biosensing Composites. *Molecules* **2021**, *26* (21), 6674. https://doi.org/10.3390/molecules26216674.

(47) Kimmel, D. W.; LeBlanc, G.; Meschievitz, M. E.; Cliffel, D. E. Electrochemical Sensors and Biosensors. *Anal. Chem.* **2012**, *84* (2), 685–707. https://doi.org/10.1021/ac202878q.

(48) Stradiotto, N. R.; Yamanaka, H.; Zanoni, M. V. B. Electrochemical Sensors: A Powerful Tool in Analytical Chemistry. *J. Braz. Chem. Soc.* **2003**, *14*, 159–173. https://doi.org/10.1590/S0103-50532003000200003.

(49) Pullano, S. A.; Greco, M.; Bianco, M. G.; Foti, D.; Brunetti, A.; Fiorillo, A. S. Glucose Biosensors in Clinical Practice: Principles, Limits and Perspectives of Currently Used Devices. *Theranostics* **2022**, *12* (2), 493–511. https://doi.org/10.7150/thno.64035.

(50) McCreery, R. L. Advanced Carbon Electrode Materials for Molecular Electrochemistry. *Chem. Rev.* **2008**, *108* (7), 2646–2687. https://doi.org/10.1021/cr068076m.

(51) Faridbod, F.; Gupta, V. K.; Zamani, H. A. Electrochemical Sensors and Biosensors. *International Journal of Electrochemistry* **2012**, *2011*, e352546. https://doi.org/10.4061/2011/352546.

(52) Hoffman, M.; MD. *How the Blood Sugar of Diabetes Affects the Body*. WebMD. https://www.webmd.com/diabetes/how-sugar-affects-diabetes (accessed 2022-04-13).

(53) Ventura, E. E.; Davis, J. N.; Goran, M. I. Sugar Content of Popular Sweetened Beverages Based on Objective Laboratory Analysis: Focus on Fructose Content. *Obesity (Silver Spring)* **2011**, *19* (4), 868–874. https://doi.org/10.1038/oby.2010.255.

(54) Tsai, Y.-C.; Li, S.-C.; Chen, J.-M. Cast Thin Film Biosensor Design Based on a Nafion Backbone, a Multiwalled Carbon Nanotube Conduit, and a Glucose Oxidase Function. *Langmuir* **2005**, *21* (8), 3653–3658. https://doi.org/10.1021/la0470535.

(55) Newman, J. D.; White, S. F.; Tothill, I. E.; Turner, A. P. F. Catalytic Materials, Membranes and Fabrication Technologies Suitable for the Construction of Amperometric Biosensors. *Analytical Chemistry* **1995**, *67* (24), 4594–4599.

(56) Guiseppi-Elie, A.; Lei, C.; Baughman, R. H. Direct Electron Transfer of Glucose Oxidase on Carbon Nanotubes. *Nanotechnology* **2002**, *13* (5), 559. https://doi.org/10.1088/0957-4484/13/5/303.

(57) Zhao, Y.-D.; Zhang, W.-D.; Chen, H.; Luo, Q.-M. Direct Electron Transfer of Glucose Oxidase Molecules Adsorbed onto Carbon Nanotube Powder Microelectrode. *ANAL. SCI.* **2002**, *18* (8), 939–941. https://doi.org/10.2116/analsci.18.939.

(58) Liu, Y.; Wang, M.; Zhao, F.; Xu, Z.; Dong, S. The Direct Electron Transfer of Glucose Oxidase and Glucose Biosensor Based on Carbon Nanotubes/Chitosan Matrix. *Biosens Bioelectron* **2005**, *21* (6), 984–988. https://doi.org/10.1016/j.bios.2005.03.003.

(59) Hassan, M. H.; Vyas, C.; Grieve, B.; Bartolo, P. Recent Advances in Enzymatic and Non-Enzymatic Electrochemical Glucose Sensing. *Sensors* **2021**, *21* (14), 4672. https://doi.org/10.3390/s21144672.

(60) Heller, A.; Feldman, B. Electrochemical Glucose Sensors and Their Applications in Diabetes Management. *Chem. Rev.* **2008**, *108* (7), 2482–2505. https://doi.org/10.1021/cr068069y.

(61) Bhalla, N.; Jolly, P.; Formisano, N.; Estrela, P. Introduction to Biosensors. *Essays Biochem* **2016**, *60* (1), 1–8. https://doi.org/10.1042/EBC20150001.

(62) Bhalla, N.; Jolly, P.; Formisano, N.; Estrela, P. Introduction to Biosensors. *Essays Biochem* **2016**, *60* (1), 1–8. https://doi.org/10.1042/EBC20150001.

(63) Nguyen, H. H.; Lee, S. H.; Lee, U. J.; Fermin, C. D.; Kim, M. Immobilized Enzymes in Biosensor Applications. *Materials (Basel)* **2019**, *12* (1), 121. https://doi.org/10.3390/ma12010121.

(64) Naresh, V.; Lee, N. A Review on Biosensors and Recent Development of Nanostructured Materials-Enabled Biosensors. *Sensors* **2021**, *21* (4), 1109. https://doi.org/10.3390/s21041109.

(65) Khor, S. M.; Choi, J.; Won, P.; Ko, S. H. Challenges and Strategies in Developing an Enzymatic Wearable Sweat Glucose Biosensor as a Practical Point-Of-Care Monitoring Tool for Type II Diabetes. *Nanomaterials (Basel)* **2022**, *12* (2), 221. https://doi.org/10.3390/nano12020221.

(66) Wilson, R.; Turner, A. P. F. Glucose Oxidase: An Ideal Enzyme. *Biosensors and Bioelectronics* **1992**, *7* (3), 165.

(67) Leong, K. L.; Ho, M. Y.; Lee, X. Y.; Yee, M. S.-L. A Review on the Development of Non-Enzymatic Glucose Sensor Based on Graphene-Based Nanocomposites. *NANO* **2020**, *15* (11), 2030004. https://doi.org/10.1142/S1793292020300042.

(68) Strakosas, X.; Selberg, J.; Pansodtee, P.; Yonas, N.; Manapongpun, P.; Teodorescu, M.; Rolandi, M. A Non-Enzymatic Glucose Sensor Enabled by Bioelectronic PH Control. *Sci Rep* **2019**, *9* (1), 1–7. https://doi.org/10.1038/s41598-019-46302-9.

(69) Park, S.; Boo, H.; Chung, T. D. Electrochemical Non-Enzymatic Glucose Sensors. *Analytica Chimica Acta* **2006**, *556* (1), 46–57. https://doi.org/10.1016/j.aca.2005.05.080.

(70) Wei, M.; Qiao, Y.; Zhao, H.; Liang, J.; Li, T.; Luo, Y.; Lu, S.; Shi, X.; Lu, W.; Sun, X. Electrochemical Non-Enzymatic Glucose Sensors: Recent Progress and Perspectives. *Chem. Commun.* **2020**, *56* (93), 14553–14569. https://doi.org/10.1039/D0CC05650B.

(71) Gong, X.; Gu, Y.; Zhang, F.; Liu, Z.; Li, Y.; Chen, G.; Wang, B. High-Performance Non-Enzymatic Glucose Sensors Based on CoNiCu Alloy Nanotubes Arrays Prepared by Electrodeposition. *Frontiers in Materials* **2019**, *6*.

(72) Ahmad, R.; Tripathy, N.; Ahn, M.-S.; Bhat, K. S.; Mahmoudi, T.; Wang, Y.; Yoo, J.-Y.; Kwon, D.-W.; Yang, H.-Y.; Hahn, Y.-B. Highly Efficient Non-Enzymatic Glucose Sensor Based on CuO Modified Vertically-Grown ZnO Nanorods on Electrode. *Sci Rep* **2017**, *7* (1), 1–10. https://doi.org/10.1038/s41598-017-06064-8.

(73) Naikoo, G. A.; Salim, H.; Hassan, I. U.; Awan, T.; Arshad, F.; Pedram, M. Z.; Ahmed, W.; Qurashi, A. Recent Advances in Non-Enzymatic Glucose Sensors Based on Metal and Metal Oxide Nanostructures for Diabetes Management- A Review. *Frontiers in Chemistry* **2021**, *9*.

(74) Zhu, H.; Li, L.; Zhou, W.; Shao, Z.; Chen, X. Advances in Non-Enzymatic Glucose Biosensors Based on Metal Oxides. *J. Mater. Chem. B* **2016**, *4*. https://doi.org/10.1039/C6TB02037B.

(75) Hwang, D.-W.; Lee, S.; Seo, M.; Chung, T. D. Recent Advances in Electrochemical Non-Enzymatic Glucose Sensors – A Review. *Analytica Chimica Acta* **2018**, *1033*, 1–34. https://doi.org/10.1016/j.aca.2018.05.051.

(76) Rahman, Md. M.; Saleh Ahammad, A. J.; Jin, J.-H.; Ahn, S. J.; Lee, J.-J. A Comprehensive Review of Glucose Biosensors Based on Nanostructured Metal-Oxides. *Sensors (Basel)* **2010**, *10* (5), 4855–4886. https://doi.org/10.3390/s100504855.

(77) Bengas, R.; Lahmar, H.; Mohamed Redha, K.; Mentar, L.; Azizi, A.; Schmerber, G.; Dinia, A. Electrochemical Synthesis of N-Type ZnS Layers on p-Cu_2O/n-ZnO Heterojunctions with Different Deposition Temperatures. *RSC Advances* **2019**, *9* (50), 29056–29069. https://doi.org/10.1039/C9RA04670D.

(78) Jones, M. A. G.; Britz, D. A.; Morton, J. J. L.; Khlobystov, A. N.; Porfyrakis, K.; Ardavan, A.; Briggs, G. A. D. Synthesis and Reactivity of N@C_{60}O. *Phys. Chem. Chem. Phys.* **2006**, *8* (17), 2083–2088. https://doi.org/10.1039/B601171C.

(79) Lee, S. M.; Lee, Y. H. Structures and Stabilities of Directly-Linked and Oxygen-Bridged Fullerene Dimers: A Density-Functional-Theory

Study. *Journal of the Korean Physical Society* **2011**, *58* (3), 482–486. https://doi.org/10.3938/jkps.58.482.

(80) Patil, V. B.; Sawkar, R. R.; Ilager, D.; Shetti, N. P.; Tuwar, S. M.; Aminabhavi, T. M. Glucose-Based Carbon Electrode for Trace-Level Detection of Acetaminophen. *Electrochemical Science Advances* **2022**, *2* (5), e202100117. https://doi.org/10.1002/elsa.202100117.

(81) Li, J.; Hu, H.; Li, H.; Yao, C. Recent Developments in Electrochemical Sensors Based on Nanomaterials for Determining Glucose and Its Byproduct H_2O_2. *Journal of Materials Science* **2017**, *52* (17), 10455–10470.

(82) Cui, H.-F.; Ye, J.-S.; Zhang, W.-D.; Li, C.-M.; Luong, J. H. T.; Sheu, F.-S. Selective and Sensitive Electrochemical Detection of Glucose in Neutral Solution Using Platinum-Lead Alloy Nanoparticle/Carbon Nanotube Nanocomposites. *Anal Chim Acta* **2007**, *594* (2), 175–183. https://doi.org/10.1016/j.aca.2007.05.047.

(83) Chen, C.; Ran, R.; Yang, Z.; Lv, R.; Shen, W.; Kang, F.; Huang, Z.-H. An Efficient Flexible Electrochemical Glucose Sensor Based on Carbon Nanotubes/Carbonized Silk Fabrics Decorated with Pt Microspheres. *Sensors and Actuators B: Chemical* **2018**, *256*, 63–70. https://doi.org/10.1016/j.snb.2017.10.067.

(84) Kang, B.-C.; Park, B.-S.; Ha, T.-J. Highly Sensitive Wearable Glucose Sensor Systems Based on Functionalized Single-Wall Carbon Nanotubes with Glucose Oxidase-Nafion Composites. *Applied Surface Science* **2019**, *470*, 13–18. https://doi.org/10.1016/j.apsusc.2018.11.101.

(85) Safavi, A.; Maleki, N.; Farjami, E. Fabrication of a Glucose Sensor Based on a Novel Nanocomposite Electrode. *Biosens Bioelectron* **2009**, *24* (6), 1655–1660. https://doi.org/10.1016/j.bios.2008.08.040.

(86) Shi, L.; Zhu, X.; Liu, T.; Zhao, H.; Lan, M. Encapsulating Cu Nanoparticles into Metal-Organic Frameworks for Nonenzymatic Glucose Sensing. *Sensors and Actuators B: Chemical* **2016**, *227*, 583–590. https://doi.org/10.1016/j.snb.2015.12.092.

(87) Meng, Z.-D.; Zhu, L.; Choi, J.-G.; Chen, M.-L.; Oh, W.-C. Effect of Pt Treated Fullerene/TiO_2 on the Photocatalytic Degradation of MO under Visible Light. *J. Mater. Chem.* **2011**, *21* (21), 7596–7603. https://doi.org/10.1039/C1JM10301F.

(88) Arif, D.; Hussain, Z.; Sohail, M.; Liaqat, M. A.; Khan, M. A.; Noor, T. A Non-Enzymatic Electrochemical Sensor for Glucose Detection Based on Ag@TiO_2@ Metal-Organic Framework (ZIF-67) Nanocomposite. *Frontiers in Chemistry* **2020**, *8*.

CHAPTER 4

HYDRAZINE REDUCTION OF HYDROGEN BONDED FULLEROL CLUSTERS FOR ELECTROCHEMICAL SENSING

4.1. Introduction

4.1.1. Introduction to fullerols

Fullerene cages are readily susceptible to addition reactions. [1] Hydroxylated fullerene, known as fullerols or fullerenols in which –OH groups are attached on the surface of the fullerene cage can be easily dispersed in water as nano-sized hydrogen bonded clusters. [2–4] Its water dispersibility increases with the increase in the number of hydroxyl groups attached to the C_{60} cage [5–7]. Fullerol aggregates have attracted lot of attention because of their energy related applications and their use in the field of biology as excellent antioxidants and radical scavengers. [8, 9] Keshri et al. reported that there are hydration shells around the nanoparticles and the surface hydroxylation is more dominant where the –OH groups are uniformly distributed on the fullerene cage. [10] There are many reports for the synthesis of fullerols with the large number of hydroxyl groups attached to fullerene cage such as $C_{60}(OH)_{44}.8H_2O$ prepared by the direct hydroxylation of pristine C_{60} in the presence of a phase transfer catalyst, TBAH, and alternatively in the presence of quarternary ammonium hydroxides.[11, 12] Fullerol $C_{60}(OH)_{27}$ can be synthesized in high yield by the high-speed vibration milling in the air at room temperature. [13] Another method for the preparation of highly water-dispersible polyhydroxylated fullerenes, as reported by Arrais et al. is by the reduction of C_{60} with Na/K alloy followed by stirring in presence of O_2. [14] An alternative strategy reported by Cataldo et al. is by the hydroxylation reaction on fluorinated C_{60}.[15] Polyhydroxylated C_{60} derivatives are also prepared by the hydrolysis of polycyclosulphated

precursors. [6] However, in most of these methods, there is a possibility of trace level contamination, which makes the final product not so compatible for biological antioxidant applications. There are reports of direct ultrasonication of C_{60} with 30% H_2O_2 in the presence of reagents like PTC, TBAH, etc. resulting in the formation of fullerols very easily. A recent report by Afreen et al. have demonstrated that direct ultrasonication of C_{60} with 30 % H_2O_2 without using any supporting reagents is capable of providing fullerols with high purity and excellent yield. [16] Depending on the number of hydroxyl groups attached to the surface of the fullerene cage, fullerols show changes in their colour from yellow to white. [17]

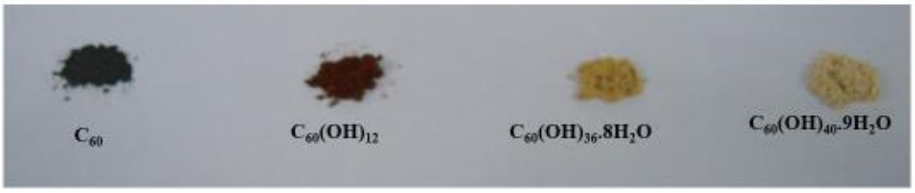

Figure 4.1: Colours of different fullerols previously reported (reprinted from kokubo et al. ref:26)

The reactivity of fullerols is significantly different from that of parent fullerenes. Fullerols are widely used as excellent hydrogen bonded catalysts in which –OH groups are employed for making hydrogen bonds with reactants and thus enhancing the reaction rate. [18] There are reports for the reduction of fullerols in water by zinc forming a hemiketal product. [19]

Fullerols are having important applications in the field of electrochemical sensing. [20]

4.1.2. Hydrazine reduction of fullerenes

C_{60} can be reduced by anhydrous hydrazine in CH_3OH to yield a mixture of fullerene hydrides like $C_{60}H_2$, $C_{60}H_4$, $C_{60}H_8$. [21] In this report, the authors suggest a probable mechanism in which the C_{60} itself may be acting as an oxidizing agent causing diimide formation from hydrazine, which is the active reducing agent causing hydrogenation. However, when pristine fullerenes are taken as the starting material, only a low degree of hydrogenation was achieved with hydrazine reagent.

4.1.3. Electrochemical sensing of H_2O_2

H_2O_2 is an important oxidative stress marker and biomarker which can be used in monitoring various diseases like diabetes, cardiovascular diseases, Alzheimer's, and neuro digestive disorders. [22] H_2O_2 concentration in the blood of a healthy person is found to be in the range of 0.8-6 μM. [23] Excessive accumulation of H_2O_2 in body cells may cause various diseases and disorders. Cancerous cells produce H_2O_2, so its detection and monitoring are found to be of very important in cancer therapy. Among the various methods proposed, electrochemical detection is more suitable for H_2O_2 monitoring because of its high selectivity, sensitivity, better reproducibility and cost effectiveness. [24] Carbon-based materials like CNTs, graphene, carbon black, etc. can be used as suitable sensing platforms in H_2O_2 sensors. [25] In the modified electrode surfaces H_2O_2 undergoes electrochemical oxidation or reduction to form products like H_2O and O_2.

In the present work, we selected the method of direct ultrasonication of C_{60} for the synthesis of fullerols.[16, 26] In this procedure, C_{60} is directly treated with 30 % H_2O_2 for 1 h followed by separation as a white precipitate by treating it with 85 ml of a mixture of three solvents, 2-propanol, diethyl ether and heptane in the volume ratio 7:5:5 respectively. White coloured, highly hydroxylated crystals of fullerols are separated and dried (figure 4.2.).

Figure 4.2: Photograph of white colored fullerol crystals separated

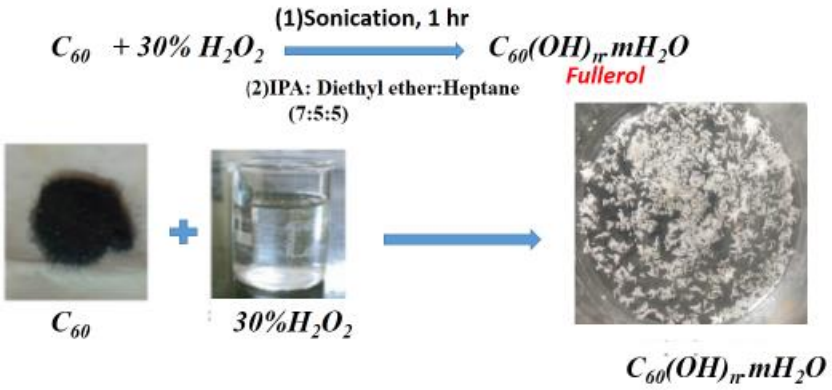

Figure 4.3: Diagram showing the preparation of fullerols

Fullerols thus prepared are subjected to hydrazine reduction resulting in the formation of a partially hydrogenated fullerol network (PHF). The various steps involved in the PHF preparation is schematically summarized in figure 4.4.

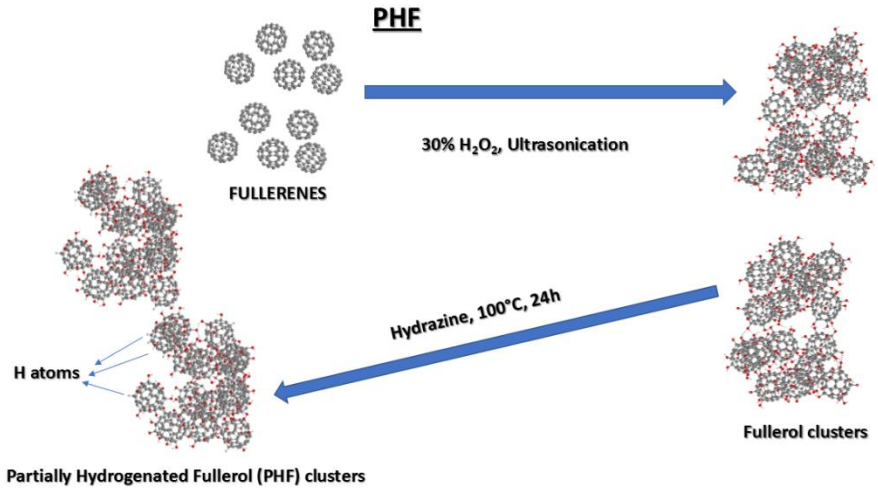

Figure 4.4: Schematic representation of preparation of Partially Hydrogenated Fullerol (PHF) network

Here, electrochemical detection of H_2O_2 is performed using PHF along with 1,10-phenanthroline, a well-known benchmark ligand. Herein, the electrochemical oxidation of 1,10-phenanthroline (phen) drop casted on a PHF modified GCE to 1,10-phenanthroline-5,6-dione (phen-dione)[27] is performed by continuous cyclic voltammetric running for15 cycles from -1 V to +1 V in a PBS solution of pH 7.4 containing 0.1 M KCl as supporting electrolyte. It is then dipped in 1 mM $CuSO_4$ solution for 180s for the binding of Cu^{2+} ions on the modified electrode surface. Its confinement to the PHF-modified glassy carbon electrode surface is ensured by repeating CV for another 15 cycles from -1 V to

+1 V in a PBS solution of pH 7.4. The resulting Cu^{2+}-phen-dione@PHF/GCE is used for the electrochemical sensing investigations of H_2O_2.

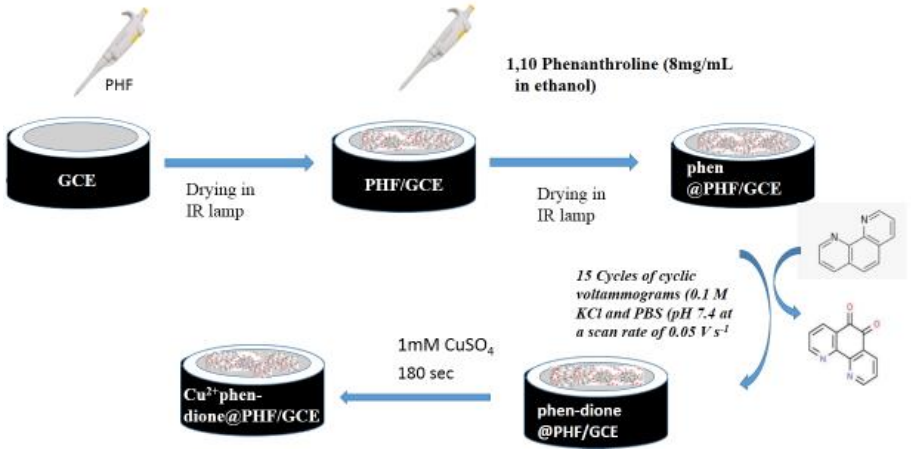

Figure 4.5: Shematic diagram showing the steps of fabrication of Cu^{2+}phen-dione@PHF/GCE sensor.

4.2 Results and discussion

White-colored highly hydroxylated fullerol crystals are separated and dried at 60 °C and is used for PHF preparation. The purpose of hydrogenation by hydrazine reduction is to reduce the water dispersibility of fullerol nanoparticles to some extent so that better binding of the fullerene-based material on the glassy carbon electrode surface can be achieved, so that it can be further utilized for H_2O_2 electrochemical sensing investigations. The characterization of the novel material developed in this study (PHF) is carried out using various spectroscopic and microscopic techniques and results obtained are presented below.

4.2.1 FTIR Analysis

Figure 4.6. shows the FTIR spectra of fullerols and PHF prepared. Fullerol shows four absorption peaks at 3442 cm^{-1}, 1634 cm^{-1}, 1380 cm^{-1}, and 1038 cm^{-1} corresponding to –OH stretching vibrations, C-OH in-plane bending, C-O stretching vibrations respectively. These four bands are the characteristic absorption band of fullerenols.[5, 6, 14, 28–31] A broad band around 3400 cm^{-1} confirms the aggregates of –OH functionalities. [32]

In PHF, after the hydrazine reduction process, even though by and large hydroxyl substitutions of fullerene balls are preserved to some extent, it can be observed that some additional peaks such as peaks at positions 2928 cm^{-1} and 2850 cm^{-1} (aliphatic C-H stretching bands) have appeared due to partial hydrogenation. Additionally, peaks corresponding to soft fragmentation of a few fullerene balls [33] resulting in the formation of aromatic products also can be seen at 3128 cm^{-1} (aromatic C-H stretching). The peak at 1719 cm^{-1} can be attributed to semi ketal C=O stretching formed due to the reduction of fullerols. [19] The peaks at 1421 cm^{-1}, 572 cm^{-1} and 524 cm^{-1} are characteristic peaks of fullerene balls formed after reduction. [34–36] The new peaks emerged in the region 1270 cm^{-1} -1200 cm^{-1} (gray shaded region in the figure 4.6) can be attributed to the newly formed C-O-C networking of fullerene balls during the reduction process.

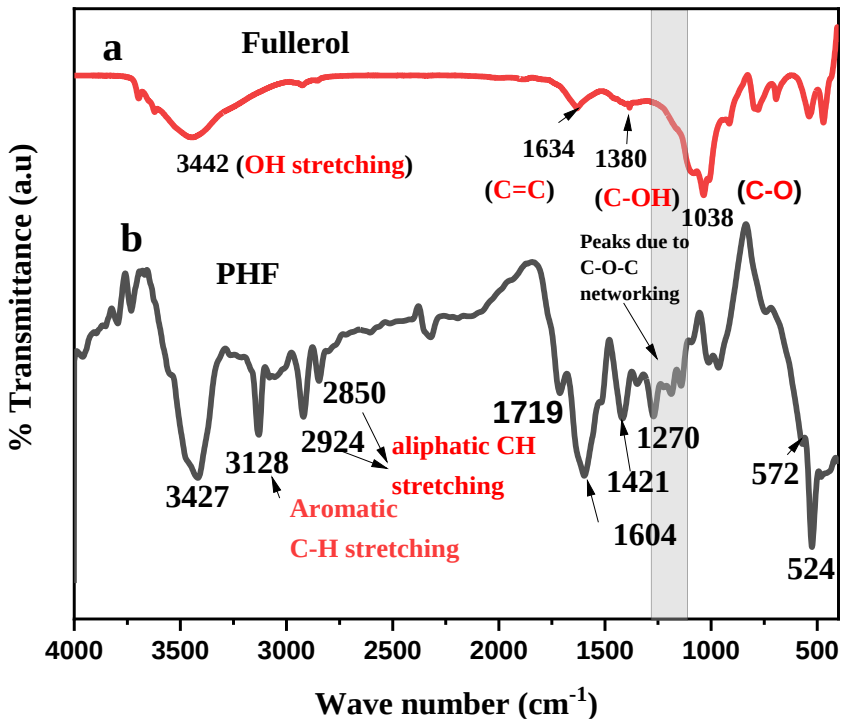

Figure 4.6: FTIR Spectra of (a) Fullerols and (b) PHF

4.2.2 Raman Analysis

Raman spectra are more sensitive to vibrations of relatively non-polar moieties such as –CH groups. Hydroxyl group vibrations are difficult to observe in Raman spectroscopic analysis. The heavily hydroxylated fullerol precursor prepared did not produce any Raman peaks (figure 4.7). For PHF, the peak at 3068 cm^{-1} corresponds to aromatic CH stretching, whereas the peak at 2914 cm^{-1} can be attributed to aliphatic–CH stretching, consistent with the results of FTIR analysis. The peak at 1598 cm^{-1} and at 1008 cm^{-1} also might have originated from the aromatic fragmentation products formed as a result of heavy

hydrogenation of few fullerene balls. The formation of these products points towards a limitation of fullerenes as a reversible hydrogen storage material by chemisorption.

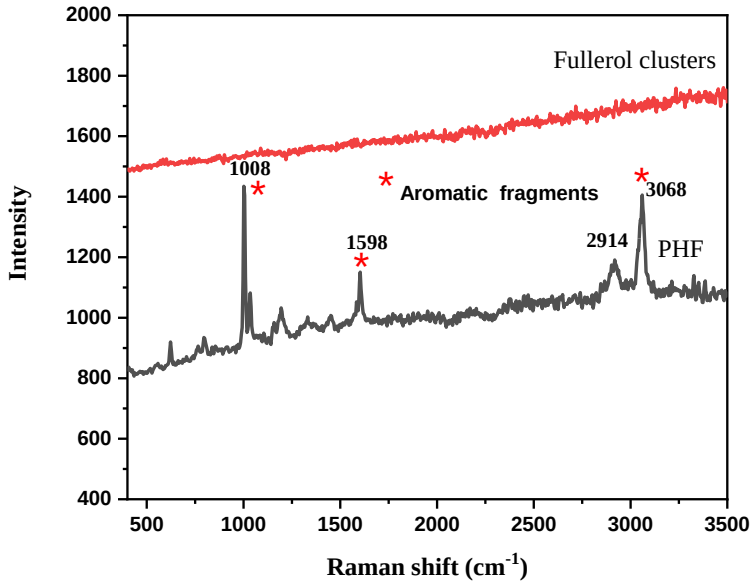

Figure 4.7: Raman Spectra of fullerol clusters and PHF

4.2.3 AFM Analysis

Figure 4.8 shows 2D and 3D AFM images of the PHF. Aggregation of partially hydrogenated fullerol balls in to small clusters is observed in the AFM image and the 3D image shows three-dimensional nature of the material with a rough surface.

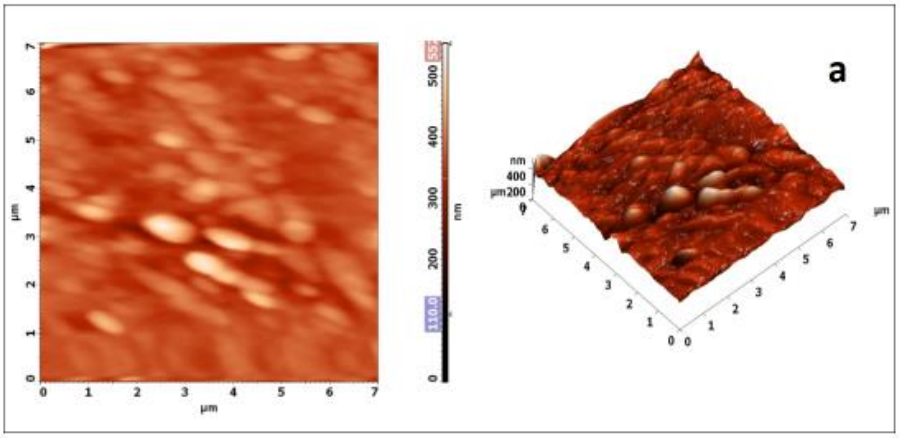

Figure 4.8: AFM images of PHF

4.2.4 SEM ANALYSIS

Since PHF is found to be a material which burns when hit with high energy electron beam, high-resolution FE SEM analysis is difficult to perform for this sample. SEM (figure 4.9) images presented here are taken with comparatively low energy electron beam. The images obtained confirm the aggregation of partially hydrogenated fullerols molecules to comparatively big particles.

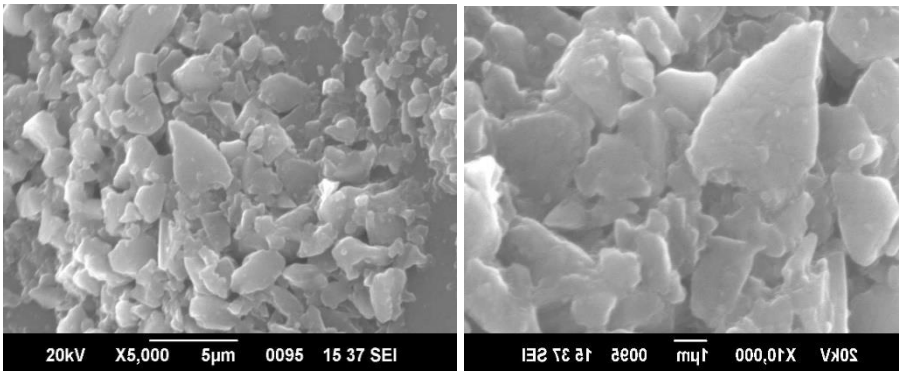

Figure 4.9: SEM images of PHF

4.2.5 XPS Analysis

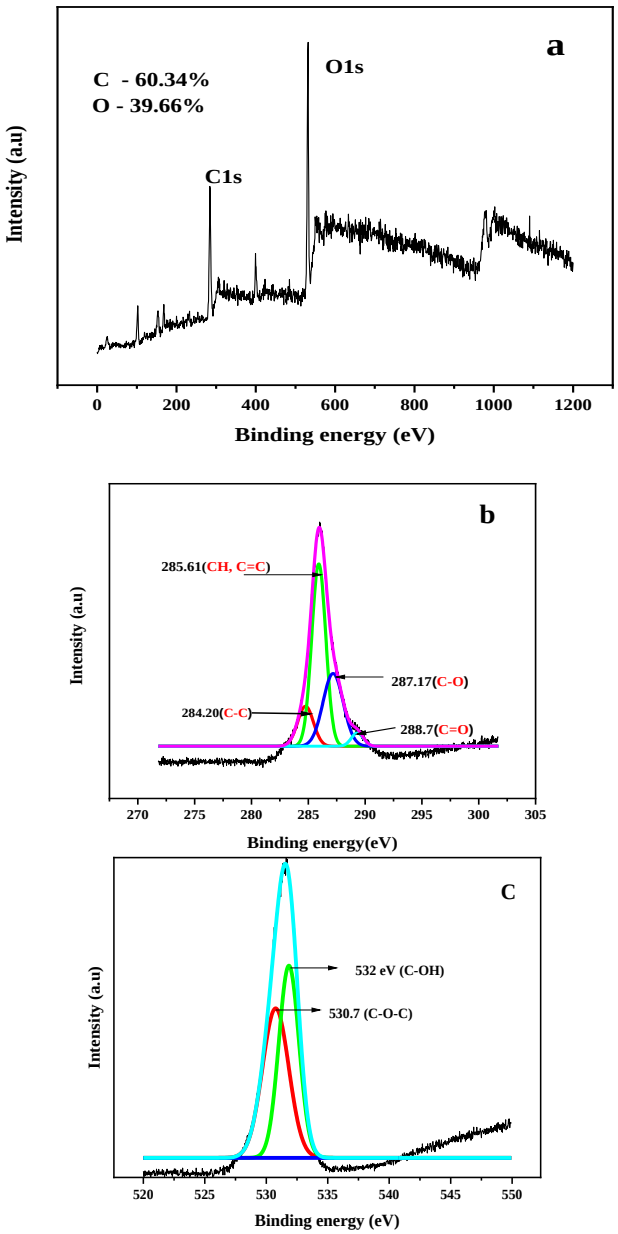

Figure 4.10: (a)XPS Survey spectrum (b) High-Resolution C1s spectrum and High-Resolution O1s spectrum of PHF

The survey spectrum of PHF is presented in figure 4.10a and it is observed that the elemental composition of PHF is 60.34 % carbon and 39.66 % oxygen, confirming that even after the hydrazine reduction process of fullerols, substantial amount of oxygen is retained in the sample. From the deconvoluted C1s spectrum, the small peak at 288.7 eV can be attributed to C=O groups of hemiacetals formed as a consequence of fullerol reduction.[19] The peak at 287.17 eV might have originated from the C-O carbon indicating the presence of retained hydroxyl groups on C_{60} cage surface and the peak at 285.61 eV can be attributed to the C-H carbon atoms and C=C carbon atoms of unmodified fullerene balls. The peak at 284.20 eV belong to the sp^3 hybridized C-C carbon atoms, emerged as a consequence of hydrogenation by the hydrazine reduction reaction. The XPS analysis of PHF is found to be consistent with the FTIR spectroscopic analysis presented earlier.

4.2.6. Proposed mechanism of fullerol hydrogenation

The hydrogen bonded nanoclusters of fullerols dispersed in water are subjected to hydrazine reduction. In this process, intermediate formation diimides are expected since fullererols may be very good oxidizing agents. Diimide intermediates are known to be formed from hydrazine is combined with a suitable oxidizing agent which are capable of adding to unsaturated bonds causing hydrogenation. [37]

4.3. Investigations on electrochemical sensing of H_2O_2

In the present work, an enzyme free sensing platform, Cu^{2+}-phen- dione@ PHF/GCE is employed for the electrochemical sensing of hydrogen peroxide. Cyclic voltammetry is the technique selected for this investigation. Initially, PHF is drop-casted on a glassy carbon electrode

by means of a binder free approach. The PHF modified GCE is then subjected to further modification with 1,10-phenanthroline (phen), again by the method of drop-casting. Since PHF is a highly oxygen rich material, some extent of oxidation of phen to phen-dione (1,10 phenanthroline 5,6 dione) happens immediately after the drop-casting and drying of the electrode under IR lamp, as evident from the initial CV obtained which shows the reduction and oxidation peaks of phen-dione at potential values -0.04 V to 1.2 V respectively;. Upon continuous potential cycling for 15 times, these peaks are getting intensified, indicating the completion of oxidation process by electrochemical means. A schematic diagram showing the process involved is presented in figure 4.12. and the CV curves obtained are shown in figure 4.11. After the completion of the electrochemical oxidation of 1,10-phenanthroline, complexation with Cu^{2+} ions is carried out and the resulting electrode is used for the sensing studies.

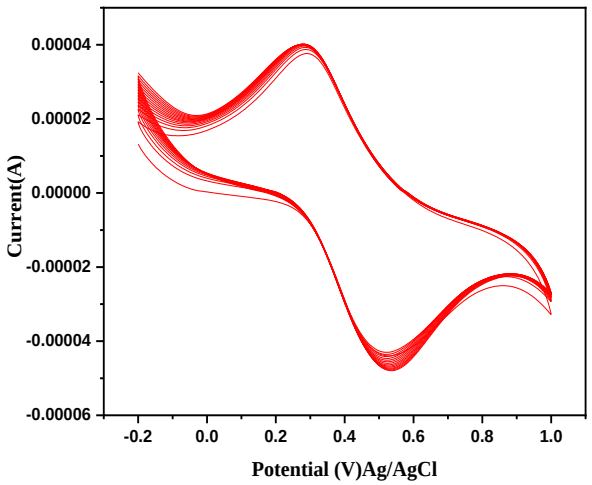

Figure 4.11: CV responses for a continuous run of 15 cycles of phendione@PHF/GCE in 0.1 M PBS (pH 7.4) with 0.1 M KCl as supporting electrolyte.

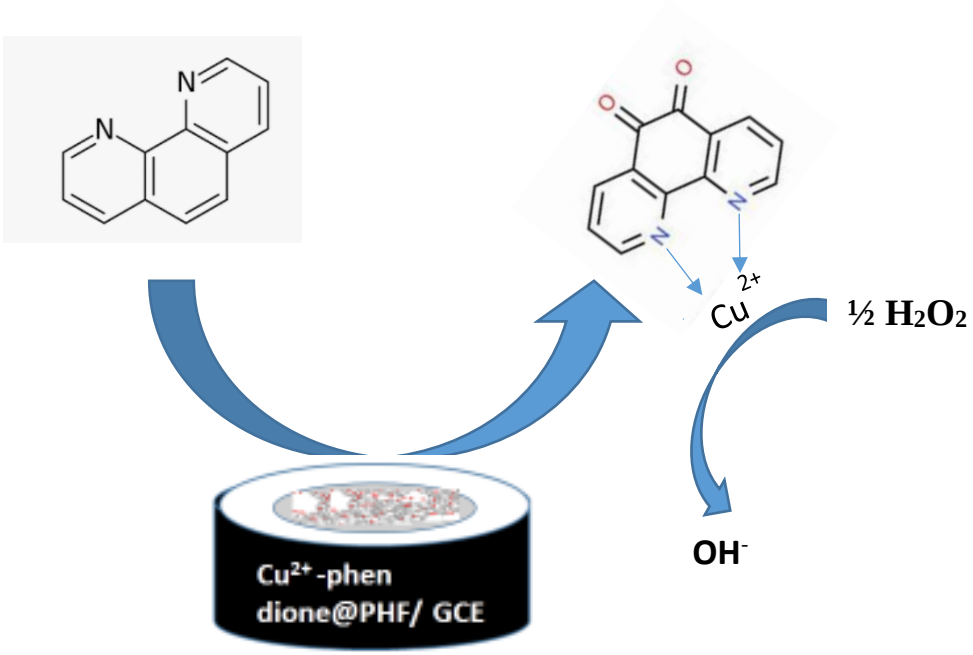

Figure 4.12: Preparation of Copper complexed phen-dione@PHF Modified Glassy Carbon Electrode

The cyclic voltametric measurement of potassium ferrocyanide/ferricyanide redox probe is carried out in a 5 mM potassium ferrocyanide solution containing 0.1 M KCl and PBS buffer using the developed sensor electrode as the working electrode and the voltammogram obtained is presented in figure 4.13.

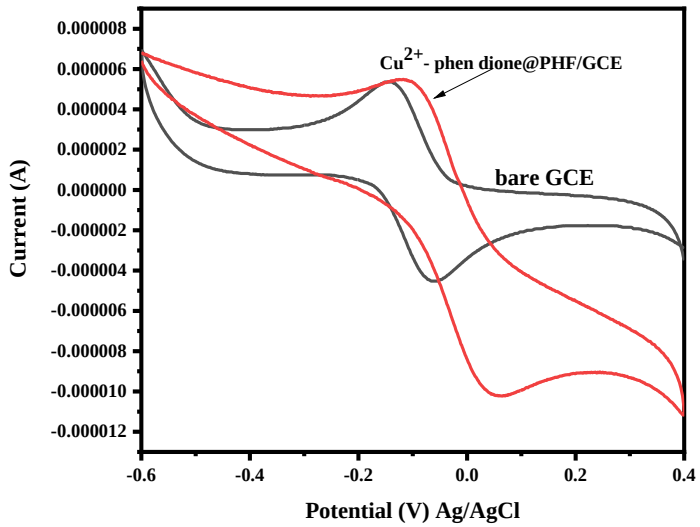

Figure 4.13: CV responses of bare GCE & Cu^{2+} phendione@PHF/GCE in 5 mM $K_3Fe(CN)_6$ (0.1 M PBS pH 7.4) with KCl supporting electrolyte.

The Electro-Chemically active Surface Area (ECSA) of the developed electrode is calculated by the Randles-Sevcik equation:

$$I_p = 2.69\times10^5 A D^{1/2} n^{3/2} \gamma^{1/2} C$$

Where Ip is the Peak current, A is the ECSA, D is the diffusion coefficient, n is the number of transferred electrons in the redox couple, γ is the scan rate and C is the concentration of the analyte. The ECSA values of bare GCE and Cu^{2+}-phendione@PHF/GCE are found to be 0.0726 cm^2, 0.089 cm^2 respectively.

To understand the nature of the electron transfer process involved with regard to the prepared sensor, cyclic voltametric measurements are carried out in a ferrocyanide/ferricyanide system

varying the scan rate. From the figure, it is clear that peak current increases with increasing scan rate, and a calibration plot of peak current vs. square root of scan rate gives a straight line with good linearity and R^2 value of 0.9971. From this, it is clear that electron transfer involving the Cu^{2+} phendione@PHF/GCE is a diffusion-controlled process.

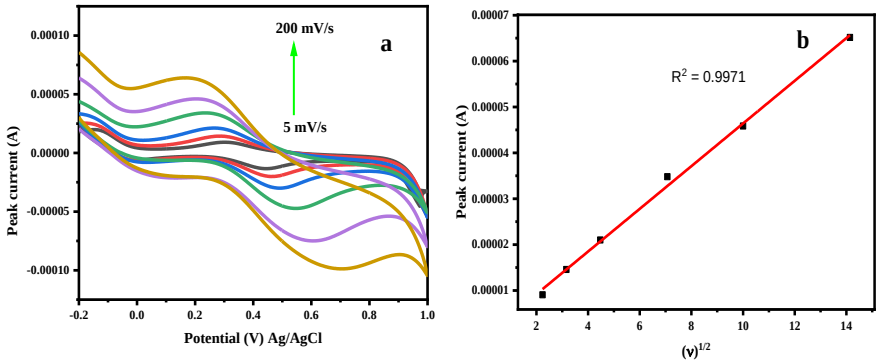

Figure 4.14: (a) CV responses of phendione@PHF/GCE (5.12 a) & Cu^{2+} phendione@PHF/GCE in 5 mM $K_3Fe(CN)_6$ (0.1 M PBS pH 7.4) with KCl supporting electrolyte at different scan rate. (b) calibration plot of peak current vs. square root of scan rate.

The efficient electrochemical sensing of H_2O_2 in micromolar concentrations in a neutral pH is carried out, again using the CV technique. After the first addition of H_2O_2 to the electrolyte 0.1 M KCl, maintained at a pH of 7.4 by PBS buffer, the peak at -0.7649 V is getting shifted to -0.8503 V and a progressive increase in the peak current at this potential value is observed (figure 4.15a). From the CV curves obtained, it is observed that the increase in peak current is linear with respect to the H_2O_2 concentration present in the electrolyte. A calibration graph is plotted with peak current vs. H_2O_2 concentration (figure 4.15b) giving a straight line with an R^2 value of 0.9992 showing good linearity.

The Limit of Detection (LOD) of hydrogen peroxide sensing on Cu^{2+}-phen-dione@PHF/GCE platform is calculated and is found to be 0.353 µM. It is calculated from the relation $3xS.D_{(bl.)}$ /m, where $S.D_{(bl)}$ is the standard deviation of the blank solution calculated from 10 consecutive measurements and m is the slope of the calibration curve. The linear range for hydrogen peroxide sensing is found to be 1 µM-10 µM and the sensitivity was found to be 8148.3 µA/mMcm^2 which is calculated as slope of the calibration curve/ECSA value of the electrode.

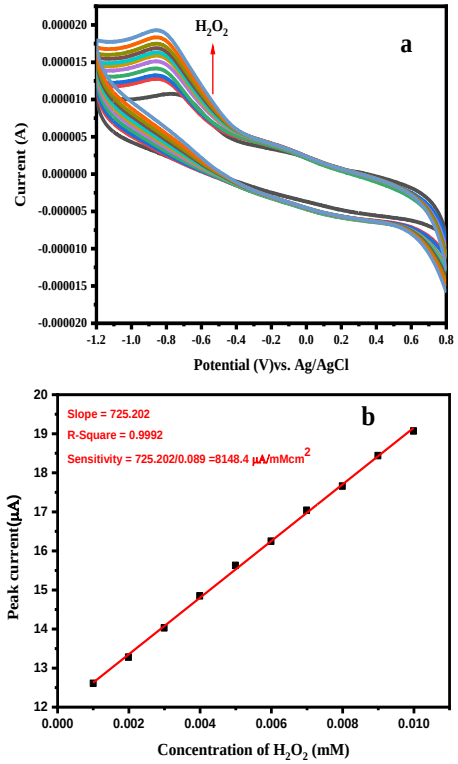

Figure 4.15: (a) Electrochemical sensing of hydrogen peroxide over Cu^{2+}-phen-dione@PHF/GCE (b) Calibration plot showing linear variation of peak current versus hydrogen peroxide concentration.

4.3.1. Interference study

To investigate the possibility of interferences for the detection of hydrogen peroxide in biological samples, 1.5 mM solutions of uric acid, ascorbic acid, and glucose are prepared. 10 µl of each these potential interfering biomarkers are added one by one to the 0.1 M PBS buffer solution and 0.1 M KCl supporting electrolyte containing 10 µM hydrogen peroxide and peak current at -0.8503 V potential value is observed in each time. The peak current remained almost unchanged with only very slight (± 1.8 %) variation by the interfering species chosen and the results are summarized in figure 4.16. Thus, the interference study reveals that no significant interference in the determination of hydrogen peroxide is present with the developed sensing platform.

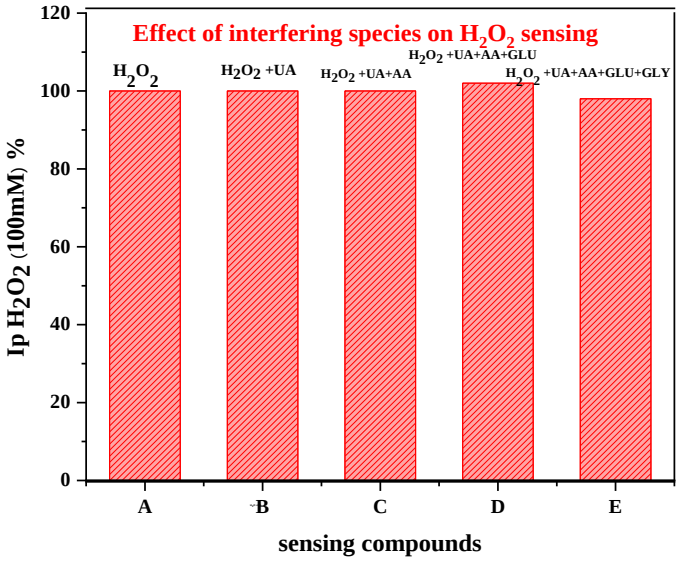

Figure 4.16: Effect of interfering compounds such as glucose, Ascorbic acid (AA), Uric acid (UA), and Glycine (GLY) on the peak current of H_2O_2.

4.3.2. Comparison of electrochemical sensing studies of H_2O_2 in literature with the present work

The summary of the comparison of electrochemical performances of various electrodes in non-enzymatic H_2O_2 sensing with the developed sensor is presented in Table 4.1. From this, it is observed that Cu^{2+} phendione PHF/GCE act an efficient non-enzymatic electrochemical sensor for H_2O_2 detection when various sensing parameters such as linear range, sensitivity, limit of detection are considered.

Table 4.1: Performance of various electrodes in the non-enzymatic electrochemical H_2O_2 sensing.

Sl No.	Electrode material	Technique used	Linear range	Sensitivity ($\mu A/mMcm^2$)	Limit of Detection (μM)	Ref
1	AgNPs/CNTs/GCE	CV	0.1-10 mM	9.79	2	39
2	GCE/MWCNTs@	CV	100 µM-4 mM	48	---	27
3	MWCNTs/Pt NPs/GCE	AMP	0.01-2.0 mM	205.8	0.3	40
4	Se/Pt	CV	0 .01-1.5 µM	39.89	3.1	41
5	GO/AuNPs/CS	CV	0.2-4.2 mM	99.5	----	48
6	AuNSs/GCE	CV	20-2.5x10^3 M	---	9.7	49
7	Hemin-OMC-Nafion GCE	CV	2-250 µM	23.4	0.3	44
8	Ag-Bt	CV	10-5000 µM	45	9.1	51
9	Cu^{2+} phendione PHF/GCE	CV	1 µM-10 µM	8148.3	0.353	This work

4.4. Conclusions

In summary, hydroxylated C_{60} derivatives called fullerols are prepared by the sonochemical reaction of C_{60} with H_2O_2 and they are networked by C-O-C bonds and partially hydrogenated by hydrazine reduction reactions. The partially hydrogenated fullerol network (PHF) obtained is characterized by various spectroscopic and microscopic techniques. High-resolution SEM and TEM analyses could not be performed due to the burning of the partially hydrogenated fullerol network when subjected to high energy electron beam. From FTIR Raman and XPS analyses, partial hydrogenation of PHF is confirmed. Enzyme-free electrochemical H_2O_2 sensing studies are successfully carried out using the PHF based sensor electrode, Cu^{2+}-phen-dione@PHF/GCE and it is found to be an efficient sensor for hydrogen peroxide.

References

(1) Taylor, R. Addition Reactions of Fullerenes. *Comptes Rendus Chimie* **2006**, *9* (7), 982–1000. https://doi.org/10.1016/j.crci.2006.01.004.

(2) Zygouri, P.; Spyrou, K.; Mitsari, E.; Barrio, M.; Macovez, R.; Patila, M.; Stamatis, H.; Verginadis, I. I.; Velalopoulou, A. P.; Evangelou, A. M.; Sideratou, Z.; Gournis, D.; Rudolf, P. A Facile Approach to Hydrophilic Oxidized Fullerenes and Their Derivatives as Cytotoxic Agents and Supports for Nanobiocatalytic Systems. *Sci Rep* **2020**, *10* (1), 1–13. https://doi.org/10.1038/s41598-020-65117-7.

(3) Brant, J.; Labille, J.; Hendren, C.; Wiesner, M. Fullerol Cluster Formation in Aqueous Solutions: Implications for Environmental Release. *Journal of colloid and interface science* **2007**, *314*, 281–288. https://doi.org/10.1016/j.jcis.2007.05.020.

(4) Djordjevic, A.; Srdjenovic, B.; Seke, M.; Petrovic, D.; Injac, R.; Mrdjanovic, J. Review of Synthesis and Antioxidant Potential of Fullerenol Nanoparticles. *Journal of Nanomaterials* **2015**, *2015*, e567073. https://doi.org/10.1155/2015/567073.

(5) Chiang, L. Y.; Bhonsle, J. B.; Wang, L.; Shu, S. F.; Chang, T. M.; Hwu, J. R. Efficient One-Flask Synthesis of Water-Soluble [60]Fullerenols. *Tetrahedron* **1996**, *52* (14), 4963–4972. https://doi.org/10.1016/0040-4020(96)00104-4.

(6) Chiang, L. Y.; Wang, L.-Y.; Swirczewski, J. W.; Soled, S.; Cameron, S. Efficient Synthesis of Polyhydroxylated Fullerene Derivatives via Hydrolysis of Polycyclosulfated Precursors. *J. Org. Chem.* **1994**, *59* (14), 3960–3968. https://doi.org/10.1021/jo00093a030.

(7) Chiang, L. Y.; Swirczewski, J. W.; Hsu, C. S.; Chowdhury, S. K.; Cameron, S.; Creegan, K. Multi-Hydroxy Additions onto C_{60} Fullerene Molecules. *J. Chem. Soc., Chem. Commun.* **1992**, No. 24, 1791–1793. https://doi.org/10.1039/C39920001791.

(8) Grebowski, J.; Konopko, A.; Krokosz, A.; DiLabio, G. A.; Litwinienko, G. Antioxidant Activity of Highly Hydroxylated Fullerene C_{60} and Its Interactions with the Analogue of α-Tocopherol. *Free Radical Biology and Medicine* **2020**, *160*, 734–744. https://doi.org/10.1016/j.freeradbiomed.2020.08.017.

(9) Roy, P.; Bag, S.; Chakraborty, D.; Dasgupta, S. Exploring the Inhibitory and Antioxidant Effects of Fullerene and Fullerenol on Ribonuclease A. *ACS Omega* **2018**, *3* (9), 12270–12283. https://doi.org/10.1021/acsomega.8b01584.

(10) Keshri, S. Insights into the Structural and Thermodynamic Properties of Fullerols [$C_{60}(OH)_n$, n=12, 14, 16, 18, 20, 22, 24] in Aqueous Media. *Fluid Phase Equilibria* **2020**, *525*, 112805. https://doi.org/10.1016/j.fluid.2020.112805.

(11) Kokubo, K.; Shirakawa, S.; Kobayashi, N.; Aoshima, H.; Oshima, T. Facile and Scalable Synthesis of a Highly Hydroxylated Water-Soluble Fullerenol as a Single Nanoparticle. *Nano Research* **2011**, *4*, 204–215. https://doi.org/10.1007/s12274-010-0071-z.

(12) Li, J.; Takeuchi, A.; Ozawa, M.; Li, X.; Saigo, K.; Kitazawa, K. C_{60} Fullerol Formation Catalysed by Quaternary Ammonium Hydroxides. *J. Chem. Soc., Chem. Commun.* **1993**, No. 23, 1784–1785. https://doi.org/10.1039/C39930001784.

(13) Zhang, P.; Pan, H.; Liu, D.; Guo, Z.-X.; Zhang, F.; Zhu, D. Effective Mechanochemical Synthesis of [60]Fullerols. *Synthetic Communications* **2003**, *33* (14), 2469–2474. https://doi.org/10.1081/SCC-120021836.

(14) Arrais, A.; Diana, E. Highly Water Soluble C_{60} Derivatives: A New Synthesis. *Fullerenes, Nanotubes and Carbon Nanostructures* **2003**, *11* (1), 35–46. https://doi.org/10.1081/FST-120018667.

(15) Cataldo, F. New Developments on the Photochlorination of C_{60} and C_{70} Fullerene and Preparation of Fullerene Derivatives: Polyfluorofullerenes and Polyfullerols. *Fullerene Science and Technology* **1996**, *4* (5), 1041–1059. https://doi.org/10.1080/10641229608001161.

(16) Afreen, S.; Kokubo, K.; Muthoosamy, K.; Manickam, S. Hydration or Hydroxylation: Direct Synthesis of Fullerenol from Pristine Fullerene [C_{60}] via Acoustic Cavitation in the Presence of Hydrogen Peroxide. *RSC Advances* **2017**, *7* (51), 31930–31939. https://doi.org/10.1039/C7RA03799F.

(17) Kokubo, K.; Matsubayashi, K.; Tategaki, H.; Takada, H.; Oshima, T. Facile Synthesis of Highly Water-Soluble Fullerenes More than Half-

Covered by Hydroxyl Groups. *ACS Nano* **2008**, *2* (2), 327–333. https://doi.org/10.1021/nn700151z.

(18) Niu, F.; Wu, J.; Zhang, L.; Li, P.; Zhu, J.; Wu, Z.; Wang, C.; Song, W. Hydroxyl Group Rich C_{60} Fullerenol: An Excellent Hydrogen Bond Catalyst with Superb Activity, Selectivity, and Stability. *ACS Catal.* **2011**, *1* (10), 1158–1161. https://doi.org/10.1021/cs200317d.

(19) Wu, J.; Alemany, L. B.; Li, W.; Petrie, L.; Welker, C.; Fortner, J. D. Reduction of Hydroxylated Fullerene (Fullerol) in Water by Zinc: Reaction and Hemiketal Product Characterization. *Environ. Sci. Technol.* **2014**, *48* (13), 7384–7392. https://doi.org/10.1021/es5012912.

(20) Bourlinos, A. B.; Georgakilas, V.; Mouselimis, V.; Kouloumpis, A.; Mouzourakis, E.; Koutsioukis, A.; Antoniou, M.-K.; Gournis, D.; Karakassides, M. A.; Deligiannakis, Y.; Urbanova, V.; Cepe, K.; Bakandritsos, A.; Zboril, R. Fullerol–Graphene Nanobuds: Novel Water Dispersible and Highly Conductive Nanocarbon for Electrochemical Sensing. *Applied Materials Today* **2017**, *9*, 71–76. https://doi.org/10.1016/j.apmt.2017.05.006.

(21) Billups, W. E.; Luo, W.; Gonzalez, A.; Arguello, D.; Alemany, L. B.; Marriott, T.; Saunders, M.; Jiménez-Vázquez, H. A.; Khong, A. Reduction of C_{60} Using Anhydrous Hydrazine. *Tetrahedron Letters* **1997**, *38* (2), 171–174. https://doi.org/10.1016/S0040-4039(97)83014-6.

(22) Patel, V.; Kruse, P.; Selvaganapathy, P. R. Solid State Sensors for Hydrogen Peroxide Detection. *Biosensors* **2021**, *11* (1), 9. https://doi.org/10.3390/bios11010009.

(23) Gaikwad, R.; Thangaraj, P. R.; Sen, A. K. Direct and Rapid Measurement of Hydrogen Peroxide in Human Blood Using a Microfluidic Device. *Sci Rep* **2021**, *11* (1), 1–10. https://doi.org/10.1038/s41598-021-82623-4.

(24) Ahmad, T.; Iqbal, A.; Halim, S. A.; Uddin, J.; Khan, A.; El Deeb, S.; Al-Harrasi, A. Recent Advances in Electrochemical Sensing of Hydrogen Peroxide (H_2O_2) Released from Cancer Cells. *Nanomaterials (Basel)* **2022**, *12* (9), 1475. https://doi.org/10.3390/nano12091475.

(25) Nestor, U.; Frodouard, H.; Theoneste, M. A Brief Review of How to Construct an Enzyme-Based H_2O_2 Sensor Involved in Nanomaterials. *Advances in Nanoparticles* **2020**, *10* (1), 1–25. https://doi.org/10.4236/anp.2021.101001.

(26) Ko, W.-B.; Heo, J.-Y.; Nam, J.-H.; Lee, K.-B. Synthesis of a Water-Soluble Fullerene [C_{60}] under Ultrasonication. *Ultrasonics* **2004**, *41* (9), 727–730. https://doi.org/10.1016/j.ultras.2003.12.029.

(27) Gayathri, P.; Senthil Kumar, A. Electrochemical Behavior of the 1,10-Phenanthroline Ligand on a Multiwalled Carbon Nanotube Surface and Its Relevant Electrochemistry for Selective Recognition of Copper Ion and Hydrogen Peroxide Sensing. *Langmuir* **2014**, *30* (34), 10513–10521. https://doi.org/10.1021/la502651w.

(28) Wang, S.; He, P.; Zhang, J.; Jiang, H.; Zhu, S. Novel and Efficient Synthesis of Water-Soluble [60]Fullerenol by Solvent-Free Reaction. *Synthetic Communications* **2005**, *35* (13), 1803–1808. https://doi.org/10.1081/SCC-200063958.

(29) Chiang, L. Y.; Upasani, R. B.; Swirczewski, J. W. Versatile Nitronium Chemistry for C_{60} Fullerene Functionalization. *J. Am. Chem. Soc.* **1992**, *114* (26), 10154–10157. https://doi.org/10.1021/ja00052a010.

(30) Vileno, B.; Marcoux, P. R.; Lekka, M.; Sienkiewicz, A.; Fehér, T.; Forró, L. Spectroscopic and Photophysical Properties of a Highly Derivatized C_{60} Fullerol. *Advanced Functional Materials* **2006**, *16* (1), 120–128. https://doi.org/10.1002/adfm.200500425.

(31) Xing, G.; Zhang, J.; Zhao, Y.; Tang, J.; Zhang, B.; Gao, X.; Yuan, H.; Qu, L.; Cao, W.; Chai, Z.; Ibrahim, K.; Su, R. Influences of Structural Properties on Stability of Fullerenols. *J. Phys. Chem. B* **2004**, *108* (31), 11473–11479. https://doi.org/10.1021/jp0487962.

(32) Velarde-Salcedo, M. V.; Gallo, M.; Guirado-López, R. A. Low Hydroxylated Fullerenes: Stability, Thermal Behavior, and Vibrational Properties. *J. Phys. Chem. C* **2018**, *122* (24), 13117–13129. https://doi.org/10.1021/acs.jpcc.8b01628.

(33) Talyzin, A. V.; Sundqvist, B.; Shulga, Y. M.; Peera, A. A.; Imus, P.; Billups, W. E. Gentle Fragmentation of C_{60} by Strong Hydrogenation: A Route to Synthesizing New Materials. *Chemical Physics Letters* **2004**, *400* (1), 112–116. https://doi.org/10.1016/j.cplett.2004.10.087.

(34) Hare, J. P.; Dennis, T. J.; Kroto, H. W.; Taylor, R.; Allaf, A. W.; Balm, S.; Walton, D. R. M. The IR Spectra of Fullerene-60 and -70. *J. Chem. Soc., Chem. Commun.* **1991**, No. 6, 412–413. https://doi.org/10.1039/C39910000412.

(35) Kuzmany, H.; Winkler, R.; Pichler, T. Infrared Spectroscopy of Fullerenes. *J. Phys.: Condens. Matter* **1995**, *7* (33), 6601. https://doi.org/10.1088/0953-8984/7/33/003.

(36) Saraswati, T. E.; Setiawan, U. H.; Ihsan, M. R.; Isnaeni, I.; Herbani, Y. The Study of the Optical Properties of C_{60} Fullerene in Different Organic Solvents. *Open Chemistry* **2019**, *17* (1), 1198–1212. https://doi.org/10.1515/chem-2019-0117.

(37) Corey, E. J.; Mock, W. L. *Chemistry of Diimide. III. Hydrogen Transfer to Multiple Bonds by Dissociation of the Diimide-Anthracene Adduct, Anthracene-9,10-Biimine.* ACS Publications. https://doi.org/10.1021/ja00863a045.

(38) Zheng, C.; Chen, S.; Shang, Y.; Li, M. A Modified Glassy Carbon Electrode for Hydrogen Peroxide Sensing. *Annali di Chimica* **2007**, *97* (11–12), 1227–1235. https://doi.org/10.1002/adic.200790108.

(39) Afraz, A.; Rafati, A. A.; Hajian, A. Analytical Sensing of Hydrogen Peroxide on Ag Nanoparticles–Multiwalled Carbon Nanotube-Modified Glassy Carbon Electrode. *J Solid State Electrochem* **2013**, *17* (7), 2017–2025. https://doi.org/10.1007/s10008-013-2057-8.

(40) Miao, Z.; Zhang, D.; Chen, Q. Non-Enzymatic Hydrogen Peroxide Sensors Based on Multi-Wall Carbon Nanotube/Pt Nanoparticle Nanohybrids. *Materials (Basel)* **2014**, *7* (4), 2945–2955. https://doi.org/10.3390/ma7042945.

(41) Li, J.; Hu, H.; Li, H.; Yao, C. Recent Developments in Electrochemical Sensors Based on Nanomaterials for Determining Glucose and Its Byproduct H_2O_2. *Journal of Materials Science* **2017**, *52* (17), 10455–10469.

(42) Shan, C.; Yang, H.; Han, D.; Zhang, Q.; Ivaska, A.; Niu, L. Graphene/AuNPs/Chitosan Nanocomposites Film for Glucose Biosensing. *Biosensors and Bioelectronics* **2010**, *25* (5), 1070–1074. https://doi.org/10.1016/j.bios.2009.09.024.

(43) Li, Y.; Ma, J.; Ma, Z. Synthesis of Gold Nanostars with Tunable Morphology and Their Electrochemical Application for Hydrogen Peroxide Sensing. *Electrochimica Acta* **2013**, *108*, 435–440. https://doi.org/10.1016/j.electacta.2013.06.141.

(44) Cao, H.; Sun, X.; Zhang, Y.; Hu, C.; Jia, N. Electrochemical Sensing Based on Hemin-Ordered Mesoporous Carbon Nanocomposites for Hydrogen Peroxide. *Anal. Methods* **2012**, *4* (8), 2412–2416. https://doi.org/10.1039/C2AY25358E.

(45) Yadav, D. K.; Gupta, R.; Ganesan, V.; Sonkar, P. K.; Rastogi, P. K. Electrochemical Sensing Platform for Hydrogen Peroxide Determination at Low Reduction Potential Using Silver Nanoparticle-Incorporated Bentonite Clay. *J Appl Electrochem* **2016**, *46* (1), 103–112. https://doi.org/10.1007/s10800-015-0904-2.

CHAPTER 5

PREPARATION OF HYDROGENATED AND HYDROXY FUNCTIONALIZED GRAPHENE-NANOTUBE-FULLERENE TERNARY HYBRIDS AND THEIR ELECTROCHEMICAL SENSING APPLICATIONS

5.1 Introduction

Combined materials of nano-allotropes of carbon such as graphene, carbon nanotubes and fullerenes are anticipated to possess many novel properties, different from their individual unique and superior properties, making them suitable for a variety of promising applications. [1] Similarly, surface decoration of these nanocomposites with various functional groups by chemical means can be used as an effective strategy to tune these properties to fit into many desired applications. The discovery of Carbon Nano Tubes (CNTs) in 1991 by Iijima, one of the amazing nano-allotropes of carbon, opened up a new area in material science research. CNTs are regarded as the rolled up forms of graphene sheets with sp^2 carbon networks. [2–4] These systems have outstanding mechanical, thermal, electrical and optical properties which makes them a promising material in nanotechnology. [5] There are reports for the existence of C_{60} decorated SWCNTs and its composites with metal oxide that shows outstanding photocatalytic activity. Similarly, C_{60}-CNTs/Bismuth based oxide composites are reported to exhibit excellent photocatalytic activity. [6] The electrochemical hydrogen storage capacities of CNTs were reported to be 110 mb/g. [7]

Even though, theoretically, CNTs are always pictured as rolled up forms of graphene sheets, experimental reports of such rolling up and zipping are only a few. There are reports for the synthesis of CNTs from metal incorporated graphite in which graphite layers grows on the selected crystal planes of the metal. [8] Guo et al. reported the synthesis of CNTs on the graphite surface under microwave irradiation. [9]

5.1.1 Carbon nanostructures for electrochemical sensing

The extraordinary electric, mechanical, plasmonic properties and large surface-to-volume ratio makes CNTs a suitable candidate for biochemical sensing. [10–12] CNTs exhibit high selectivity, better sensitivity and high electrochemical response to some biomolecules, which makes them as an important sensing platform for biomolecules.[13, 14] CNT based sensors are able to mediate electron transfer reactions with various electro active species present in a solution.[15–17] Functionalization of CNT surfaces can bring about drastic changes in the solubility, improved biocompatibility and they can even act as a better sensing platform for heavy metal ions.[18, 19] CNT based sensing is found to be highly reliable, accurate and fast because of their unique material properties. [20] Nitrogen doped CNT surfaces shows a fast chemical disproportionation of H_2O_2 and their analytical sensitivity higher than that of undoped CNTs. [21]

Graphene as well as functionalized graphene are also equally competent platforms widely employed for electrochemical sensing. [22–24]

Hydrogen peroxide act as a signaling molecule which is involved in various biological processes occurring in our body. [25] High biological specificity makes them function as as a modulator in gene expression during protein synthesis. [26] Moreover, it is an important biomarker for various human diseases. A fast, selective, and a stable quantification of H_2O_2 is a key factor in the proper maintenance of H_2O_2 level in our body.[27,28] CNTs based materials can act as a better bio analytical sensing

platform for the detection of H_2O_2 even in trace level. [29] CNT/clay nanocomposites shows better sensitivity and selectivity in H_2O_2 sensing. [30] Graphene based nanomaterials also are considered important functional materials suitable for functioning as efficient electrochemical sensing platform for important biomarkers such as H_2O_2.[31, 32]

In the present work, we observed accidental incorporation of CNTs in the nanocomposites of hydroxy functionalized fullerenes and hydroxy graphene prepared via hydrazine reduction. Another interesting aspect observed is the heavy hydrogenation of the carbon nano structures present in the nanocomposite by the hydrazine reduction, probably by via the formation of the active reducing agent diimide. [33]

5.2. (A) Hydrogenated and hydroxy functionalized ternary hybrid of Graphene, Nanotube, and Fullerene (GNF1): Hydrazine reduction of a mixed aqueous dispersion of oxidized mixture of PFO and Reduced hydroxy graphene (RHG)

Reduced hydroxy graphene (RHG) is prepared solvothermally from fluorographite derived hydroxygraphene (HG), following a procedure reported from this lab previously. [34] The aqueous dispersion of a PFO/RHG mixture in 1:1 ratio, obtained by mechanical mixing followed by calcination at 250 °C in a muffle furnace for 5 h, converts the water insoluble PFO network and RHG to a completely water dispersible forms. It is presumed that the mechanical mixing and calcination treatment in the presence of air might have resulted in the plausible oxidation of PFO & RHG and resulting in the breaking of PFO network and its conversion to water dispersible hydroxy functionalized fullerenes (fullerols). Conversion of RHG to hydroxy graphene also

possible by the oxidative treatment which is again water dispersible. This black colored aqueous dispersion obtained, when subjected to hydrazine reduction comes out from the aqueous medium, getting transformed into a highly hydrogenated and hydroxy functionalized ternary composite of graphene, nanotubes and fullerenes, designated as GNF1. The scheme of formation of GNF1 is shown in figure 5.1. In the ternary hybrid thus formed, CNT formation may have resulted by the rapping of some of the functionalized graphene sheets present.

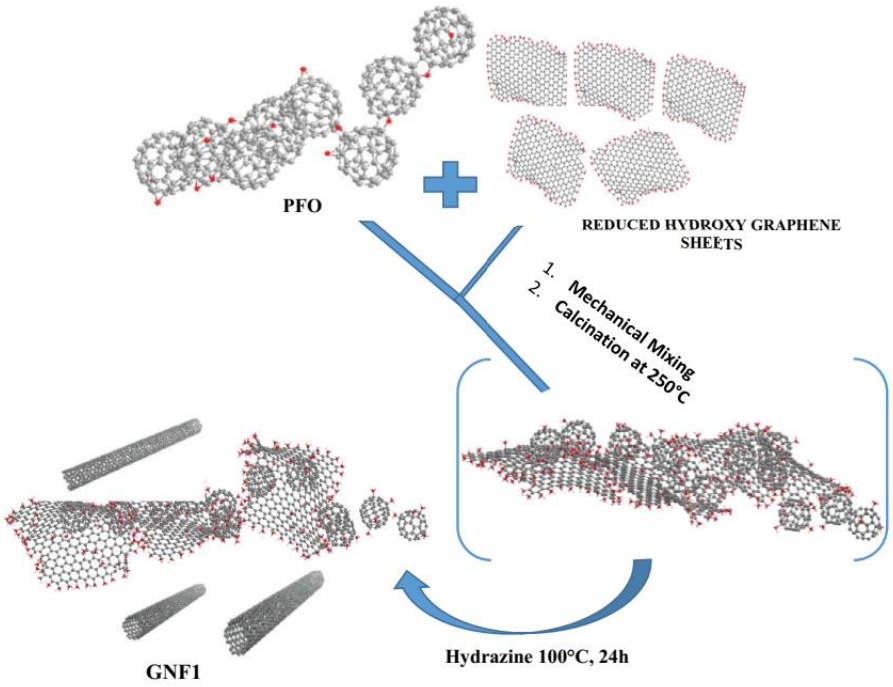

Figure 5.1: Schematic representation of the formation of hydrogenated and hydroxy functionalized ternary hybrid of Graphene, Nanotube, and Fullerene (GNF1) prepared by the hydrazine reduction of aqueous dispersion of oxidized PFO/RHG mixture.

5.2. (B) Hydrogenated and hydroxy functionalized ternary hybrid of Graphene, Nanotube, and Fullerene (GNF2) : Hydrazine reduction of a mixed aqueous dispersion of fullerol clusters and hydroxygraphene.

In an alternative strategy, another hydrogenated and hydroxy functionalized ternary hybrid of Graphene, Nanotube, and Fullerene (GNF2) is prepared by the hydrazine reduction of an aqueous dispersion of fullerols prepared sonochemically with H_2O_2 reagent, as described in the previous chapter and fluorographite derived hydroxygraphene, taken in a 1:1 ratio. In GNF2, CNTs formed are found to be externally decorated with fullerol molecules. A schematic of the GNF2 formation is represented in figure 5.2.

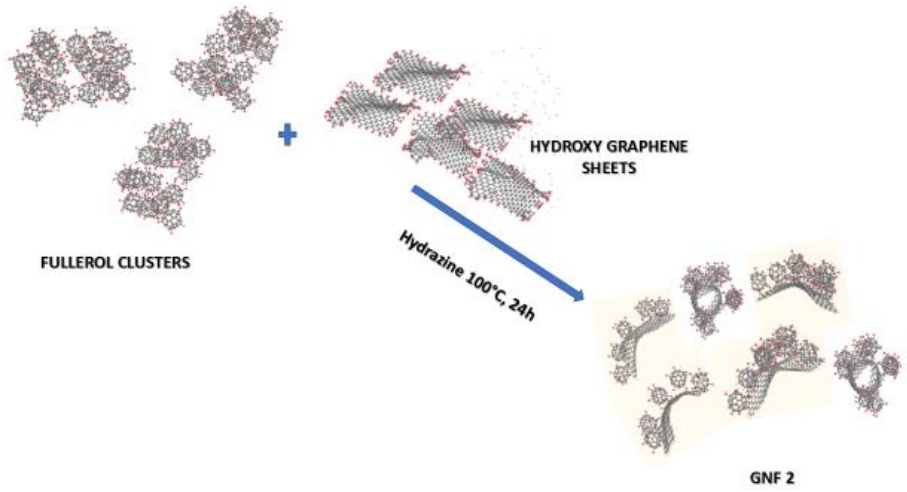

Fig 5.2: Schematic for the preparation of ternary hybrid of Graphene, Nanotube, and Fullerene (GNF2) prepared by the hydrazine reduction of fullerol and hydroxy graphene dispersion.

5.3. Results and discussion

Both the ternary nanohybrids, GNF1 and GNF2 are characterized by means of various spectroscopic and microscopic techniques and the results are presented below.

5.3.1 FTIR Analysis

FTIR analysis of GNF1 and GNF2 are performed and the spectra obtained are presented in figure 5.3. In GNF1, the two intense peaks observed at 2916 cm^{-1}, 2856 cm^{-1} corresponds to aliphatic –CH stretching. Similarly, two sharp peaks at 2920 cm^{-1} and 2844 cm^{-1} are observed in GNF2 also corresponding to aliphatic C-H stretching, confirming the hydrogenation of the carbon nanomaterials present in the composite. The hydrogenation is presumed to have happened during the hydrazine reduction plausibly via imide formation and subsequent hydrogen incorporation as in the case of PHF. A striking difference observed here is the absence of aromatic C-H stretching. Probably, graphene and nanotube parts of the composite are more susceptible to hydrogenation in the nanocomposite than the fullerene part. As a result, the soft fragmentation of few fullerene balls as a consequence of their heavy hydrogenation, producing aromatic fragments are almost absent in both these cases. The sharp peak at 1702 cm^{-1} can be attributed to C=O stretching vibrations of the hemiacetals formed in the reduction process which is again more intensified in the case of GNF1 compared to GNF2 and PHF. Many cage vibrations of hydrogenated C_{60} are observed in the frequency range 500-1700 cm^{-1} both in GNF1 and GNF2. In the FTIR analysis, striking resemblance in peak positions can

be observed between the spectra of GNF1 and GNF2, supporting our hypothesis that water dispersible fullerols are formed after the breaking of PFO network. The shaded region in the spectra of GNF1 and GNF2 indicate the vibrations due to the newly formed C-O-C interlinkages of the framework, centered around 1200 cm^{-1}.

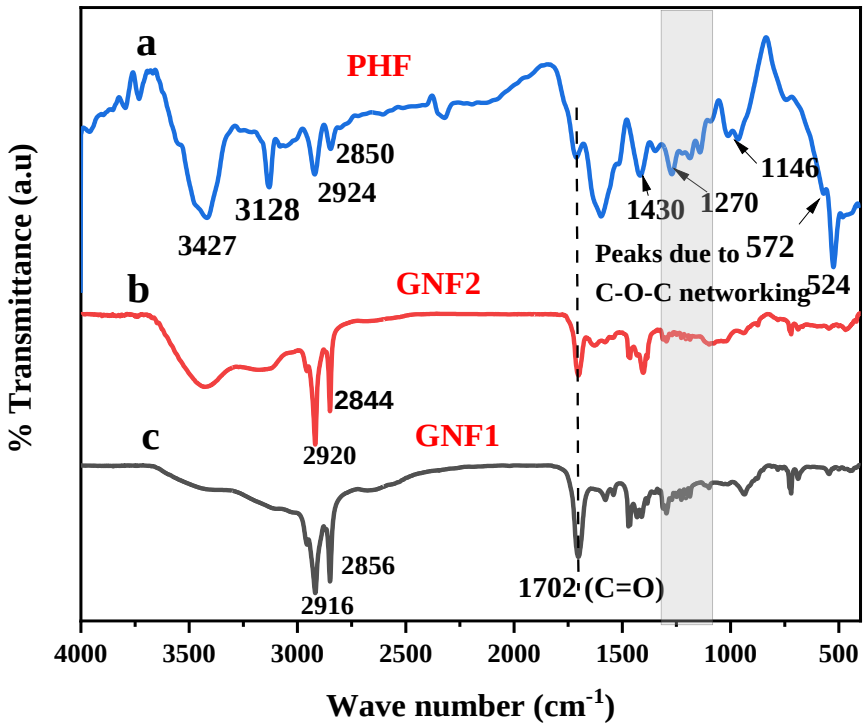

Figure 5.3: FTIR Spectra of (a) PHF (b) GNF2 (c) GNF1.

5.3.2 Raman Analysis

In Raman analysis as well, there is a one-to-one correspondence of peak positions, except for small shifts when the spectra of GNF1 and GNF2 are compared, consistent with FTIR analysis. In both GNF1 and

GNF2, sharp and intense peaks are observed for aliphatic C-H stretching vibrations (at 2881 cm^{-1} in GNF1 and 2865 cm^{-1} in GNF2), strong evidence for hydrogenation. In Raman spectra also, the signature bands of aromatic fragments found in PHF are completely absent, again consistent with FTIR data. Due to hydrogenation, the expected G band for graphene and nanotubes are almost absent in the Raman spectra, consistent with the literature. [35] The weak signals found at 1362 cm^{-1} (D band), 1645 cm^{-1} (G band) and the medium signal at 2725 cm^{-1} (2D band) can be attributed to the characteristic Raman signatures of graphene and nanotubes. In the Raman spectra of GNF2 and GNF1, the peaks observed at 1443 cm^{-1} in GNF2 and 1445 cm^{-1} in GNF1can be attributed to the characteristic pentagonal pinch mode of fullerene balls shifted due to the structural changes such as hydroxylation, hydrogenation and attachment to CNT or graphene surface.

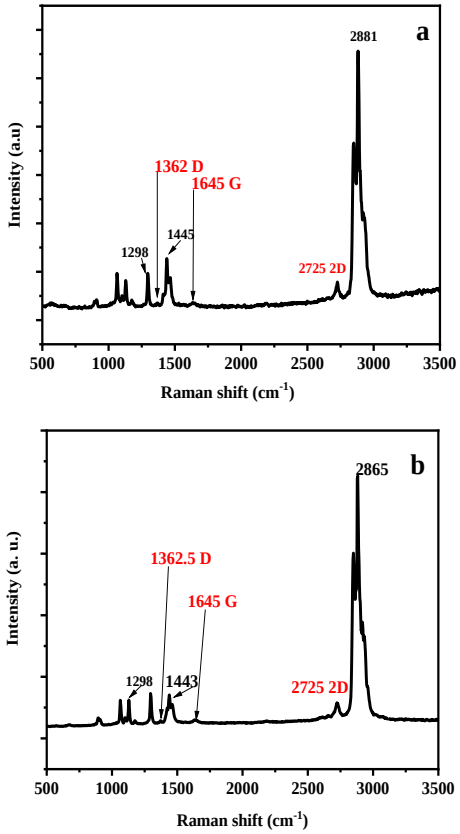

Fig 5.4: Raman spectra of (a) GNF1and (b) GNF2

5.3.3 AFM Analysis

The surface morphology and topological features of the prepared nancomposites, GNF1 and GNF2, are analysed by Atomic Force microscopy (AFM). The 2D and 3D images obtained for both the samples are presented in figure 5.5. In the AFM images of GNF1(figure 5.5a), nanotubes as well as interconnected fullerol clusters originated from PFO, lying on the graphene nanosheets are visible in an ordered manner. Similarly, in GNF2, bundles of oriented nanotubes are visible whereas separate fullerol clusters are not observed (figure 5.5b).

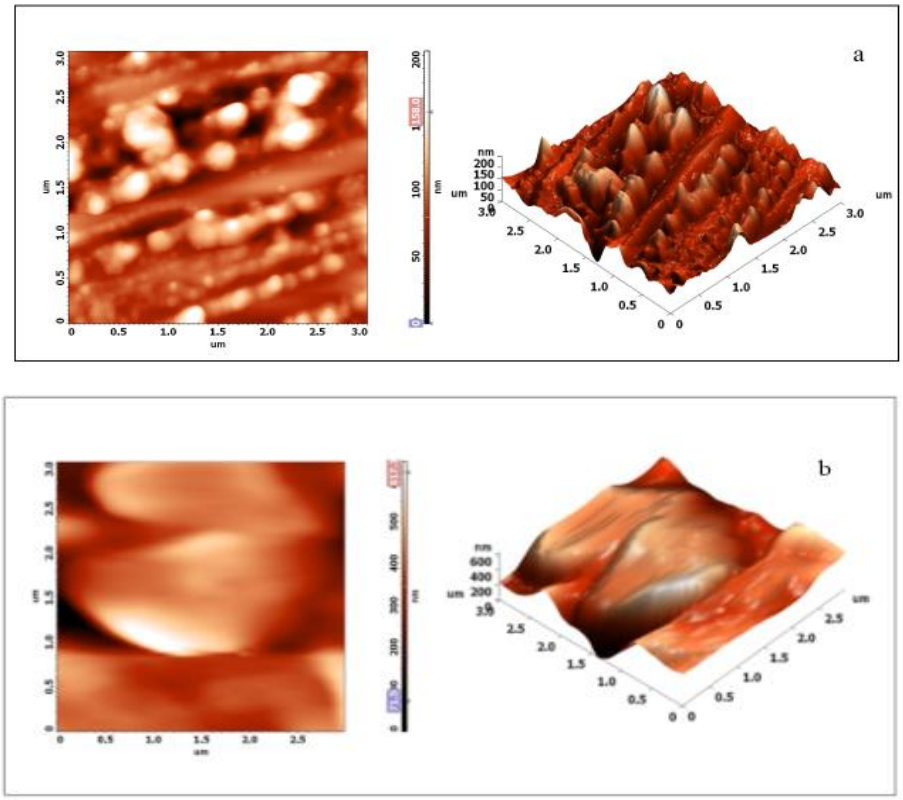

Figure 5.5: AFM images of (a) GNF1 (b) GNF2

5.3.4 SEM Analysis

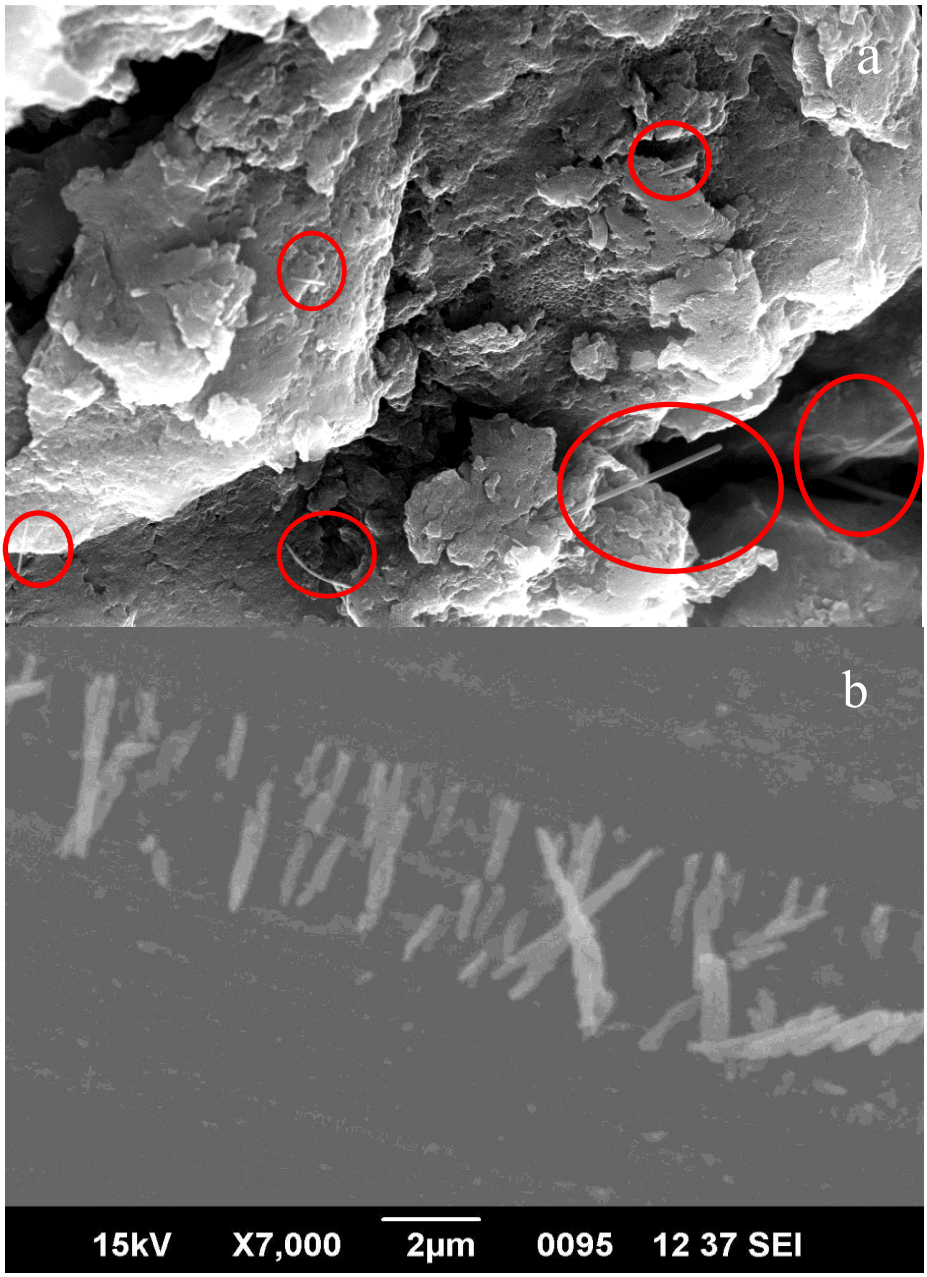

Fig 5.6: FE SEM image of a) GNF1 and b) SEM image of GNF2.

The FE SEM image of GNF1 is obtained successfully whereas that of GNF2 is not obtained because of the burning of the sample while striking with high energy electron beam. Extensive hydroxylation of the fullerene balls makes the sample sensitive to high energy electrons. Note that in GNF1, fullerols are originated from PFO which is expected to be less hydroxylated whereas the fullerols employed for GNF2 preparation is from H_2O_2 assisted sono-chemical preparation and therefore the fullerene balls will be extensively covered with hydroxy groups. Therefore, ordinary SEM image is collected for GNF2 with low energy electron beam. Presence of CNTs is well observed both in GNF1 and GNF2 as per the SEM analysis. In FE SEM image of GNF1, the nanotubes which are observed to be protruded from the composite are marked with red circles (figure 5.6a). In the SEM image of GNF2 (figure 5.6b)., the formed nanotubes are found to be externally covered with the fullerols, plausibly by C-O-C bonds as evident from XPS and FTIR studies as well. From figure 5.6b, it is observed that CNTs formed are arranged in an ordered pattern in GNF2.

5.3.5 TEM Analysis

TEM images are collected both for GNF1 and GNF2, even though burning of the external covering is observed for GNF2. The TEM analysis confirms formation carbon nanotubes both in GNF1 and GNF2. In GNF1and GNF2, functionalized graphene sheets are found getting rolled up to form CNTs, in the presence fullerols. In GNF2, the formed nanotubes are externally covered with fullerol balls which are also observed in TEM analysis, (inset of figure 5.7d). Unfortunately,

high resolution TEM images could not be obtained due to the electron beam sensitivity of the sample. Both in GNF1 and GNF2, the nanotubes formed are found to be multiwalled in nature.

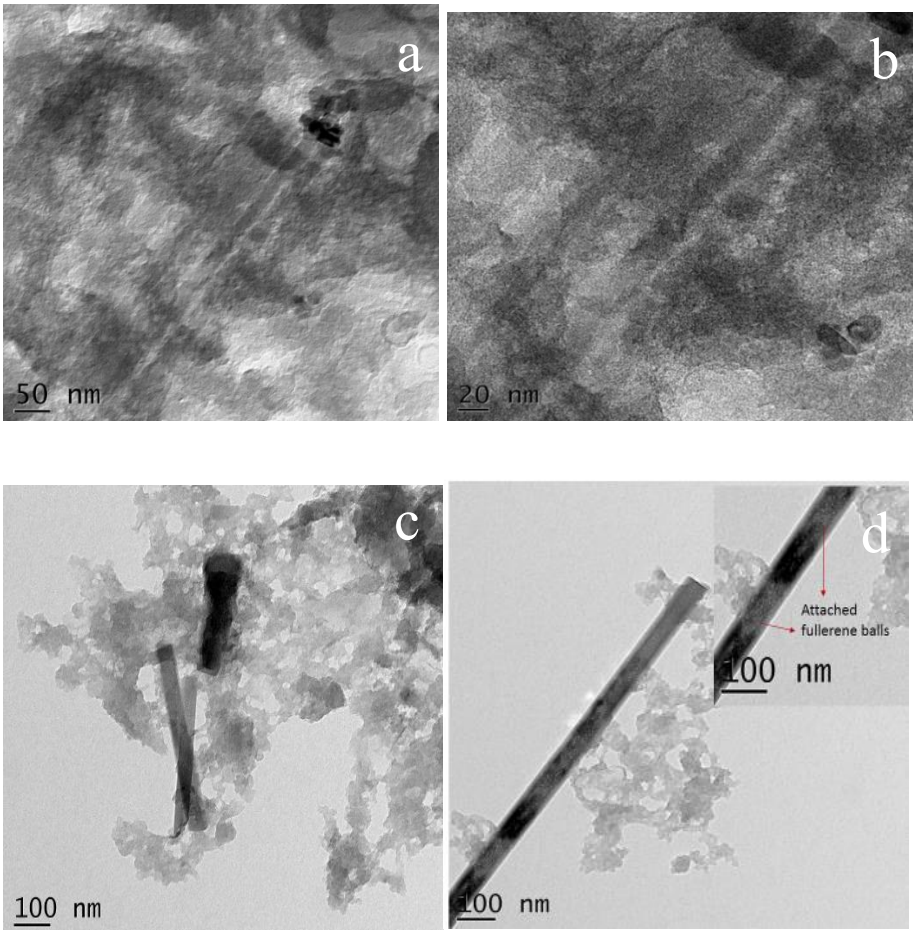

Figure 5.7: TEM images (a)&(b) of GNF1, (c)& (d) of GNF2

5.3.6 XPS Analysis

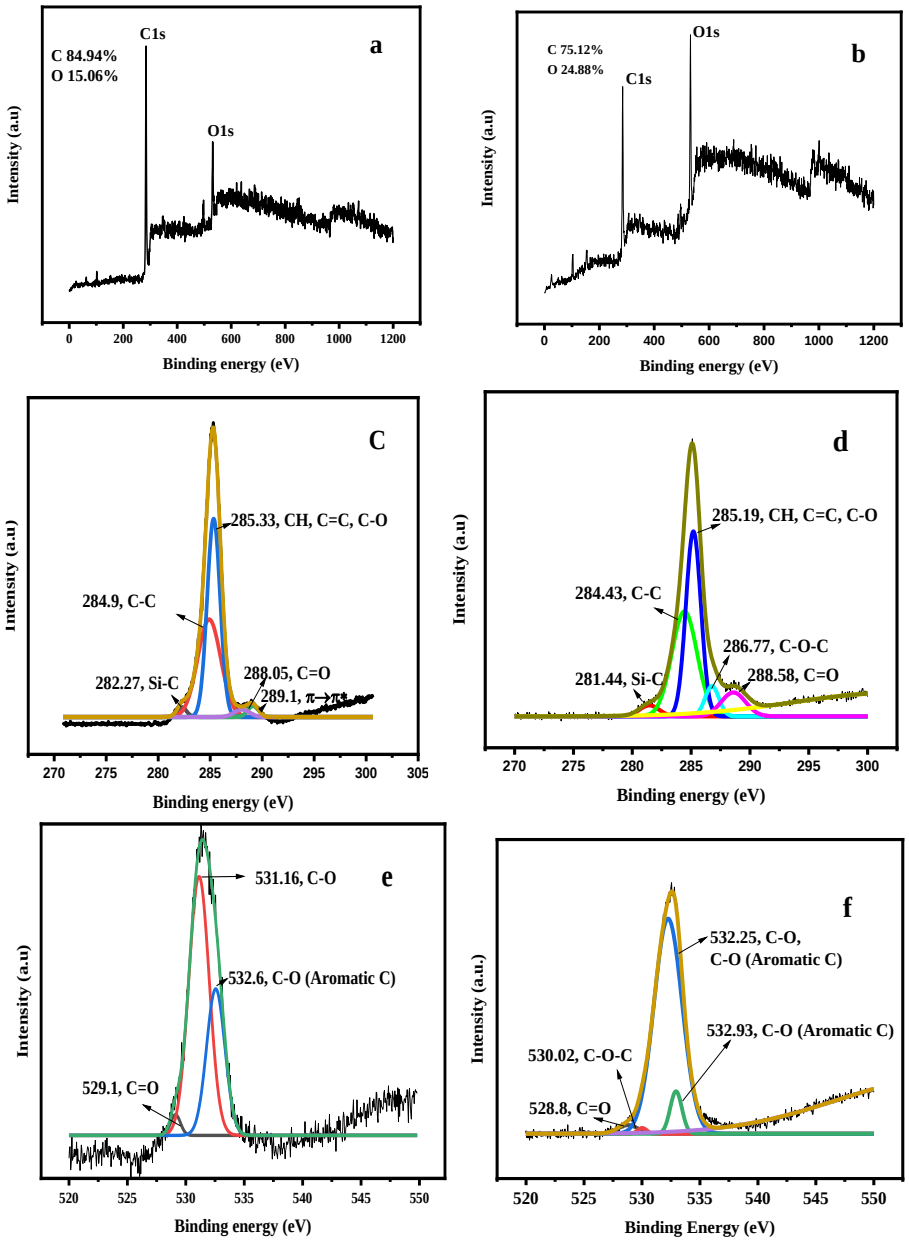

Figure 5.8 : XPS Survey spectra of (a) GNF1 & **(**b) GNF2
High Resolution C1s spectra of (c) GNF1 & (d) GNF2
High Resolution O1s spectra of (e) GNF1 & (f) GNF2

Even though XPS is regarded as a powerful characterization technique for functionalized carbon nanostructures, unfortunately it is less useful in probing hydrogenation, mainly for two reasons. [36] The first one is the inability of XPS to detect hydrogen and the second reason is the chemical shift of the hydrogenated carbon observed in the C1s high resolution spectrum is too small to be distinguished separately. The results obtained in the XPS analysis of GNF1 and GNF2 are presented in figure 5.8. From the XPS survey spectra (figure 5.8a & b), lower oxygen content is observed in GNF1compared to GNF2, which implies that the fullerols originated from PFO are far less hydroxylated than the ones used in the GNF2 preparation. The high-resolution C1s spectra for GNF1 and GNF2 reveal almost same chemical constitution of the two nanocomposites. Hemiacetal formation is also observed in both the nanocomposites as evidenced by the presence of C=O, both in high resolution C1s and O1s of both nanocomposites. The carbonyl content is observed to be slightly more in GNF1 compared to GNF2. There are weak signals in the high resolution C1s spectra at 282.27 eV for GNF1 and 281.44 eV for GNF2 indicating chemisorption and Si-C bond formation during the coating of the sample on the glass substrate used in the sample preparation for XPS analysis.

A tentative assignment of the peaks observed in the high resolution XPS spectra of C1s and O 1s regions of both GNF1 and GNF2 are summarized in table 5.1

Table 5.1: Peaks observed in the high resolution XPS spectra of C1s and O 1s regions of both GNF1 and GNF2

Sample	C1s Bindingenergy (eV) (Functional group)	O1s Bindingenergy(eV) (Functional group)
GNF1	282.27 (Si-C) 284.9(C-C) 285.3 (CH), C=C, C-O 288.05 (C=O) 289.1(π-π*)	529.1 (C=O) 531.16 (C-O) 532.6 (C-O)
GNF2	281.44(Si-C) 284.43 (C-C) 285.19(CH), C=C, C-O 286.77 (C-O-C) 288.58 (C=O)	528.8(C=O) 530.02 (C-O-C) 532.25 (C-O, Aromatic C) 532.93 (C-O, Aromatic C)

5.4. Electrochemical H_2O_2 sensing studies of GNF1 and GNF2

Herein, electrochemical sensing of H_2O_2 is performed with both GNF1 and GNF2 modified GCE, in which 1,10-phenanthroline (phen) drop-casted on the GNF1/GNF2 modified glassy carbon electrode surfaces whose electrochemical oxidation is performed by continuous cyclic voltammetric running for 15 cycles in PBS solution of pH 7.4. Cu^{2+} complexed with immobilised1,10-phenanthroline-5.6-dione (phen-dione) on GNF1 modified GCE act as a better sensing platform for H_2O_2 detection than the PHF based sensor developed in the previous work. whereas Cu^{2+} complexed with immobilised1,10-phenanthroline-5,6-dione (phen-dione) on GNF2 modified GCE showed lower activity than PHF based sensor.

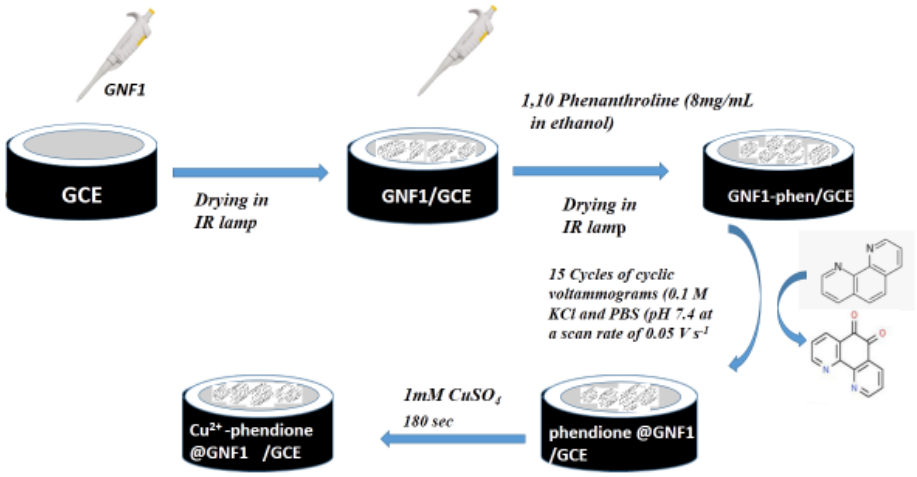

Fig 5.9: Preparation of Cu^{2+}-phen-dione@GNF1/GCE and Cu^{2+}-phen-dione@GNF2/GCE sensors.

The oxidized 1,10-phenanthroline can act as a mediator in the H_2O_2 sensing in an GNF1//GNF2 modified GCE surfaces. By continuous cyclic voltammetric running for 15 cycles 1,10-phenanthroline (Phen) undergoes oxidation to its dione form as evident by the continuous increase in its oxidation peak current as shown in figure 5.10. The phen-dione immobilized electrode is then subjected to dipping in 1 mM $CuSO_4$ solution for 180 s which result in the formation of copper complexed phen-dione@GNF1/GCE. A similar procedure is adapted for the preparation of copper complexed phen-dione@GNF2/GCE as well. All electrochemical measurements are performed with Phosphate Buffer Solution (pH 7.4) with 0.1 M KCl as supporting electrolyte.

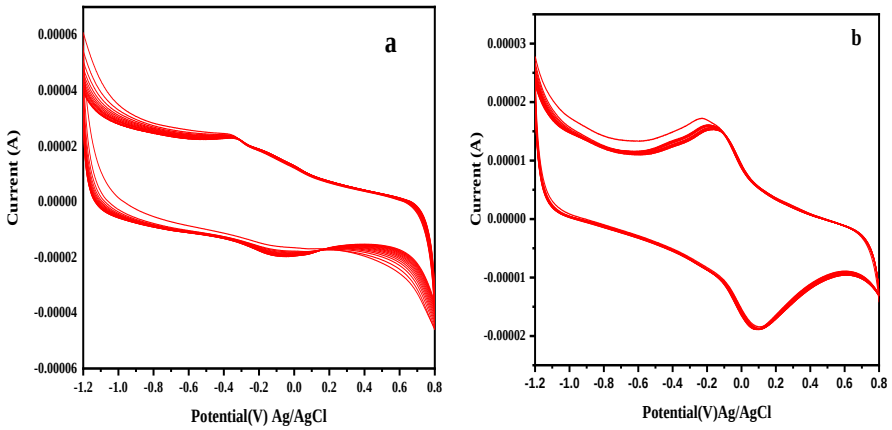

Figure 5.10: CV responses for a continuous run of 15 cycles for the preparation of phen-dione@GNF1/GCE (b) phen-dione@GNF2/GCE in 0.1 M PBS (pH 7.4) with 0.1 M KCl as supporting electrolyte.

Cyclic voltammetric responses of both GNF1 and GNF2 modified electrode surfaces in potassium ferro/ferri cyanide redox probe are recorded with KCl as supporting electrolyte in PBS (pH 7.4) solution as shown in figure:

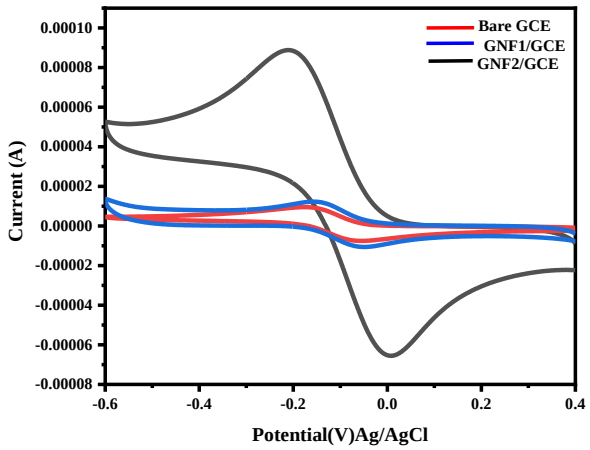

Figure 5.11: CV responses of (a) bare GCE (b)Cu^{2+}-phen-dione@GNF1/GCE(c)Cu^{2+}-phen-dione@GNF2/GCE in 0.5 mM $K_3Fe(CN)_6$ (0.1 M PBS pH 7.4) with KCl supporting electrolyte.

The Electro-Chemically active Surface Area (ECSA) of the modified electrodes are calculated by the Randles-Sevcik equation. ECSA values for bare GCE, Cu^{2+}-phen-dione@GNF1/GCE and Cu^{2+}-phen-dione@GNF2/GCE are 0.044 cm^2, 0.053 cm^2, 0.3778 cm^2 respectively.

Cyclic voltammetric responses of Cu^{2+}-1,10-phen-dione @GNF1/GCE and Cu^{2+}-1,10-phen-dione@GNF2/GCE in a potassium ferrocyanide/ferricyanide system are recorded at different scan rate. Peak current is found to be increasing with the increase in scan rate as shown in figure 5.12a and figure 5.13a. The plot of peak current vs. square root of scan rate gives a straight line in both cases with R^2 values of 0.9950 and 0.9944 respectively. From the linearity of the plots obtained, it is clear that electron transfer in both Cu^{2+}-phen-dione@GNF/GCE and Cu^{2+}-phen-dione@GNF2/GCE involves diffusion controlled processes.

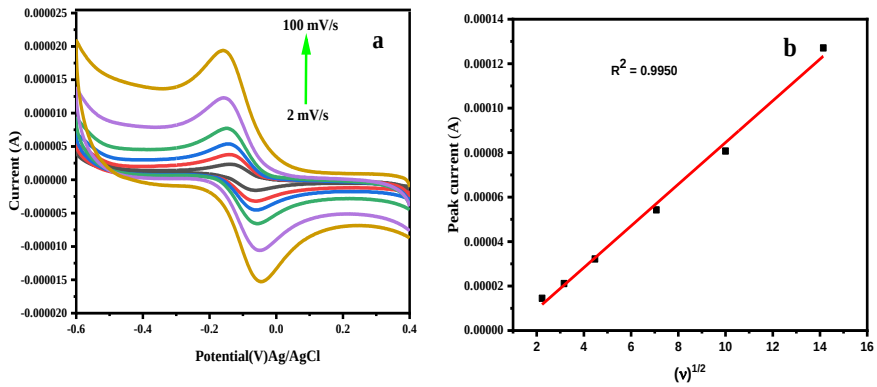

Figure 5.12: CV curves of Cu^{2+}-1,10-phen-dione@GNF1/GCE in 0.1M PBS containing 5 mM $Fe(CN)_6$ at at different scan rate

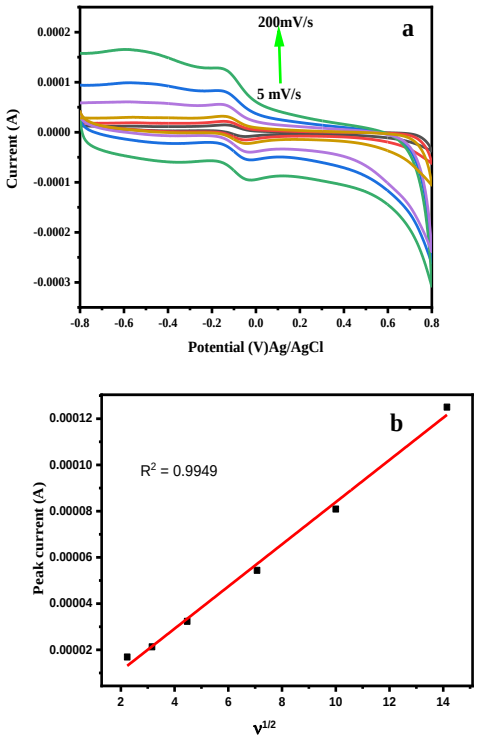

Figure 5.13: CV curves of Cu^{2+}-phen-dione@GNF2/GCE in 0.1 M PBS containing 5 mM $K_4Fe(CN)_6$ at different scan rate with Ag/AgCl as the reference electrode and 0.1 M KCl as supporting electrolyte .

Electrochemical sensing investigations of H_2O_2 are performed by means of cyclic voltammetry, by using the developed sensor electrodes in 0.1 M KCl as supporting electrolyte and phosphate buffer solution (pH 7.4) and the cyclic voltammetric responses obtained are presented in figure 5.14a & 5.15a. In both the cases, oxidation peak current values increase with the successive addition of H_2O_2 and calibration graphs are plotted with peak current vs. concentration of H_2O_2 giving straight line with R^2 values of 0.994 and 0.9971 respectively for Cu^{2+}-phen-dione@GNF1/GCE and Cu^{2+}-phen-

dione@GNF2/GCE showing good linearity over a range of concentrations in the micromolar level (figure 5.14b and figure 5.15b respectively).

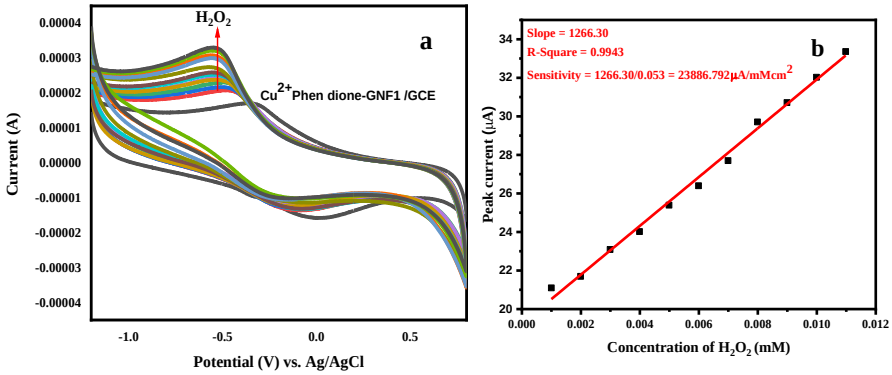

Figure 5.14: (a) Electrochemical sensing of hydrogen Cu^{2+}-1,10-phen-dione@GNF1/GCE (b) Corresponding calibration plot.

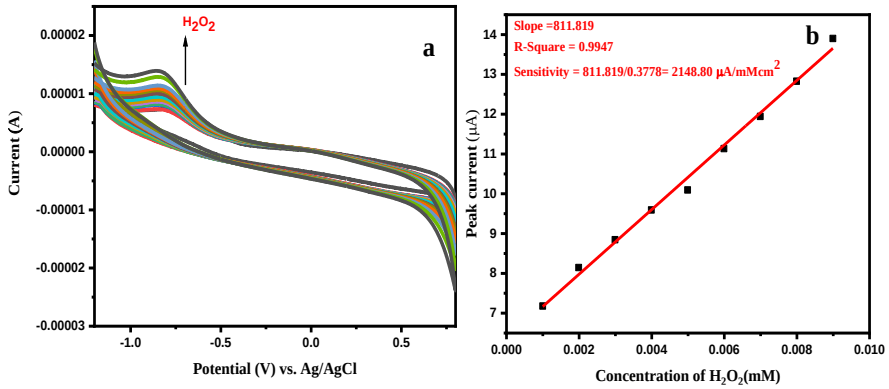

Figure 5.15: (a) Electrochemical sensing of hydrogen peroxide Cu^{2+}-phen-dione@GNF2/GCE (b) corresponding calibration plot.

The Limits Of Detection (LOD) of the prepared hydrogen peroxide sensors are evaluated by the relation $3xS.D_{(bl.)}$ /m, where S.D(bl) is the standard deviation of the blank solution calculated from

10 consecutive measurements and m is the slope of the calibration curve.The LOD values of Cu^{2+} -phen-dione@GNF1/GCE and Cu^{2+}-phen-dione@GNF2/GCE are found to be 3.018µM and 0.502µM respectively and the linear range they exhibited are 1 µM-11.02 µM & 1.03 µM – 8.9 µM respectively. Sensitivity of the developed electrode materials are calculated as 23886.7µA/mM cm^2, and 2148.806 µA/mM cm^2 respectively which is calculated as slope of the calibration curve/ECSA value of the electrode.

5.4.1 Interference study

Investigations to find out the interferences from other probable interfering biomarkers like Uric acid, Ascorbic acid, and glucose for the detection of H_2O_2 are performed cyclic voltammetrically. For this, 1.5 mM solutions of Uric acid (UA), Ascorbic acid, and glucose are prepared. 10 µl of each of these solutions of glucose, UA, and AA are added to 10 ml of Phosphate Buffer Saline solution (PBS, pH 7.4) and 0.1 M KCl, containing 10 µM concentration of H_2O_2, one by one and variation in the peak current are noted. The peak current for H_2O_2 is affected only very slightly (± 1.2 %) by these interfering species for both the developed sensors. Thus, it is observed that no significant interferences are present in the determination of H_2O_2, in both the cases. The results obtained are summarized in figure 5.16.

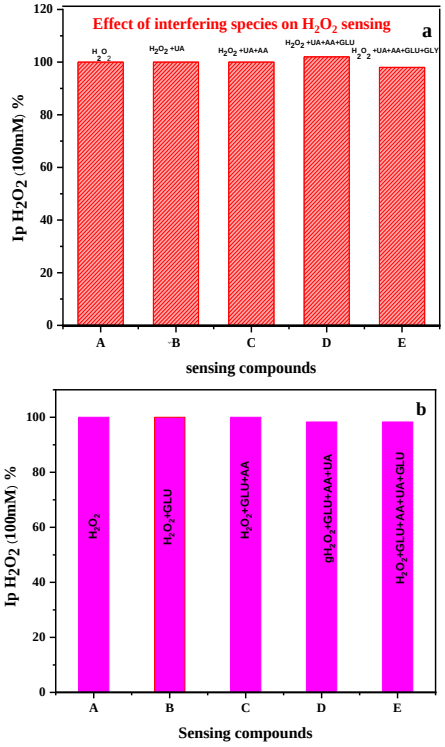

Figure 5.16 : Bar diagram showing the effect of interfering species on H_2O_2 sensing for (a) Cu^{2+}-1,10-phen -dione@GNF1/GCE (b) Cu^{2+}-phen-dione@GNF2/GCE.

The electrochemical performances of developed electrodes in H_2O_2 sensing are compared with that of other electrode materials found in literature as well as PHF based sensor investigated in the previous work and the results are presented in Table 5.2. The comparison shows that in terms of sensitivity, GNF1 is found to be an excellent sensor. However, owing to higher standard deviation values for blank measurements, the calculated LOD value for GNF1 is slightly high (3.018 μM) compared to other H_2O_2 sensors examined. The sensitivity of GNF2 is found to be lower than PHF and the overall sensing

performance of GNF2 have not shown expected improvement even after the incorporation of graphene and CNTs, in spite of achieving tremendous enhancement in the peak current and electrochemically active surface area, when the redox probe ferrocyanide/ferricyanide is used. Apparently, heavy hydroxylation and hydrogenation are not favorable for these materials to function as the electrocatalytic material for H_2O_2 sensing activity even though mild functionalization of the surfaces can improve the adsorption of the analyte molecules to their surfaces. Thus, GNF1 for which oxygen content is comparatively less, function as a more sensitive sensing platform compared to PHF and GNF2.

Table 5.2 : Electrochemical responses of various electrodes in H_2O_2 sensing

Sl No.	Electrode material	Technique used	Linear range	Sensitivity (μA/mMcm2)	Limit of Detection (μM)	Ref
1	Ag-PIL-GE	CV	0.1 μM-2.1 mM	38.73	0.05	39
2	β-MnO_2 nanorods/GCE	CV	2.45 μM-42.85 mM	21.74	2.45	27
3	MnO_2/graphene oxide	CV	5 μM-0.6 mM	38.2	0.8	40
4	AgNPs/PQ11/graphene	CV	100 μM-40 mM	39.89	2.8	41
5	Graphene/Au NPs/CHIT	CV	200 μM-4.2 mM	99.5	----	48
6	HRP/$NiFe_2O_4$NPs/ CHIT/Fe	CV	10 μM-2 mM	---	2	49
7	CoOX.NPs/ERGO	AMP	5 μM-1 mM	148.6	0.2	44
8	Cu^{2+} phendione@ PHF/GCE	CV	1 μM-10 μM	8148.3	0.353	Previous work
9	Cu^{2+} phendione@GNF1/GCE	CV	1 μM-11.02 μM	23886.7	3.018	This work
10	Cu^{2+}phendione@GNF2/GCE	CV	1.0 μM-8.9 μM	2148.80	0.502	This work

5.5 Conclusions

Hydrogen and hydroxy functionalized Graphene-Nanotube-Fullerene ternary nanohybrids (GNF1) are prepared by the hydrazine reduction of aqueous dispersion of oxidized PFO/RHG mixture and Graphene-Nanotube-Fullerene ternary hybrid (GNF2) is prepared by the hydrazine reduction of a mixture of fullerol and hydroxygraphene dispersion in water. Characterization of the prepared nano-materials using various spectroscopic and microscopic techniques are performed. From SEM and TEM, formation of nanotubes by the rapping of graphene sheets are observed both for GNF1 and GNF2. In addition, in GNF2, the formed nanotubes are found to be externally covered with the fullerol network, plausibly by C-O-C bonds as evident from XPS. Even though both GNF1 and GNF2 is thought to be originated from the hydrazine reduction of fullerols and hydroxy graphene precursors, the fullerols used in GNF2 preparation is more hydroxylated than the fullerols formed from PFO. This might have resulted in more interlinking and external covering of nanotubes with hydrogenated fullerol clusters through covalent bonds.

Another promising aspect of this work is the observation of high degree of hydrogenation present in the nanohybrids prepared. Similar to the hydrogenation of fullerol clusters observed in the previous work, the hydrazine reduction is thought to be proceeded via diimide formation where the fullerols formed from PFO acting as the required oxidizer in GNF1 and in GNF2 fullerols are one of the precursors which function as the oxidizing agent producing highly reactive diimides from hydrazine molecules. Hydrogen being perceived as the important future fuel; its safe storage is an area which have attracted tremendous research

attention. The observed degree of hydrogenation promises a landmark by providing a simple and straightforward hydrogenation strategy via diimides, of the most investigated hydrogen storage materials, viz., carbon nanomaterials.

Enzyme-free electrochemical sensing studies are performed for H_2O_2 using the modified glassy carbon electrodes, Cu^{2+}-phen-dione@GNF1/GCE and Cu^{2+}-phen-dione@GNF2/GCE. Cu^{2+}-phen-dione@GNF1/GCE is found to be a better sensor for H_2O_2 detection in terms of sensitivity. However, in terms of LOD, GNF1 based sensor did not show the best value. By and large, the developed sensors are excellent for the trace-level detection of the important biomarker H_2O_2, which can contribute to the global efforts for early-stage cancer diagnosis.

References

(1) Nasir, S.; Hussein, M. Z.; Zainal, Z.; Yusof, N. A. Carbon-Based Nanomaterials/Allotropes: A Glimpse of Their Synthesis, Properties and Some Applications. *Materials* **2018**, *11* (2), 295. https://doi.org/10.3390/ma11020295.

(2) Li, Y. Carbon Nanotube Research in Its 30th Year. *ACS Nano* **2021**, *15* (6), 9197–9200. https://doi.org/10.1021/acsnano.1c04972.

(3) Hamada, N.; Sawada, S.; Oshiyama, A. New One-Dimensional Conductors: Graphitic Microtubules. *Phys. Rev. Lett.* **1992**, *68* (10), 1579–1581. https://doi.org/10.1103/PhysRevLett.68.1579.

(4) Dresselhaus, M. S.; etc; Dresselhaus, G.; Eklund, P. C. *Science of Fullerenes and Carbon Nanotubes*; Academic Press Inc: San Diego, 1996.

(5) Kokarneswaran, M.; Selvaraj, P.; Ashokan, T.; Perumal, S.; Sellappan, P.; Murugan, K. D.; Ramalingam, S.; Mohan, N.; Chandrasekaran, V. Discovery of Carbon Nanotubes in Sixth Century BC Potteries from Keeladi, India. *Sci. Rep.* **2020**, *10* (1), 19786. https://doi.org/10.1038/s41598-020-76720-z.

(6) Lin, X.; Xi, Y.; Zhao, R.; Shi, J.; Yan, N. Construction of C_{60}-Decorated SWCNTs (C_{60}-CNTs)/Bismuth-Based Oxide Ternary Heterostructures with Enhanced Photocatalytic Activity. *RSC Adv.* **2017**, *7* (85), 53847–53854. https://doi.org/10.1039/C7RA11056A.

(7) Froudakis, G. E. Hydrogen Storage in Nanotubes & Nanostructures. *Mater. Today* **2011**, *14* (7), 324–328. https://doi.org/10.1016/S1369-7021(11)70162-6.

(8) Aqel, A.; El-Nour, K. M. M. A.; Ammar, R. A. A.; Al-Warthan, A. Carbon Nanotubes, Science and Technology Part (I) Structure, Synthesis and Characterisation. *Arab. J. Chem.* **2012**, *5* (1), 1–23. https://doi.org/10.1016/j.arabjc.2010.08.022.

(9) Guo, S.; Dai, Q.; Wang, Z.; Yao, H. Rapid Microwave Irradiation Synthesis of Carbon Nanotubes on Graphite Surface and Its Application on Asphalt Reinforcement. *Compos. Part B Eng.* **2017**, *124*, 134–143. https://doi.org/10.1016/j.compositesb.2017.05.033.

(10) Gong, K.; Yan, Y.; Zhang, M.; Su, L.; Xiong, S.; Mao, L. Electrochemistry and Electroanalytical Applications of Carbon Nanotubes: A Review. *Anal. Sci.* **2005**, *21* (12), 1383–1393. https://doi.org/10.2116/analsci.21.1383.

(11) Wang, J. Carbon-Nanotube Based Electrochemical Biosensors: A Review. *Electroanalysis* **2005**, *17* (1), 7–14. https://doi.org/10.1002/elan.200403113.

(12) Merkoçi, A. Carbon Nanotubes in Analytical Sciences. *Microchim. Acta* **2006**, *152* (3), 157–174. https://doi.org/10.1007/s00604-005-0439-z.

(13) Mondal, J.; An, J. M.; Surwase, S. S.; Chakraborty, K.; Sutradhar, S. C.; Hwang, J.; Lee, J.; Lee, Y.-K. Carbon Nanotube and Its Derived Nanomaterials Based High Performance Biosensing Platform. *Biosensors* **2022**, *12* (9), 731. https://doi.org/10.3390/bios12090731.

(14) Fathi, A.; Hassanzadazar, M. *CNT as a Sensor Platform*. Handbook of Research on Nanoelectronic Sensor Modeling and Applications. https://doi.org/10.4018/978-1-5225-0736-9.ch001.

(15) Britto, P. J.; Santhanam, K. S. V.; Rubio, A.; Alonso, J. A.; Ajayan, P. M. Improved Charge Transfer at Carbon Nanotube Electrodes. *Adv. Mater.* **1999**, *11* (2), 154–157. https://doi.org/10.1002/(SICI)1521-4095(199902)11:2<154::AID-ADMA154>3.0.CO;2-B.

(16) H, L.; Z, S.; N, L.; Z, G.; Q, Z. Investigation of the Electrochemical and Electrocatalytic Behavior of Single-Wall Carbon Nanotube Film on a Glassy Carbon Electrode. *Anal. Chem.* **2001**, *73* (5). https://doi.org/10.1021/ac000967l.

(17) Sun, L.; Crooks, R. M. Single Carbon Nanotube Membranes: A Well-Defined Model for Studying Mass Transport through Nanoporous Materials. *J. Am. Chem. Soc.* **2000**, *122* (49), 12340–12345. https://doi.org/10.1021/ja002429w.

(18) Ferrier, D. C.; Honeychurch, K. C. Carbon Nanotube (CNT)-Based Biosensors. *Biosensors* **2021**, *11* (12), 486. https://doi.org/10.3390/bios11120486.

(19) Martinez Jimenez, M. J.; Avila, A.; de Barros, A.; Lopez, E. O.; Alvarez, F.; Riul, A. J.; Perez-Taborda, J. A. Polyethyleneimine-Functionalized Carbon Nanotube/Graphene Oxide Composite: A

Novel Sensing Platform for Pb(II) Acetate in Aqueous Solution. *ACS Omega* **2021**, *6* (28), 18190–18199. https://doi.org/10.1021/acsomega.1c02085.

(20) Zhu, Z. An Overview of Carbon Nanotubes and Graphene for Biosensing Applications. *Nano-Micro Lett.* **2017**, *9* (3), 1–24. https://doi.org/10.1007/s40820-017-0128-6.

(21) Goran, J. M.; Phan, E. N. H.; Favela, C. A.; Stevenson, K. J. H_2O_2 Detection at Carbon Nanotubes and Nitrogen-Doped Carbon Nanotubes: Oxidation, Reduction, or Disproportionation? *Anal. Chem.* **2015**, *87* (12), 5989–5996. https://doi.org/10.1021/acs.analchem.5b00059.

(22) Pumera, M.; Ambrosi, A.; Bonanni, A.; Chng, E. L. K.; Poh, H. L. Graphene for Electrochemical Sensing and Biosensing. *TrAC Trends Anal. Chem.* **2010**, *29* (9), 954–965. https://doi.org/10.1016/j.trac.2010.05.011.

(23) Zhou, M.; Zhai, Y.; Dong, S. Electrochemical Sensing and Biosensing Platform Based on Chemically Reduced Graphene Oxide. *Anal. Chem.* **2009**, *81* (14), 5603–5613. https://doi.org/10.1021/ac900136z.

(24) Gan, T.; Hu, S. Electrochemical Sensors Based on Graphene Materials. *Microchim. Acta* **2011**, *175* (1), 1–19. https://doi.org/10.1007/s00604-011-0639-7.

(25) Veal, E. A.; Day, A. M.; Morgan, B. A. Hydrogen Peroxide Sensing and Signaling. *Mol. Cell* **2007**, *26* (1), 1–14. https://doi.org/10.1016/j.molcel.2007.03.016.

(26) Marinho, H. S.; Real, C.; Cyrne, L.; Soares, H.; Antunes, F. Hydrogen Peroxide Sensing, Signaling and Regulation of Transcription Factors. *Redox Biol.* **2014**, *2*, 535–562. https://doi.org/10.1016/j.redox.2014.02.006.

(27) Niamlaem, M.; Boonyuen, C.; Sangthong, W.; Limtrakul, J.; Zigah, D.; Kuhn, A.; Warakulwit, C. Highly Defective Carbon Nanotubes for Sensitive, Low-Cost and Environmentally Friendly Electrochemical H_2O_2 Sensors: Insight into Carbon Supports. *Carbon* **2020**, *170*, 154–164. https://doi.org/10.1016/j.carbon.2020.07.081.

(28) Luo, Y.; Liu, H.; Rui, Q.; Tian, Y. Detection of Extracellular H_2O_2 Released from Human Liver Cancer Cells Based on TiO_2 Nanoneedles

with Enhanced Electron Transfer of Cytochrome c. *Anal. Chem.* **2009**, *81* (8), 3035–3041. https://doi.org/10.1021/ac802721x.

(29) Eguílaz, M.; Dalmasso, P. R.; Rubianes, M. D.; Gutierrez, F.; Rodríguez, M. C.; Gallay, P. A.; López Mujica, M. E. J.; Ramírez, M. L.; Tettamanti, C. S.; Montemerlo, A. E.; Rivas, G. A. Recent Advances in the Development of Electrochemical Hydrogen Peroxide Carbon Nanotube–Based (Bio)Sensors. *Curr. Opin. Electrochem.* **2019**, *14*, 157–165. https://doi.org/10.1016/j.coelec.2019.02.007.

(30) Zeng, Q.; Li, Z.; Zhou, Y. Synthesis and Application of Carbon Nanotubes. *J. Nat. Gas Chem.* **2006**, *15* (3), 235–246. https://doi.org/10.1016/S1003-9953(06)60032-7.

(31) Wang, M.; Ma, J.; Guan, X.; Peng, W.; Fan, X.; Zhang, G.; Zhang, F.; Li, Y. A Novel H_2O_2 Electrochemical Sensor Based on $NiCo_2S_4$ Functionalized Reduced Graphene Oxide. *J. Alloys Compd.* **2019**, *784*, 827–833. https://doi.org/10.1016/j.jallcom.2019.01.043.

(32) Sreejesh, M.; Huang, N. M.; Nagaraja, H. S. Solar Exfoliated Graphene and Its Application in Supercapacitors and Electrochemical H_2O_2 Sensing. **2015**.

(33) Corey, E. J.0; Mock, W. L. Chemistry of Diimide. III. Hydrogen Transfer to Multiple Bonds by Dissociation of the Diimide-Anthracene Adduct, Anthracene-9,10-Biimine. *J. Am. Chem. Soc.* **1962**, *84* (4), 685–686. https://doi.org/10.1021/ja00863a045.

(34) U, R.; M, A.; P, R.; Rm, R. Graphene reduction of P25 titania: Ti^{3+}-doped titania/graphene nanohybrids for enhanced photocatalytic hydrogen production. *Int. J. Hydrog. Energy* **2020**, *45* (16), 9564–9574.

(35) Pakornchote, T.; Geballe, Z. M.; Pinsook, U.; Taychatanapat, T.; Busayaporn, W.; Bovornratanaraks, T.; Goncharov, A. F. Raman Spectroscopy on Hydrogenated Graphene under High Pressure. *Carbon* **2020**, *156*, 549–557. https://doi.org/10.1016/j.carbon.2019.09.077.

(36) Stojilovic, N. *Why Can't We See Hydrogen in X-ray Photoelectron Spectroscopy?* ACS Publications. https://doi.org/10.1021/ed300057j.

CHAPTER 6

CONCLUSIONS

In this dissertation, the first topic investigated is the networking of fullerene balls via five membered furan ring systems resulting in the development of a nanostructured polymeric fullerene oxide (PFO) framework via thermal [3+2] cycloadditions of fullerene oxides formed by the thermal decomposition of $C_{60}Br_{24}$. Photocatalytic dye degradation of model dye methylene blue as well as the photocatalytic hydrogen peroxide generation are investigated. Thus, the prepared PFO is found to be a highly efficient metal-free, sunlight-active, photocatalyst with narrow bandgap and can be considered as excellent material for visible light harvesting. With the proposed band diagram for PFO, the plausible mechanism of ROS production and the photocatalytic process have been put forward. In addition, electrochemical glucose sensing applications of PFO are also investigated and it is found to be an efficient metal-free, mediator-free fourth generation sensing platform for the trace level detection of glucose. The pore architectures of PFO are revealed by various characterization techniques, which is made up of macropores and mesopores with some extent of mesoscale ordering.

In the next work presented in this dissertation, networking of fullerene balls is achieved alternately via C-O-C bridges, by a reduction strategy employing hydrazine reagent to hydrogen bonded clusters of highly hydroxylated fullerenes called fullerols. Since fullerols are oxygen rich species, they are capable of acting as good oxidizing agents. Hydrazine is known produce diimides in the presence of oxidizers which are capable of hydrogenate multiple bonds.[1] Thus, along with C-O-C networking, partial hydrogenation of the fullerene balls also take place

resulting in the formation of partially hydrogenated fullerol (PHF) networks. This will make the material slightly less hydrophilic, suitable for modification of glassy carbon electrodes, in the development of an enzyme free sensing platform for hydrogen peroxide. The H_2O_2 sensor thus developed using Cu^{2+} ions attached on 1,10-phenanthroline-5,6-dione as the mediator on a PHF modified GCE, is found to be an efficient one in terms of sensitivity, selectivity, limit of detection and linear range when compared to other H_2O_2 sensors present in literature.

In the next study, successful development of functional ternary nanohybrids of graphene, carbon nanotubes and fullerenes are achieved by two different strategies. In the first one, hydroxy graphene is prepared from fluorographite and is solvothermaly reduced to RHG (reduced hydroxygraphene). PFO and RHG are taken in 1:1 ratio, mechanically mixed in a mortar and the mixture is calcined. This process is thought to be breaking the PFO network and converting it to fullerols by oxidation. RHG also is getting oxidized back to hydroxy graphene, such that the entire mixture becomes completely dispersible in water. This black aqueous dispersion is then subjected to hydrazine reduction. Apart from formation of hydrogenated fullerol balls and hydrogenated graphene sheets, accidental formation of few carbon nanotubes also by the zipping of curved hydroxylated graphene sheets during the reduction process. The hydrazine reduction is again thought to be proceeded via diimide formation where the fullerols formed acting as the required oxidizers. The composite formed is termed as GNF1. It is then characterized by various spectroscopic and microscopic techniques and successfully

employed as an efficient electrochemical sensing platform for H_2O_2. Another composite, GNF2 is prepared with an alternative strategy, mixing aqueous dispersions of fluorographite derived hydroxygraphene (HG) and fullerols (prepared by sonochemical H_2O_2 oxidation of C_{60}), in 1:1 ratio, followed by hydrazine reduction. GNF2 also is characterized in a similar way. The interesting finding is that regardless of the difference in preparation methods, GNF2 exhibit striking resemblance with GNF1, especially in FTIR and Raman spectroscopic analysis, which confirms that GNF1 and GNF2 possess similar chemical constitutions. However, in XPS analysis, GNF2 is found to have more oxygen content than GNF1, probably because the fullerol precursor used in GNF2 preparation is more hydroxylated than the ones originated from PFO. Moreover, in the HR TEM analysis of GNF2, the carbon nanotubes are observed to have attachment of fullerene balls on their surface, again hypothesised as a result of the heavy hydroxylation of fullerene balls used here, resulting in C-O-C linkages with nanotubes. Similar to PHF, burning of a part of GNF2 in high energy electron beam is observed, except the nanotube part, in the HR TEM and FE SEM analyses. Instead of FE SEM images, ordinary SEM images are presented here. The H_2O_2 sensing studies are carried out by using Cu^{2+} ions attached on 1,10-phenanthroline-5,6-dione as the mediator on a GNF1/GNF2 modified GCE. Efficiency of the developed sensors are evaluated in terms of sensitivity, selectivity, limit of detection and linear range and PHF, GNF1 and GNF2 are compared as H_2O_2 sensor material. GNF1is demonstrated to be a better electrochemical sensing platform for H_2O_2 than PHF and GNF2.

References

(1) Corey, E. J.; Mock, W. L. Chemistry of Diimide. III. Hydrogen Transfer to Multiple Bonds by Dissociation of the Diimide-Anthracene Adduct, Anthracene-9,10-Biimine. ACS Publications. https://doi.org/10.1021/ja00863a045.

CHAPTER 7

FUTURE OUTLOOK

The present dissertation focusses mainly on networking of oxidized fullerenes to form novel functional materials and their diverse applications. Oxidized fullerenes have attracted researchers' attention recently as an interstellar material. Detailed investigations leading to better understanding of their material properties and possible chemical transformations are relevant in the current scenario and offer possibilities for extended research in this direction. Designing photovoltaic devices utilizing the newly prepared fullerene-based polymeric framework will be another future prospect of this research work.

The photocatalysts developed here are highly efficient in the harvesting of sunlight to carry out diverse chemical transformations which can be exploited further. Similarly, the electrochemical sensors for important biomolecules like glucose and hydrogen peroxide can indeed contribute towards the global urge for cost effective and sensitive sensing platforms for their trace level detection in biological media in a non-invasive manner, especially in the health monitoring of neonatal babies.

Further, the high degree of hydrogenation observed in both these nanohybrids offer lot of possibilities for their potential use as hydrogen storage materials. This is the first report of utilization of hydrazine reduction with hydrogenation of double bonds via diimide formation in presence of an oxidizing agent, in graphene and carbon nanotubes. This opens up immense possibility and important future direction for further investigations with these interesting nanomaterials in the field of hydrogen storage.

PUBLICATION AND PAPERS PRESENTED

Publications

1. M Usha, K Sreeja, U Rajeena, P Chakkingal Parambil, P Raveendran, RM Ramakrishnan, Preparation of mesoporous poly (fullerene oxide) framework by thermal [3+ 2] cycloadditions and its application as a semiconductor photocatalyst, *Fullerenes, Nanotubes and Carbon Nanostructures* **31** (4), 2023, 317-326
2. K Sreeja, M Usha, U Rajeena, P Raveendran, RM Ramakrishnan, Fluorine-rich graphene quantum dots by selective oxidative cutting of hydroxy fluorographene and their application for sensing of Fe (III) ions, *Journal of Fluorine Chemistry* **268**, 2023, 110130

Paper presented

1. Presented a paper entitled " Synthesis, characterization and Biological study of Curcumin Reduced Silver nanoparticles" day National seminar on "Emerging trends in Nanomaterials science and Technology" organized by Dept. of chemistry,SNGS College, Pattambi

2. Presented a paper entitled " Azodyes of synthetic curcuminoids " day National seminar on "Emerging trends in Nanomaterials science and Technology" organized by Dept. of chemistrySri vyasa NSS College, Wadakkanchery